EUROPEAN RESPIRATORY journal

FLAGSHIP SCIENTIFIC JOURNAL OF ERS

Early View

Original research article

Computed tomography-based radiomics decodes prognostic and molecular differences in interstitial lung disease related to systemic sclerosis

Janine Schniering, Malgorzata Maciukiewicz, Hubert S. Gabrys, Matthias Brunner, Christian Blüthgen, Chantal Meier, Sophie Braga-Lagache, Anne-Christine Uldry, Manfred Heller, Matthias Guckenberger, Håvard Fretheim, Christos T. Nakas, Anna-Maria Hoffmann-Vold, Oliver Distler, Thomas Frauenfelder, Stephanie Tanadini-Lang, Britta Maurer

Please cite this article as: Schniering J, Maciukiewicz M, Gabrys HS, *et al*. Computed tomography-based radiomics decodes prognostic and molecular differences in interstitial lung disease related to systemic sclerosis. *Eur Respir J* 2021; in press (https://doi.org/10.1183/13993003.04503-2020).

Computed tomography-based radiomics decodes prognostic and molecular differences in interstitial lung disease related to systemic sclerosis

Janine Schniering[1,2], Malgorzata Maciukiewicz[1], Hubert S. Gabrys[3], Matthias Brunner[1,4], Christian Blüthgen[5], Chantal Meier[1], Sophie Braga-Lagache[6], Anne-Christine Uldry[6], Manfred Heller[6], Matthias Guckenberger[3], Håvard Fretheim[7], Christos T. Nakas[8,9], Anna-Maria Hoffmann-Vold[7], Oliver Distler[1], Thomas Frauenfelder[5], Stephanie Tanadini-Lang[3], Britta Maurer[1,4]

[1]Center of Experimental Rheumatology, Department of Rheumatology, University Hospital Zurich, University of Zurich, Zurich, Switzerland, [2]Institute of Lung Biology and Disease and Comprehensive Pneumology Center, Helmholtz Zentrum München, Member of the German Center for Lung Research (DZL), Munich, Germany,
[3]Department of Radiation Oncology, University Hospital Zurich, University of Zurich, Zurich, Switzerland, [4]Department of Rheumatology and Immunology, University Hospital Bern, University Bern, Switzerland, [5]Institute of Diagnostic and Interventional Radiology, University Hospital Zurich, University of Zurich, Zurich, Switzerland, [6]Proteomics and Mass Spectrometry Core Facility, Department for BioMedical Research (DBMR), University of Bern, Bern, Switzerland, [7]Department of Rheumatology, Oslo University Hospital, and Institute of Clinical Medicine, University of Oslo, Oslo, Norway, [8]Laboratory of Biometry, University of Thessaly, Volos, Greece, [9]University Institute of Clinical Chemistry, Inselspital, Bern University Hospital, University of Bern, Bern, Switzerland

*__Corresponding Author__: Britta Maurer, MD, Department of Rheumatology and Immunology, University Hospital Bern, University Bern, Switzerland, Phone +41 31 632 98 40, e-mail britta.maurer@insel.ch

Funding: This work was supported by the Forschungskredit PostDoc from University of Zurich (to J.S.; FK-19-046), the Bangerter Foundation and Swiss Academy of Medical Sciences (to C.M.), as well as the Gebauer Foundation, Lunge Zürich Foundation, OPO Foundation, and Prof. Max Cloetta Foundation (to B.M.).

Conflicts of Interests: J.S., M.M., H.S.G, M.B., C.M., C.B., M.G., S.B., A.U., M.H., C.T.N., T.F, S.T. have no competing interests to declare. H.F. received travel bursaries from Actelion and GSK, and remuneration from Bayer. A.M.H.V had grant/research support from Boehringer-Ingelheim and received speaker and personal fees from Boehringer-Ingelheim, Roche, Actelion, MSD, Medscape, and Bayer. O.D. had consultancy relationship and/or has received research funding from Abbvie, Actelion, Acceleron Pharma, Amgen, AnaMar, Baecon Discovery, Blade Therapeutics, Bayer, Boehringer Ingelheim, Catenion, Competitive Drug Development International Ltd , CSL Behring, ChemomAb, Curzion Pharmaceuticals, Ergonex, Galapagos NV, Glenmark Pharmaceuticals, GSK, Inventiva, Italfarmaco, iQone, iQvia, Lilly, medac, Medscape, Mitsubishi Tanabe Pharma, MSD, Novartis, Pfizer, Roche, Sanofi, Target Bio Science and UCB in the area of potential treatments of scleroderma and its complications. In addition, O.D. has a patent mir-29 for the treatment of systemic sclerosis issued (US8247389, EP2331143). B. M. has consultancies with Novartis, Boehringer Ingelheim,

Janssen-Cilag, had grant/research support from AbbVie, Protagen, Novartis Biomedical Research, received speaker fees from Boehringer-Ingelheim as well as congress support from Medtalk, Pfizer, Roche, Actelion, mepha, and MSD. In addition, B.M. has a patent mir-29 for the treatment of systemic sclerosis issued (US8247389, EP2331143).

Author Contributions: J.S. contributed to the design and conception of the work, was involved in acquisition, analysis and interpretation of radiomics, clinical and molecular data, and wrote the manuscript. M.M. contributed to the design and conception of the work, performed the statistical analysis, and drafted the manuscript. M.B. contributed to the acquisition and analysis of radiomics, clinical and molecular data, and revised the manuscript. H.S.G., C.B. were involved in the acquisition and analysis of radiomics data, and revised the manuscript. S.B., A.U., M.H. contributed to the acquisition and interpretation of proteomics data, and revised the manuscript. M.G. contributed to the analysis and interpretation of radiomics and clinical data, and revised the manuscript. C.M., H.F., A.M.H.V. contributed to the acquisition and interpretation of clinical data, and revised the manuscript. C.T.N. contributed to the statistical analysis and interpretation of data, and revised the manuscript. O.D. contributed to the analysis and interpretation of clinical and molecular data, and revised the manuscript. T.F., S.T. contributed to the acquisition, analysis and interpretation of radiomics data, and revised the manuscript. B.M. was central for the design and conception of the work, was involved in acquisition, analysis and interpretation of radiomics, clinical and molecular data, and wrote the manuscript.

Abstract

Background: Radiomic features calculated from routine medical images show great potential for personalized medicine in cancer. Patients with systemic sclerosis (SSc), a rare, multi-organ autoimmune disorder, have a similarly poor prognosis due to interstitial lung disease (ILD).

Objectives: To explore computed tomography (CT)-based high-dimensional image analysis (radiomics) for disease characterisation, risk stratification, and relaying information on lung pathophysiology in SSc-ILD.

Methods: We investigated two independent, prospectively followed SSc-ILD cohorts (Zurich, derivation cohort, *n*=90; Oslo, validation cohort, *n*=66). For every subject, we defined 1’355 robust radiomic features from standard-of-care CT images. We performed unsupervised clustering to identify and characterize imaging-based patient clusters. A clinically applicable prognostic quantitative radiomic risk score (qRISSc) for progression-free survival was derived from radiomic profiles using supervised analysis. The biological basis of qRISSc was assessed in a cross-species approach by correlation with lung proteomics, histological and gene expression data derived from mice with bleomycin-induced lung fibrosis.

Results: Radiomic profiling identified two clinically and prognostically distinct SSc-ILD patient clusters. To evaluate the clinical applicability, we derived and externally validated a binary, quantitative radiomic risk score composed of 26 features, qRISSc, that

accurately predicted progression-free survival and significantly improved upon clinical risk stratification parameters in multivariable Cox regression analyses in the pooled cohorts. A high qRISSc score, which identifies patients at risk for progression, was reverse translatable from human to experimental ILD and correlated with fibrotic pathway activation.

Conclusions: Radiomics-based risk stratification using routine CT images provides complementary phenotypic, clinical and prognostic information significantly impacting clinical decision-making in SSc-ILD.

Key Words: computed tomography, risk stratification, imaging biomarker, animal model, pathophysiology

Short Message. CT-based radiomics decodes phenotypic, prognostic and molecular differences in SSc-ILD and predicts progression-free survival with a significant impact on future clinical decision-making in SSc-ILD.

Introduction

Despite the emergence of targeted therapies, interstitial lung disease (ILD), the leading cause of death in systemic sclerosis (SSc), remains a key challenge due to the high variability in patient-specific disease trajectories and progression rates [1]. This high interindividual variability warrants valid prognostic biomarkers for individual risk stratification and personalized management, which so far are lacking [2]. Traditionally, molecular data from tissue biopsies have been explored for precision medicine strategies. However, the invasiveness of tissue biopsies, the unsuitability for longitudinal assessments, the high risk of non-representative sampling due to spatial disease heterogeneity and the high costs associated with molecular profiling have mostly limited the clinical implementation. This applies even more to SSc-ILD, where lung biopsies are only exceptionally performed since they are not required for diagnosis [3]. Medical imaging, particularly high-resolution computed tomography (HRCT), is an integral part of the standard-of-care of SSc-ILD, as it allows both diagnosis and longitudinal monitoring of the entire lung pathology with high sensitivity [4–6].

Recently, high-dimensional image analysis, termed “radiomics”, has opened novel avenues for imaging-based disease subtyping and outcome prediction [7–10]. Radiomic features are computationally retrieved, quantitative data derived from medical images, which describe the tissue in terms of its intensity, texture and advanced statistical properties [11]. Their unique and added value compared with visual or other quantitative imaging methodologies [12–14] lies in their ability to capture tissue phenotypes on different spatial scales ranging from the radiological/macroscopic to the molecular/microscopic level [8, 10, 15], which adds another dimension. Thereby, they

provide novel and complementary information compared to clinical reports, laboratory, and functional tests.

To address the high, unmet need for validated risk parameters, herein, we explored the potential of HRCT-based radiomics for disease characterization and outcome prediction in SSc-ILD.

Methods

Study Design and Datasets

We retrospectively investigated two independent prospectively followed cohorts of SSc-ILD including 90 patients (76.7% female, median age 57.5 years) from the University Hospital Zurich (=derivation cohort) and 66 patients (75.8% female, median age 61.0 years) from the Oslo University Hospital (=validation cohort). All included patients met the following criteria: diagnosis of SSc according to the Very Early Diagnosis of Systemic Sclerosis (VEDOSS) [16] or the 2013 American College of Rheumatology//European League [17] against Rheumatism (ACR/EULAR) classification criteria [18], presence of ILD on HRCT, and availability of an HRCT scan fulfilling the predefined quality criteria (ref. Supplementary Methods). A summary of the patient's demographics and clinical characteristics at baseline for both study cohorts is given in **Table 1**.

A third dataset derived from an experimental cohort of 30 mice with bleomycin-induced lung fibrosis, a widely acknowledged preclinical model for ILD [19], was used for correlation studies with biological features, including proteomic, histological, and gene

expression data. For every subject, we defined and extracted 1'386 radiomic features (**Supplementary File 1**) from semi-automated segmented HRCT images, including 17 intensity, 137 texture, and 1'232 wavelet features using our in-house developed radiomics software Z-Rad. A detailed description of the study workflow is available in **Fig.1**. The local ethics committees approved the study (approval numbers: pre-BASEC-EK-839 (KEK-no.-2016-01515), KEK-ZH-no. 2010-158/5, BASEC-no. 2018-02165, BASEC-no. 2018-01873) and written informed consent was obtained from every patient.

Statistical Analyses

Robustness of radiomic features against semi-automated lung delineation was assessed by intra- and inter-reader intraclass correlation (ICC) analysis, and unstable features (ICC < 0.75) were excluded from further analyses, resulting in a final set of 1,355 robust radiomic features (**Supplementary Fig.1**). Unsupervised *k*-Means clustering was performed to identify homogeneous imaging-based patient clusters without a priori assumptions in the derivation cohort (Zurich; *n*=90). Next, a quantitative composite radiomic risk score (qRISSc) for progression-free survival (PFS) was built to evaluate the clinical applicability. PFS was defined as the time from the date of the HRCT to the date of the first occurrence of ILD progression (=relative decline in FVC% predicted ≥ 15%). qRISSc, composed of 26 features, was derived by two-step feature selection, including univariable Cox regression and cross-validated LASSO penalised regression, and was further developed into a binary score with an optimal cut-off value of 0.21. Associations with clinical characteristics and PFS among the obtained patient clusters and qRISSc-based risk groups were assessed by Fisher's Exact and Mann-Whitney U test, or

univariable Cox regression, respectively. Multivariable Cox regression analyses with Hazards ratio (HR) and 95% confidence interval (CI) and C-index were applied to analyse the predictive ability of conventional clinical risk factors and qRISSc for progressive ILD in the pooled cohorts (*n*=156). The C-index is equivalent to the area under the curve in ROC analysis and can be used in Cox regression analysis [20]. Spearman correlation analysis with histological, gene expression and whole-lung proteomics data obtained from mice with bleomycin-induced lung fibrosis and pathway enrichment analysis was performed to define the biological basis of qRISSc.

A detailed description of the methods is provided in the online data supplement.

Results

Radiomic profiling captures clinical and prognostic differences among SSc-ILD patients

In a first discovery approach, we explored the radiomic phenotypes of the 90 SSc-ILD patients from the Zurich cohort with unsupervised clustering and examined their associations with clinical characteristics and patient outcome among the obtained clusters. Clustering of the 1,355 robust radiomic features revealed two distinct and stable patient clusters based on their radiomic profiles (Jaccard coefficient for cluster 1: 0.90 and for cluster 2: 0.82, wherein 1 indicates perfect stability; **Fig.2a/b**). The differences in clinical characteristics were substantial (**Fig.2** and **Supplementary Tab.1**) with patients from cluster 2 (*n*=31) having a significantly more impaired lung function (*p*<0.001, **Fig.2c**), worse performance in the 6-min walk test (**Fig.2c**), and a higher frequency of pulmonary hypertension (*p*=0.001, Fig.**2a/c**) than patients of cluster 1 (*n*=59). Cluster 2 was also

significantly enriched for honeycombing (p=0.009) as a radiological sign of more severe fibrotic lung remodelling.

Most notably, radiomic clusters did not stratify patients according to classical definitions of ILD severity, including limited and extensive disease extent as defined by HRCT analysis (HRCT threshold <20% or ≥20%) or PFTs (FVC ≥ 70% or <70%) [21], respectively. However, significant associations with both disease classifiers were detected (p=0.002 and p<0.001, respectively).

Furthermore, the clusters did not differ in common SSc clinical, demographic and serological characteristics, including age, sex, SSc disease duration, active immunomodulatory therapy, the extent of skin involvement, autoantibody profiles or CRP levels [18, 22] (**Fig. 2a/c** and **Supplementary Tab.1**).

We next assessed whether the patients of the two clusters also differed in their outcome by survival analysis with the Kaplan-Meier estimator. Consistent with their worse disease phenotype, patients of cluster 2 showed a higher probability of faster disease progression and a decrease in PFS defined by either the time to a relative decline of ≥ 15% in FVC% predicted (p=0.001, HR=3.52, 95% CI=(1.66-7.45), **Fig.2d**) or the time to decline assessed by a recently proposed FVC-DLCO composite index [22] (p=0.005, HR=2.73, 95% CI=(1.36 - 5.50), **Fig.2e**). In addition, a marginal association with time to visual disease progression on HRCT (p=0.102) and overall survival (p=0.104) was detected, suggesting a higher risk for visual ILD progression and all-cause death for patients of cluster 2 (**Fig.2f/g**).

Collectively, this exploratory analysis demonstrated that HRCT-based radiomic profiling captured clinical and prognostic differences in SSc-ILD that were complementary to the information provided by routine clinical, functional, and imaging tests.

A clinically applicable radiomic risk score predicts progression-free survival in SSc-ILD and improves upon existing stratification parameters

Having found that radiomic features identified prognostically distinct SSc-ILD patient clusters, we next assessed the clinical applicability of radiomics for outcome prediction. To that end, we derived a prognostic composite radiomic signature as recently proposed by Lu et al. [10] for risk stratification in ovarian cancer using the Zurich cohort as a derivation cohort. The resulting quantitative radiomic risk score for PFS, qRISSc, comprising 26 radiomic features (*n*=4 intensity, *n*=9 texture and *n*=13 wavelet features, **Supplementary Tab.2**), accurately stratified patients according to their risk for future lung decline with an optimal cut-off value of 0.21. In the derivation cohort (Zurich), high-risk patients had a higher probability of earlier lung function decline than low-risk patients (median PFS time = 48.0 months vs 82.30 months; **Fig.3a**). Most importantly, the final, binary version of qRISSc for risk stratification was independently confirmed. In the external validation cohort from Oslo, qRISSc-identified high-risk patients were at significant risk for progression (HR=5.14; 95% CI=14 - 23.20) with a median PFS time of 41.7 months compared with 88 months in the low-risk group (*p*=0.03) (**Fig.3b**).

Similarly to what was previously shown for the two distinct radiomic patient clusters, qRISSc-stratified high- and low-risk patient groups differed in their clinical characteristics (**Fig.3c**, **Supplementary Tabs. 3/4**). High-risk patients consistently presented with worse lung function parameters and showed an association with the presence of pulmonary

hypertension, the extent of fibrosis on HRCT, and specific visual ILD HRCT patterns including honeycombing, and traction bronchiectasis (**Fig.3c**).

Next, we evaluated whether qRISSc improved upon previously proposed clinical risk factors for SSc-ILD progression, including age, sex, baseline FVC and DLCO, disease extent on HRCT, radiological subtype, SSc subtype, auto-antibody status, and CRP [23–30] in both univariable and multivariable Cox regression analysis.

The univariable analysis only revealed baseline DLCO apart from qRISSc to be significantly and consistently associated with PFS among the two study cohorts (Fig.4a), yet with significantly weaker hazard ratios (HR=0.95-0.97, $p<0.05$) than qRISSc (HR=4.07-5.14, $p<0.05$, **Supplementary Tab. 5**).

In multivariable Cox regression analysis of the pooled cohorts, the integration of qRISSc into models composed of different combinations of the clinically pertinent risk factors for SSc-ILD progression significantly improved the power of outcome prediction as measured by the C-index (**Fig.4b, Supplementary Fig.2b**) compared to the models exclusively composed of the clinical risk factors **(Supplementary Tab. 6-8)**. In addition, in multivariable analysis same as in univariate analysis, qRISSc remained the strongest (HR=3.07-4.23) and often the only significant predictor in the combined models (**Fig.4c/Supplementary Fig.2a, Supplementary Tabs. 7/8**).

Of note, in the pooled study cohorts, qRISSc revealed to be also associated with other clinically used definitions of ILD progression, including different thresholds of FVC decline (i.e. an absolute FVC decline of ≥10% or ≥15%, or a relative FVC decline of ≥5% or ≥10%, $p<0.05$, **Supplementary Fig3b-e**), the FVC-DLCO composite index ($p<0.001$, **Supplementary Fig.3af**), visual ILD progression on HRCT ($p=0.031$, **Supplementary**

Fig.3~~b~~g), and overall survival (p<0.001, **Supplementary Fig.3~~c~~h**). No significant association of qRISSc was found with an absolute FVC decline of 5% (p=0.16, **Supplementary Fig.3a**).

Furthermore, we compared the prognostic performance of qRISSc to a quantitative score only composed of less complex, first order densitometric (intensity) features that were used in the past to quantify disease extent and progression in SSc-ILD [31–34]. While the intensity score was prognostic for future lung function decline in the derivation cohort (p=0.004), it was not significant in the external validation cohort (p=0.08), thus showing that the consideration of more abstract radiomic features provides additional important prognostic information (Supplementary Fig.4).

The clinical applicability of qRISSc was further confirmed by demonstrating that radiomic features, including qRISSc features, did not separate patients according to different imaging sites and settings employed in Zurich vs Oslo (**Supplementary Fig.5**; **Supplementary Tab.9**) [35].

In summary, our newly derived binary radiomic risk score, qRISSc, accurately predicted progression-free survival and significantly improved upon conventional risk stratification tools in two independent cohorts of SSc-ILD.

The quantitative radiomic risk score is associated with fibrotic pathway activation on a molecular level

The added and complementary value of radiomic profiling might ultimately arise from the integrated in-depth analysis of tissue heterogeneity covering the spatial spectrum from the radiological/macroscopic to the molecular/microscopic level covering pathologic

information of the whole organ [36]. Therefore, we next assessed the association of qRISSc with specific pathophysiological processes to define the biological underpinning for the stratification into high- and low-risk patients.

Since lung biopsies are only rarely performed in SSc-ILD [3] and consequently, imaging-matched human biosamples were not available, we used a cross-species correlation approach, employing the mouse model of bleomycin-induced lung fibrosis as a model system for SSc-ILD. For this model, we have recently confirmed that radiomic signatures largely translate between experimental ILD in bleomycin-treated mice and ILD in SSc patients [37].

We firstly compared qRISSc values obtained in mice and our two patients' cohorts to ensure that qRISSc reverse translates from patients to mice. We found a very similar score distribution between all three datasets confirming the suitability of this animal model as a preclinical "radiomic surrogate" for human ILD (**Fig.5a**).

We then performed pathway enrichment analysis for significantly qRISSc-correlated proteins (634 out of 5,311 identified proteins (11.94%) with rho ≥ |0.3|, $p<0.05$) derived from whole-lung tissue proteomics to reveal associations of qRISSc with molecular pathways and processes related to ILD (**Fig.5d**). We observed that pathways related to fibrosis development, particularly pathways associated with ECM organization and formation, were most significantly associated with qRISSc (**Fig.5f/g**). Consistently, the enriched biological processes that significantly correlated with qRISSc were also linked mainly to pro-fibrotic remodelling processes underlying ILD, including processes related to protein polymerization and ECM assembly (**Fig.5e**).

Among the highly and significantly qRISSc-correlated proteins were multiple ECM proteins, such as collagen 5α1, (CO5A1, *rho*=0.48), collagen 7α1 (CO7A1, *rho*=0.55), collagen 12α1 (COCA1, *rho*=0.46), collagen 15α1 (COFA1, *rho*=0.48), collagen 18α1 (COIA1, *rho*=0.47), filamin-C (FLNC, *rho*=0.66), and elastin (ELN, *rho*=0.63) as well as proteins required for ECM assembly and crosslinking, including members of the lysyl oxidase family, such as LOXL1 (*rho*=0.56) and LOXL2 (*rho*=0.68), or peroxidasin (PXDN, *rho*=0.64). In addition, proteins involved in TGF-β activation, including latent-transforming growth factor beta-binding protein 2 (LTBP2: *rho*=0.50) and integrin β6 (ITB6, *rho*=0.55), were strongly correlated with qRISSc (**Fig.5g**).

To complement the proteomic analysis, we additionally performed whole-slide digital histopathological and gene expression analysis of established fibrotic and inflammatory markers [38–40] (**Fig.5b/c)**. In line with the proteomic data, qRISSc was also significantly correlated with fibrotic markers on a histological level with a higher qRISSc value corresponding to a higher fibrosis score (Ashcroft score [41], *rho*=0.55), and increased expression of αSMA, a marker for activated fibroblasts (*rho*=0.38). Consistently, qRISSc also showed significant association with the expression of fibrotic genes, including collagen 1α1 (*Col1a1, rho*=-0.62), collagen 3α1 (*Col3a1, rho*=-0.59), and fibronectin 1 (*Fn1, rho*=-0.65), where a lower ΔCt value and thus negative correlation indicates higher gene expression. Most notably, neither on the histological nor on the gene level, qRISSc correlated with inflammatory markers, such as the number of CD45+ inflammatory cells in tissue sections, interleukin 6 (*Il6*), and monocyte chemoattractant protein 1 (*Mcp1*) mRNA expression (**Fig.5b/c**).

Collectively, this demonstrates that qRISSc specifically reflects the underlying fibrotic remodelling processes in experimental ILD and suggests that fibrotic and not inflammatory pathway activation may be dominant in individuals identified by a high qRISSc score.

Discussion

Herein, we showed that radiomics performed on standard-of-care HRCT images provided complementary clinical, prognostic and pathophysiologic information with great potential for risk stratification and outcome prediction in SSc-ILD.

Radiomic profiles captured ILD-specific differences based on image intensity, texture, and wavelet transformation and contained prognostic information. Clinical applicability was demonstrated by the accurate prediction of PFS in the combined SSc-ILD cohorts using a newly derived quantitative, binary radiomic risk score for SSc-ILD that can be calculated from a patient's routine HRCT scan. The integration of qRISSc into models composed of previously suggested risk factors [22–30] significantly improved the predictive power measured by the C-index. In all analyses, qRISSc was the strongest (HR=3.07-4.23) and often the only significant predictor in the combined models, thereby underlining the added value of qRISSc.

In both independent study cohorts, "high risk-patients" identified by clustering or risk scoring (qRISSc) were characterized by a more severe ILD phenotype, more compromised lung function, presence of pulmonary hypertension and specific visual ILD HRCT patterns including honeycombing and traction bronchiectasis, all of which have been discussed as potential risk factors in SSc-ILD [2, 42]. The fact that we did not

observe correlations with other suggested clinical risk factors such as, e.g. diffuse cutaneous SSc subset, older age, male sex, anti-topoisomerase 1-positivity [25, 43] or CRP [22] underlines that radiomic features capture lung-specific information independent of demographic and clinicoserological characteristics.

The benefit of radiomics might arise from the integrative and in-depth information obtained on whole lung pathology, where tissue heterogeneity is reflected on different spatial levels. In radiomic terms, spatial tissue heterogeneity is best described by texture features, which identify different image patterns by describing voxel intensities and their spatial arrangement [44]. In our study, most qRISSc features (e.g. “coarseness”, “cluster tendency”, “sum of variance”) belonged to the class of texture features or of wavelet transformations thereof. Investigating the added value of qRISSc compared to a radiomic score composed only of intensity features further showed that inclusion of such more complex features is crucial for prognostic performance. Our results are in line with previous studies, where texture features outperformed first order (intensity) features for prognostic purposes [8, 10, 15, 33] and where texture features were found to stratify patients according to disease severity [45]. In contrast to deep learning-based models, which require large datasets and represent “black box” approaches without an underlying biological rationale [46], radiomic features were shown to not only correlate with morphological but also with molecular tissue characteristics. This in-depth information provided by radiomics adds a new dimension to previously developed quantitative image analysis [12–14].

The hypothesis that radiomic features reflect the underlying pathophysiology was supported in our study, where we used a cross-species approach integrating imaging with molecular data to define the biological basis of qRISSc. In experimental ILD, a high qRISSc score was closely linked to specific fibrotic remodelling processes yet did not correlate with inflammation as assessed on a multiscale molecular level. The fibrotic pathway activation tied in with the worse outcome of the high-risk group of SSc-ILD patients identified by qRISSc [47]. The ability of radiomic markers to reflect the entire lung pathology is particularly attractive in a complex multi-organ disease with high molecular heterogeneity such as SSc [48]. The fact that radiomic features, including qRISSc, were reverse translatable from humans to mice demonstrates that well-characterized and representative animal models could prove valuable to test defined hypotheses in radiomics research, particularly for studying links with pathophysiology in rare diseases with low numbers of patients and limited access to biosamples.

Our study has some limitations, which despite the high-quality registry data from two independent, prospectively followed SSc cohorts from academic expert sites [49], mainly arise from the relatively low numbers of patients with this orphan disease. Appropriately, we did not impute missing data since the lack of data could not be assumed random. Furthermore, due to the modest sample size of our derivation cohort, we lacked the power to assess variable importance (measured by LASSO coefficients) and therefore assigned equal importance to each feature following a maximum-likelihood approach to construct qRISSc. Notably, despite this fact, we could fit significant multivariable models with good prognostic power on the combined cohort dataset, demonstrating the clinical applicability

of our quantitative radiomic risk score (qRISSc) and the potential to support clinical decision-making by improving upon existing risk parameters. Future large-scale collaborative studies designed to consider analytical methodologies for high-dimensional data will allow us to determine feature importance, perform proper weighting of score features, and evaluate further the added predictive value of radiomic signatures. Other limitations arise from exclusively focusing the analysis on SSc-ILD, which is relatively mild and of different aetiology compared with many other forms of fibrosing ILDs. Since the severity of ILD of the SSc patients included in our study was well in line with recently published data from the EUSTAR cohort [23], we consider our approach to apply to other SSc-ILD cohorts. Whether it applies to more severe forms and different aetiologies of fibrosing ILD, such as idiopathic pulmonary fibrosis, has yet to be determined.

Concerns about the reproducibility of radiomic features arise from their dependency on image acquisition and reconstruction methodologies and the intra-/inter-observer variability during image segmentation [50, 51]. In our study, radiomic features, including qRISSc, proved to be very stable against semi-automated lung segmentation. In addition, no batch-effects concerning different CT scanner types, scan and reconstruction protocols across two inhomogeneous cohorts of patients from independent sites occurred. This emphasizes the translational potential of our results and is a strong argument for the future clinical application of radiomics. We can, however, not exclude that the adherence to pre-defined quality criteria of the HRCT scan settings to ensure comparability between the two cohorts may have led to a specific selection bias of patients.

In conclusion, this work highlights radiomic profiling as a non-invasive means to capture the SSc-ILD heterogeneity by decoding clinical and prognostic differences and relaying pathophysiologic information. We provide a clinically applicable quantitative risk score for predicting PFS in SSc-ILD, which improves upon conventional risk factors. Whether it also allows the prediction of treatment response will be the subject of future studies.

References

1. Hoffmann-Vold A-M, Fretheim H, Halse A-K, Seip M, Bitter H, Wallenius M, Garen T, Salberg A, Brunborg C, Midtvedt Ø, Lund MB, Aaløkken TM, Molberg Ø. Tracking Impact of Interstitial Lung Disease in Systemic Sclerosis in a Complete Nationwide Cohort [Internet]. American Journal of Respiratory and Critical Care Medicine 2019. p. 1258–1266Available from: http://dx.doi.org/10.1164/rccm.201903-0486oc.

2. Distler O, Assassi S, Cottin V, Cutolo M, Danoff SK, Denton CP, Distler JHW, Hoffmann-Vold A-M, Johnson SR, Müller Ladner U, Smith V, Volkmann ER, Maher TM. Predictors of progression in systemic sclerosis patients with interstitial lung disease. *Eur. Respir. J.* [Internet] 2020; 55Available from: http://dx.doi.org/10.1183/13993003.02026-2019.

3. Silver KC, Silver RM. Management of Systemic-Sclerosis-Associated Interstitial Lung Disease. *Rheum. Dis. Clin. North Am.* 2015; 41: 439–457.

4. Hansell DM, Goldin JG, King TE Jr, Lynch DA, Richeldi L, Wells AU. CT staging and monitoring of fibrotic interstitial lung diseases in clinical practice and treatment trials: a Position Paper from the Fleischner society. *The Lancet Respiratory Medicine* 2015; 3: 483–496.

5. Winklehner A, Berger N, Maurer B, Distler O, Alkadhi H, Frauenfelder T. Screening for interstitial lung disease in systemic sclerosis: the diagnostic accuracy of HRCT image series with high increment and reduced number of slices. *Ann. Rheum. Dis.* 2012; 71: 549–552.

6. Hoffmann-Vold A-M, Aaløkken TM, Lund MB, Garen T, Midtvedt Ø, Brunborg C, Gran JT, Molberg Ø. Predictive value of serial high-resolution computed tomography analyses and concurrent lung function tests in systemic sclerosis. *Arthritis Rheumatol* 2015; 67: 2205–2212.

7. Parmar C, Leijenaar RTH, Grossmann P, Rios Velazquez E, Bussink J, Rietveld D, Rietbergen MM, Haibe-Kains B, Lambin P, Aerts HJWL. Radiomic feature clusters and prognostic signatures specific for Lung and Head & Neck cancer. *Sci. Rep.* 2015; 5: 11044.

8. Aerts HJWL, Velazquez ER, Leijenaar RTH, Parmar C, Grossmann P, Carvalho S, Bussink J, Monshouwer R, Haibe-Kains B, Rietveld D, Hoebers F, Rietbergen MM, Leemans CR, Dekker A, Quackenbush J, Gillies RJ, Lambin P. Decoding tumour phenotype by noninvasive imaging using a quantitative radiomics approach. *Nat. Commun.* 2014; 5: 4006.

9. Aerts HJWL, Grossmann P, Tan Y, Oxnard GR, Rizvi N, Schwartz LH, Zhao B. Defining a Radiomic Response Phenotype: A Pilot Study using targeted therapy in

NSCLC. *Sci. Rep.* 2016; 6: 33860.

10. Lu H, Arshad M, Thornton A, Avesani G, Cunnea P, Curry E, Kanavati F, Liang J, Nixon K, Williams ST, Hassan MA, Bowtell DDL, Gabra H, Fotopoulou C, Rockall A, Aboagye EO. A mathematical-descriptor of tumor-mesoscopic-structure from computed-tomography images annotates prognostic- and molecular-phenotypes of epithelial ovarian cancer. *Nat. Commun.* 2019; 10: 764.

11. Lambin P, Rios-Velazquez E, Leijenaar R, Carvalho S, van Stiphout RGPM, Granton P, Zegers CML, Gillies R, Boellard R, Dekker A, Aerts HJWL. Radiomics: extracting more information from medical images using advanced feature analysis. *Eur. J. Cancer* 2012; 48: 441–446.

12. Tashkin DP, Volkmann ER, Tseng C-H, Kim HJ, Goldin J, Clements P, Furst D, Khanna D, Kleerup E, Roth MD, Elashoff R. Relationship between quantitative radiographic assessments of interstitial lung disease and physiological and clinical features of systemic sclerosis. *Ann. Rheum. Dis.* 2016; 75: 374–381.

13. Abtin FG, Khanna D, Furst DE, Brown MS, Saidian L, Kim HJG, Galperin-Aizenberg M, Goldin J. Validation Of A Computer Aided Quantitative Fibrosis Score In Systemic Sclerosis Patients [Internet]. A103. INSIGHTS INTO IMAGING, DIAGNOSIS AND TREATMENT OF INTERSTITIAL LUNG DISEASE 2010.Available from: http://dx.doi.org/10.1164/ajrccm-conference.2010.181.1_meetingabstracts.a2353.

14. Kim HG, Tashkin DP, Clements PJ, Li G, Brown MS, Elashoff R, Gjertson DW, Abtin F, Lynch DA, Strollo DC, Goldin JG. A computer-aided diagnosis system for quantitative scoring of extent of lung fibrosis in scleroderma patients. *Clin. Exp. Rheumatol.* 2010; 28: S26–S35.

15. Grossmann P, Stringfield O, El-Hachem N, Bui MM, Rios Velazquez E, Parmar C, Leijenaar RT, Haibe-Kains B, Lambin P, Gillies RJ, Aerts HJ. Defining the biological basis of radiomic phenotypes in lung cancer. *Elife* [Internet] 2017; 6Available from: http://dx.doi.org/10.7554/eLife.23421.

16. Minier T, Guiducci S, Bellando-Randone S, Bruni C, Lepri G, Czirják L, Distler O, Walker UA, Fransen J, Allanore Y, Denton C, Cutolo M, Tyndall A, Müller-Ladner U, Matucci-Cerinic M, EUSTAR co-workers, EUSTAR co-workers. Preliminary analysis of the very early diagnosis of systemic sclerosis (VEDOSS) EUSTAR multicentre study: evidence for puffy fingers as a pivotal sign for suspicion of systemic sclerosis. *Ann. Rheum. Dis.* 2014; 73: 2087–2093.

17. Minier T, Guiducci S, Bellando-Randone S, Bruni C, Lepri G, Czirják L, Distler O, Walker UA, Fransen J, Allanore Y, Denton C, Cutolo M, Tyndall A, Müller-Ladner U, Matucci-Cerinic M, EUSTAR co-workers, EUSTAR co-workers. Preliminary analysis of the very early diagnosis of systemic sclerosis (VEDOSS) EUSTAR multicentre study: evidence for puffy fingers as a pivotal sign for suspicion of systemic sclerosis. *Ann. Rheum. Dis.* 2014; 73: 2087–2093.

18. van den Hoogen F, Khanna D, Fransen J, Johnson SR, Baron M, Tyndall A, Matucci-Cerinic M, Naden RP, Medsger TA Jr, Carreira PE, Riemekasten G, Clements PJ, Denton CP, Distler O, Allanore Y, Furst DE, Gabrielli A, Mayes MD, van Laar JM, Seibold JR, Czirjak L, Steen VD, Inanc M, Kowal-Bielecka O, Müller-Ladner U, Valentini G, Veale DJ, Vonk MC, Walker UA, Chung L, et al. 2013 classification criteria for systemic sclerosis: an American College of Rheumatology/European League against Rheumatism collaborative initiative. *Arthritis Rheum.* 2013; 65: 2737–2747.

19. Liu T, De Los Santos FG, Phan SH. The Bleomycin Model of Pulmonary Fibrosis. *Methods Mol. Biol.* 2017; 1627: 27–42.

20. Harrell FE. Regression Modeling Strategies: With Applications to Linear Models, Logistic and Ordinal Regression, and Survival Analysis. Cham: Springer International Publishing; 2015.

21. Goh NSL, Desai SR, Veeraraghavan S, Hansell DM, Copley SJ, Maher TM, Corte TJ, Sander CR, Ratoff J, Devaraj A, Bozovic G, Denton CP, Black CM, du Bois RM, Wells AU. Interstitial lung disease in systemic sclerosis: a simple staging system. *Am. J. Respir. Crit. Care Med.* 2008; 177: 1248–1254.

22. Wu W, Jordan S, Becker MO, Dobrota R, Maurer B, Fretheim H, Ye S, Siegert E, Allanore Y, Hoffmann-Vold A-M, Distler O. Prediction of progression of interstitial lung disease in patients with systemic sclerosis: the SPAR model. *Ann. Rheum. Dis.* 2018; 77: 1326–1332.

23. Hoffmann-Vold A-M, Allanore Y, Alves M, Brunborg C, Airó P, Ananieva LP, Czirják L, Guiducci S, Hachulla E, Li M, Mihai C, Riemekasten G, Sfikakis PP, Kowal-Bielecka O, Riccardi A, Distler O, EUSTAR collaborators. Progressive interstitial lung disease in patients with systemic sclerosis-associated interstitial lung disease in the EUSTAR database. *Ann. Rheum. Dis.* [Internet] 2020; Available from: http://dx.doi.org/10.1136/annrheumdis-2020-217455.

24. Winstone TA, Assayag D, Wilcox PG, Dunne JV, Hague CJ, Leipsic J, Collard HR, Ryerson CJ. Predictors of mortality and progression in scleroderma-associated interstitial lung disease: a systematic review. *Chest* 2014; 146: 422–436.

25. Nihtyanova SI, Schreiber BE, Ong VH, Rosenberg D, Moinzadeh P, Coghlan JG, Wells AU, Denton CP. Prediction of pulmonary complications and long-term survival in systemic sclerosis. *Arthritis Rheumatol* 2014; 66: 1625–1635.

26. Zhang XJ, Bonner A, Hudson M, Canadian Scleroderma Research Group, Baron M, Pope J. Association of gastroesophageal factors and worsening of forced vital capacity in systemic sclerosis. *J. Rheumatol.* 2013; 40: 850–858.

27. Savarino E, Bazzica M, Zentilin P, Pohl D, Parodi A, Cittadini G, Negrini S, Indiveri F, Tutuian R, Savarino V, Ghio M. Gastroesophageal reflux and pulmonary fibrosis in scleroderma: a study using pH-impedance monitoring. *Am. J. Respir. Crit. Care*

Med. 2009; 179: 408–413.

28. Assassi S, Sharif R, Lasky RE, McNearney TA, Estrada-Y-Martin RM, Draeger H, Nair DK, Fritzler MJ, Reveille JD, Arnett FC, Mayes MD, GENISOS Study Group. Predictors of interstitial lung disease in early systemic sclerosis: a prospective longitudinal study of the GENISOS cohort. *Arthritis Res. Ther.* 2010; 12: R166.

29. Plastiras SC, Karadimitrakis SP, Ziakas PD, Vlachoyiannopoulos PG, Moutsopoulos HM, Tzelepis GE. Scleroderma lung: initial forced vital capacity as predictor of pulmonary function decline. *Arthritis Rheum.* 2006; 55: 598–602.

30. Morgan C, Knight C, Lunt M, Black CM, Silman AJ. Predictors of end stage lung disease in a cohort of patients with scleroderma. *Ann. Rheum. Dis.* 2003; 62: 146–150.

31. Ufuk F, Demirci M, Altinisik G. Quantitative computed tomography assessment for systemic sclerosis-related interstitial lung disease: comparison of different methods. *Eur. Radiol.* 2020; 30: 4369–4380.

32. Bocchino M, Bruzzese D, D'Alto M, Argiento P, Borgia A, Capaccio A, Romeo E, Russo B, Sanduzzi A, Valente T, Sverzellati N, Rea G, Vettori S. Performance of a new quantitative computed tomography index for interstitial lung disease assessment in systemic sclerosis. *Sci. Rep.* 2019; 9: 9468.

33. Saldana DC, Hague CJ, Murphy D, Coxson HO, Tschirren J, Peterson S, Sieren JP, Kirby M, Ryerson CJ. Association of Computed Tomography Densitometry with Disease Severity, Functional Decline, and Survival in Systemic Sclerosis-associated Interstitial Lung Disease. *Ann. Am. Thorac. Soc.* 2020; 17: 813–820.

34. Ariani A, Silva M, Seletti V, Bravi E, Saracco M, Parisi S, De Gennaro F, Idolazzi L, Caramaschi P, Benini C, Bodini FC, Scirè CA, Carrara G, Lumetti F, Alfieri V, Bonati E, Lucchini G, Aiello M, Santilli D, Mozzani F, Imberti D, Michieletti E, Arrigoni E, Delsante G, Pellerito R, Fusaro E, Chetta A, Sverzellati N. Quantitative chest computed tomography is associated with two prediction models of mortality in interstitial lung disease related to systemic sclerosis. *Rheumatology* 2017; 56: 922–927.

35. Rizzo S, Botta F, Raimondi S, Origgi D, Fanciullo C, Morganti AG, Bellomi M. Radiomics: the facts and the challenges of image analysis. *Eur Radiol Exp* 2018; 2: 36.

36. Gillies RJ, Kinahan PE, Hricak H. Radiomics: Images Are More than Pictures, They Are Data [Internet]. Radiology 2016. p. 563–577Available from: http://dx.doi.org/10.1148/radiol.2015151169.

37. Schniering J, Gabrys H, Brunner M, Distler O, Guckenberger M, Bogowicz M, Vuong D, Karava K, Müller C, Frauenfelder T, Tanadini-Lang S, Maurer B. Computed-tomography-based radiomics features for staging of interstitial lung

disease – transferability from experimental to human lung fibrosis - a proof-of-concept study [Internet]. Imaging 2019.Available from: http://dx.doi.org/10.1183/13993003.congress-2019.pa4806.

38. Schniering J, Benešová M, Brunner M, Haller S, Cohrs S, Frauenfelder T, Vrugt B, Feghali-Bostwick C, Schibli R, Distler O, Müller C, Maurer B. F-AzaFol for Detection of Folate Receptor-β Positive Macrophages in Experimental Interstitial Lung Disease-A Proof-of-Concept Study. *Front. Immunol.* 2019; 10: 2724.

39. Schniering J, Benešová M, Brunner M, Haller S, Cohrs S, Frauenfelder T, Vrugt B, Feghali-Bostwick CA, Schibli R, Distler O, Mueller C, Maurer B. Visualisation of interstitial lung disease by molecular imaging of integrin αvβ3 and somatostatin receptor 2. *Ann. Rheum. Dis.* 2019; 78: 218–227.

40. Schniering J, Guo L, Brunner M, Schibli R, Ye S, Distler O, Béhé M, Maurer B. Evaluation of Tc-rhAnnexin V-128 SPECT/CT as a diagnostic tool for early stages of interstitial lung disease associated with systemic sclerosis. *Arthritis Res. Ther.* 2018; 20: 183.

41. Ashcroft T, Simpson JM, Timbrell V. Simple method of estimating severity of pulmonary fibrosis on a numerical scale. *J. Clin. Pathol.* 1988; 41: 467–470.

42. Perelas A, Silver RM, Arrossi AV, Highland KB. Systemic sclerosis-associated interstitial lung disease. *Lancet Respir Med* 2020; 8: 304–320.

43. Walker UA, Tyndall A, Czirjak L, Denton C, Farge-Bancel D, Kowal-Bielecka O, Muller-Ladner U, Bocelli-Tyndall C, Matucci-Cerinic M, Co-authors E. Clinical risk assessment of organ manifestations in systemic sclerosis: a report from the EULAR Scleroderma Trials And Research group database [Internet]. Annals of the Rheumatic Diseases 2007. p. 754–763Available from: http://dx.doi.org/10.1136/ard.2006.062901.

44. Zwanenburg A, Vallières M, Abdalah MA, Aerts HJWL, Andrearczyk V, Apte A, Ashrafinia S, Bakas S, Beukinga RJ, Boellaard R, Bogowicz M, Boldrini L, Buvat I, Cook GJR, Davatzikos C, Depeursinge A, Desseroit M-C, Dinapoli N, Dinh CV, Echegaray S, El Naqa I, Fedorov AY, Gatta R, Gillies RJ, Goh V, Götz M, Guckenberger M, Ha SM, Hatt M, Isensee F, et al. The Image Biomarker Standardization Initiative: Standardized Quantitative Radiomics for High-Throughput Image-based Phenotyping. *Radiology* 2020; : 191145.

45. Martini K, Baessler B, Bogowicz M, Blüthgen C, Mannil M, Tanadini-Lang S, Schniering J, Maurer B, Frauenfelder T. Applicability of radiomics in interstitial lung disease associated with systemic sclerosis: proof of concept. *Eur. Radiol.* [Internet] 2020; Available from: http://dx.doi.org/10.1007/s00330-020-07293-8.

46. Walsh SLF, Calandriello L, Silva M, Sverzellati N. Deep learning for classifying fibrotic lung disease on high-resolution computed tomography: a case-cohort study. *Lancet Respir Med* 2018; 6: 837–845.

47. Khanna D, Tashkin DP, Denton CP, Lubell MW, Vazquez-Mateo C, Wax S. Ongoing clinical trials and treatment options for patients with systemic sclerosis-associated interstitial lung disease. *Rheumatology* 2019; 58: 567–579.

48. Martyanov V, Whitfield ML. Molecular stratification and precision medicine in systemic sclerosis from genomic and proteomic data. *Curr. Opin. Rheumatol.* 2016; 28: 83–88.

49. Meier FMP, Frommer KW, Dinser R, Walker UA, Czirjak L, Denton CP, Allanore Y, Distler O, Riemekasten G, Valentini G, Müller-Ladner U, EUSTAR Co-authors. Update on the profile of the EUSTAR cohort: an analysis of the EULAR Scleroderma Trials and Research group database. *Ann. Rheum. Dis.* 2012; 71: 1355–1360.

50. Kumar V, Gu Y, Basu S, Berglund A, Eschrich SA, Schabath MB, Forster K, Aerts HJWL, Dekker A, Fenstermacher D, Goldgof DB, Hall LO, Lambin P, Balagurunathan Y, Gatenby RA, Gillies RJ. Radiomics: the process and the challenges. *Magn. Reson. Imaging* 2012; 30: 1234–1248.

51. Yip SSF, Aerts HJWL. Applications and limitations of radiomics. *Phys. Med. Biol.* 2016; 61: R150–R166.

Acknowledgements

Microscopic image recording was performed with equipment maintained by the Centre for Microscopy and Image Analysis, University of Zurich. We acknowledge Maria Comazzi (Centre of Experimental Rheumatology, University Hospital Zurich, Switzerland) for her technical assistance with the histological analyses.

Data Availability and Sharing

All data (clinical, radiomic, and molecular) and code for reproduction of the main findings of this study will be made publicly available after publication.

Tables

Table 1: Summary of the patients' demographics and clinical characteristics for the two patient cohorts included in this study. Continuous variables are described as median ± interquartile range, and categorical variables are presented as absolute counts with relative frequencies (percent). P-values of univariate comparisons of baseline characteristics between the two cohorts are shown. Fisher's exact test was used to compare categorical, and Mann-Whitney U to compare continuous variables, respectively. *Abbreviations: UIP = usual interstitial pneumonia, NSIP = nonspecific interstitial pneumonia, DIP = diffuse interstitial pneumonia, PAPsys = systolic pulmonary artery pressure, FVC = forced vital capacity, FEV1 = forced expiratory volume in 1 second, DLCO = diffusing capacity for carbon monoxide, 6-MWT = 6-min walk test, CRP = C-reactive protein*

Characteristics	**Zurich cohort** (n = 90)	**Oslo cohort** (n = 66)	**P-value**
Age (years)	57.5 ± 17.8	61.0 ± 18.8	0.641
Sex			
Male	21 (23.3%)	16 (24.2%)	1.000
Female	69 (76.7%)	50 (75.8%)	
SSc disease duration (years)*	5.0 ± 8.2	5.3 ± 9.2	0.874
SSc subset (LeRoy 1988)			
Limited cutaneous SSc	41 (45.6%)	37 (56.1%)	
Diffuse cutaneous SSc	42 (46.7%)	29 (43.9%)	**0.041**
No skin involvement	7 (7.8%)	0 (0.0%)	
Skin involvement			
Limited cutaneous	31 (34.4%)	37 (56.1%)	
Diffuse cutaneous	43 (47.8%)	29 (43.9%)	**<0.001**
No skin involvement	9 (10.0%)	0 (0.0%)	
Only sclerodactyly	7 (7.8%)	0 (0.0%)	
Autoantibodies			
Anti-centromere positive	13 (14.4%)	7 (10.6%)	1.000
Anti-topoisomerase I positive	41 (45.6%)	24 (36.4%)	0.614
Anti-RNA polymerase III positive	7 (7.8%)	8 (12.1%)	0.261
Anti-PMScl positive	18 (20.0%)	4 (6.1%)	**0.032**
FVC (% predicted)	87.5 ± 33.9	85.0 ± 36.0	0.605
FVC ≥70% predicted	64 (71.1%)	44 (66.7%)	0.851
FVC <70% predicted	24 (26.7%)	15 (22.7%)	
DLCO (% predicted)	66.5 ± 29.4	61.0 ± 29.0	0.078
FEV1 (% predicted)	88.7 ± 31.2	77.0 ± 26.5	0.088
Pulmonary hypertension†	20 (22.2%)	6 (9.1%)	**0.048**
PAPsys (mmHg)‡	26.0 ± 10.0	21.0 ± 20.0	**0.028**
CRP (mg/l)	3.1 ± 5.6	3.6 ± 8.0	0.259
6 min walk distance (m)	511.0 ± 161.0	n/a	n/a
SpO_2 before 6-MWT (%)	96.0 ± 2.0	n/a	n/a
SpO_2 after 6-MWT (%)	95.0 ± 7.0	n/a	n/a
Borg scale (unit; range 0-10)	3.0 ± 2.0	n/a	n/a
Extent of lung fibrosis on CT			

<20%	50 (55.6%)	30 (45.5%)	0.257
≥20%	40 (44.4%)	36 (54.5%)	
Ground glass opacification	45 (50.0%)	42 (63.6%)	0.104
Reticular changes	87 (96.7%)	51 (77.3%)	**<0.001**
Traction bronchiectasis	50 (55.6%)	27 (40.9%)	0.077
Honeycombing	22 (24.4%)	16 (24.2%)	1.000
Bullae	3 (3.3%)	4 (6.1%)	0.457
Radiological subtype			
NSIP	49 (54.4%)	34 (51.5%)	0.602
UIP[#]	37 (41.1%)	27 (40.9%)	
DIP	1 (1.1%)	0 (0.0%)	
Unclassifiable	3 (3.3%)	5 (7.6%)	
Immunomodulatory therapy[§]	51 (56.7%)	28 (42.4%)	0.105
Smoking status			
Never	55 (61.1%)	24 (36.4%)	**0.025**
Former	21 (23.3%)	25 (37.9%)	
Current	12 (13.3%)	5 (7.6%)	
Died during follow-up[§§]	20 (22.2%)	22 (33.3%)	**0.009**
Relative FVC decline ≥15% during follow-up	27 (30.0%)	11 (16.7%)	0.113
Visual HRCT progression during follow-up	21 (23.3%)	18 (27.3%)	0.316

*Disease duration of SSc was calculated as the difference between the date of baseline CT and the date of manifestation of the first non-Raynaud's symptom.

[†]Pulmonary hypertension was assessed by echocardiography or right heart catheterisation.

[‡]PAPsys was determined by right heart catheterisation.

[#]UIP includes the radiological diagnosis of both, "definite" and "probable" UIP.

[§]Immunomodulatory therapy included prednisone, methotrexate, rituximab, cyclophosphamide, mycophenolate mofetil, hydroxychloroquine, tocilizumab, imatinib, azathioprine, adalimumab, leflunomide, cyclosporine.

[§§]Cause of death included SSc-ILD, PAH, viral pneumonia, pulmonary embolism, septic shock, brain haemorrhage, caecal cancer, pancreatic carcinoma, lung cancer.

Figure Legends

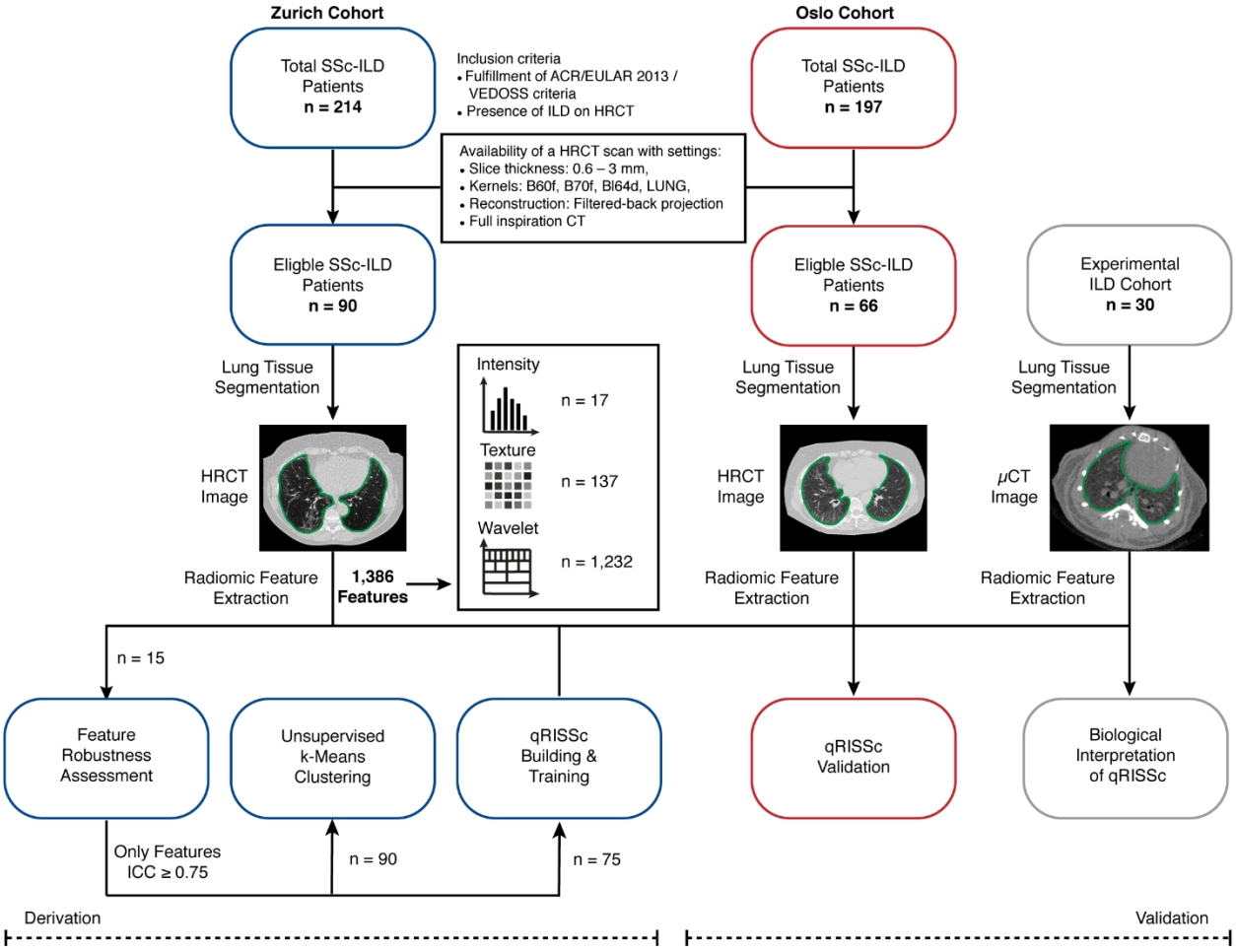

Figure 1: Study workflow. In this study, we applied radiomics to three different datasets, including two independent cohorts of SSc-ILD patients from 1) the University Hospital Zurich (derivation cohort) and 2) the Oslo University Hospital (validation cohort), and one experimental ILD cohort, composed of 30 bleomycin-treated mice for association studies with biological features (i.e. proteomic, histological, and gene expression data). Patients were retrospectively selected based on the fulfilment of early/mild SSc according to the Very Early Diagnosis of Systemic Sclerosis (VEDOSS) criteria [16] or established disease according to the 2013 American College of Rheumatology//European League against

Rheumatism (ACR/EULAR) classification criteria [18], presence of ILD on HRCT as determined by a senior radiologist, and pre-defined quality criteria for their HRCT images. For every subject, in total, 1,386 radiomic features were extracted from semi-automated segmented CT images, including 17 intensity, 137 texture, and 1,232 wavelet features using our in-house developed software Z-Rad. Filtering of robust radiomic features (ICC ≥ 0.75), unsupervised clustering, and construction of the quantitative radiomic ILD risk score (qRISSc) for progression-free survival in SSc-ILD were performed in the Zurich cohort. Independent and external validation of the built qRISSc was performed using the Oslo cohort.

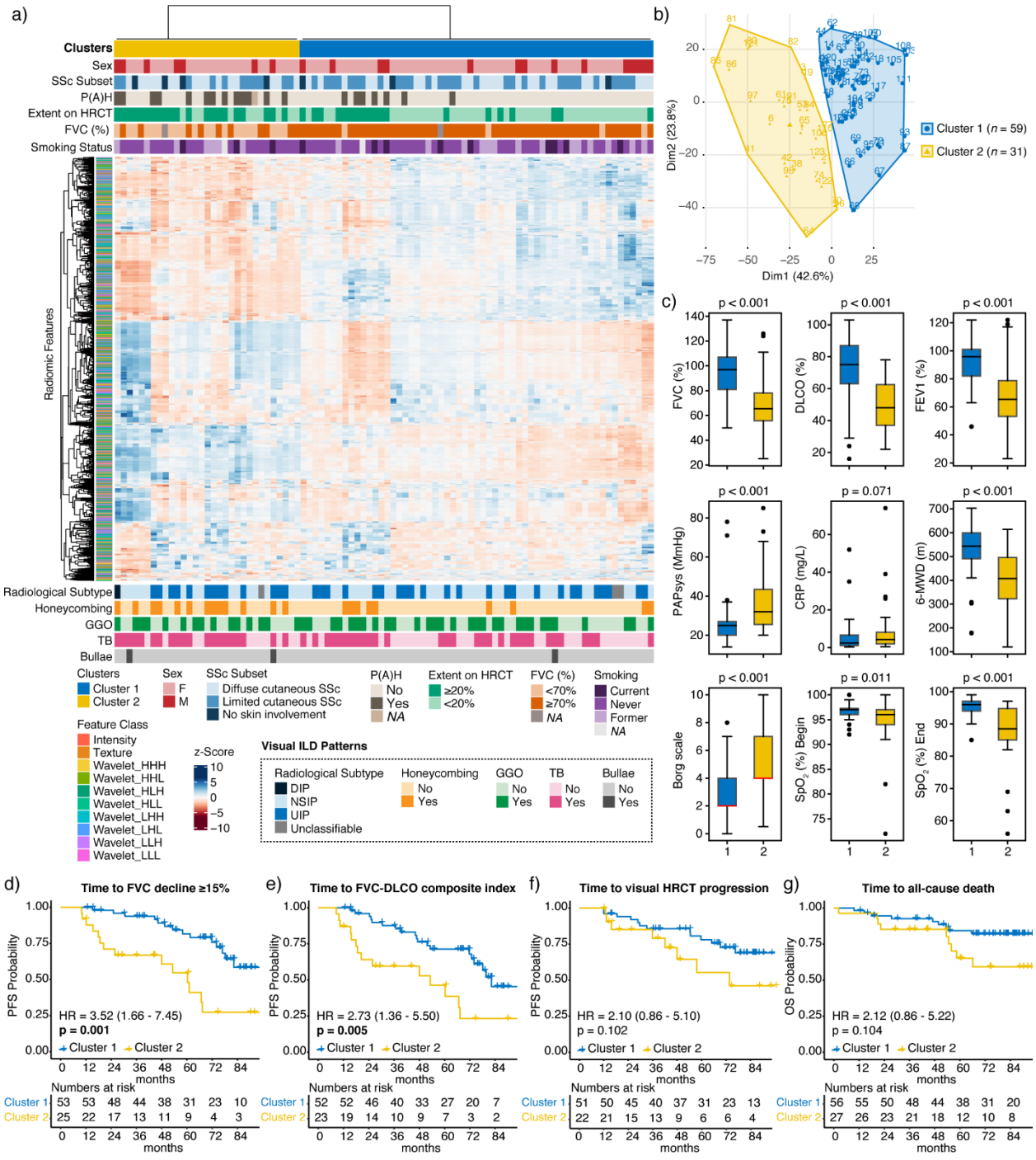

Figure 2: Unsupervised *k*-Means clustering of radiomic data from SSc-ILD patients.

(**a**) Heatmap summarizing the *k*-Means clustering results (Zurich cohort, *n*=90). Before clustering, radiomic features were z-scored. Associations between the two identified

radiomic patient clusters with categorical clinical parameters (above) and visual ILD patterns depicted on HRCT (below) are shown. (**b**) *k*-Means cluster plot indicating two stable clusters (Jaccard coefficient for cluster 1 (blue): 0.90 and for cluster 2 (yellow): 0.82, wherein 1 indicates perfect stability). (**c,** *first row*) Boxplots comparing lung function parameters between the two clusters, including FVC% predicted, DLCO% predicted and FEV1% predicted. (**c,** *second row*) Boxplots showing the systolic pulmonary artery pressure (PAPsys) and CRP values and the 6-min walk distance (6-MWD) from the 6-min walk test for both clusters. (c, third row) Boxplots indicating the Borg scale of perceived exertion (scale 0-10, 0 = no exertion, 1 = very weak, 2 = weak, 3 = moderate, 5 = strong, 7 = very strong, 10 = extreme exertion), and oxygen saturation (SpO2) at the beginning and end of the test per patient cluster. (**d**) Kaplan Meier curves for progression-free survival (PFS) defined as either the time to a relative FVC decline ≥ 15%, or (**e**) the time to the FVC-DLCO composite index (FVC-DLCO composite index = relative decrease in FVC% predicted of ≥15%, or a relative decline in FVC% predicted of ≥10% combined with DLCO% predicted of ≥15% according to [22]), or (**f**) the time to visual ILD progression on HRCT. (g) Kaplan Meier plot for overall survival (OS) defined as the time to all-cause death. The Hazard ratios (HR) with 95% confidence intervals and p-value of the univariate Cox regression are shown.

Abbreviations: SSc = systemic sclerosis, P(A)H = pulmonary (arterial) hypertension, FVC = forced vital capacity, FEV1 = forced *expiratory volume in 1 second, DLCO = diffusing capacity for carbon monoxide, CRP = C-reactive protein, F = female, M = male, DIP = diffuse interstitial pneumonia, NSIP = nonspecific interstitial pneumonia, UIP = usual interstitial pneumonia, GGO = ground glass opacification, TB = traction bronchiectasis*

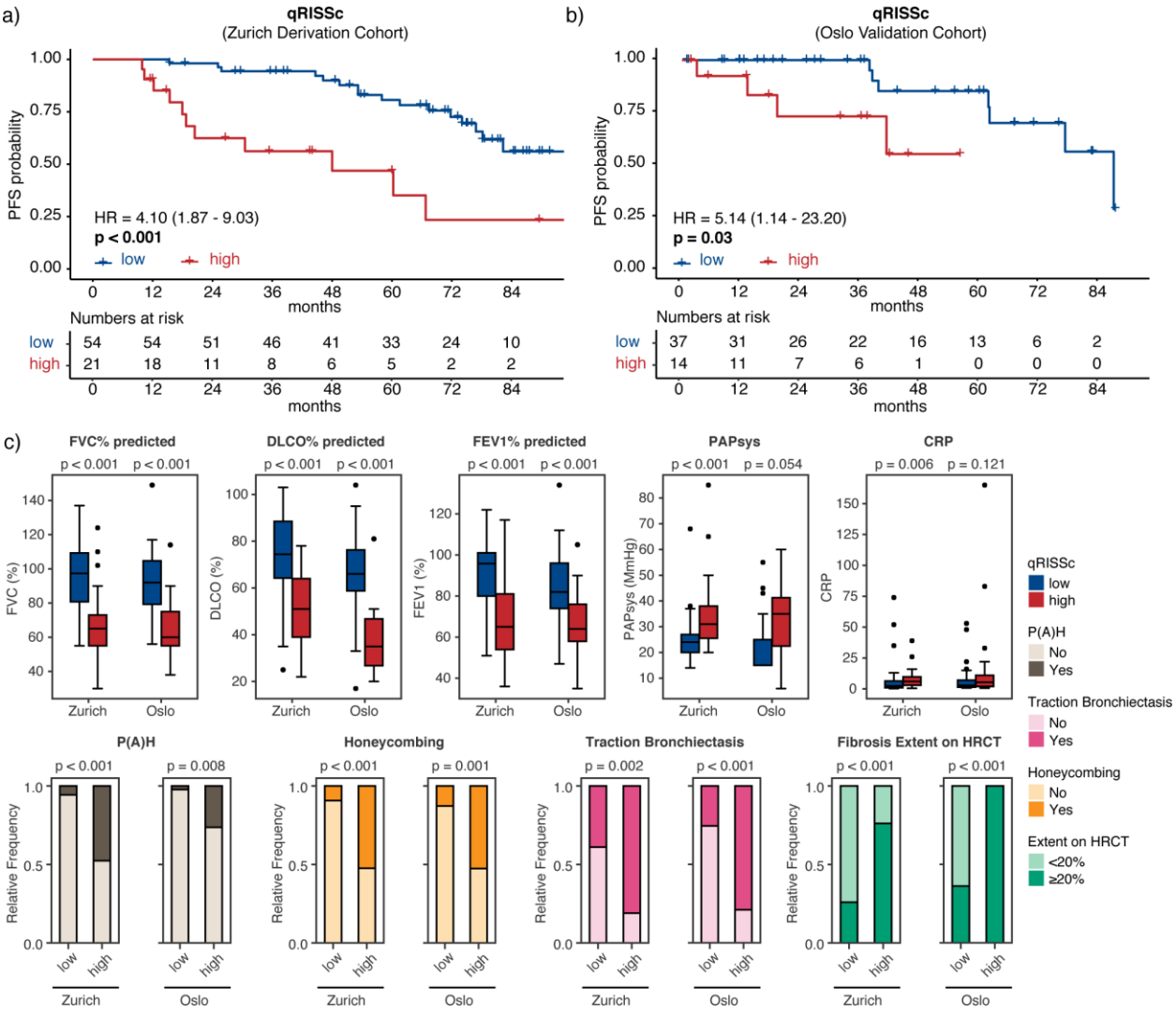

Figure 3: qRISSc-based risk stratification for future lung function decline and associations of qRISSc with clinical parameters in the derivation and validation cohort. Kaplan Meier curves of the constructed quantitative radiomic ILD risk score (qRISSc) for progression-free survival (PFS) defined as the time to relative FVC decline ≥ 15% in (**a**) the derivation cohort from Zurich and (**b**) in the external validation cohort from Oslo. The Hazard ratios (HR) with 95% confidence intervals and p-values of the univariate Cox regression are shown. (**c**) Significant associations of qRISSc with clinical parameters in both the derivation (Zurich) cohort and validation (Oslo) cohort. Fisher's

exact test was used for comparison of categorical and Mann-Whitney U test to compare numerical variables, respectively.

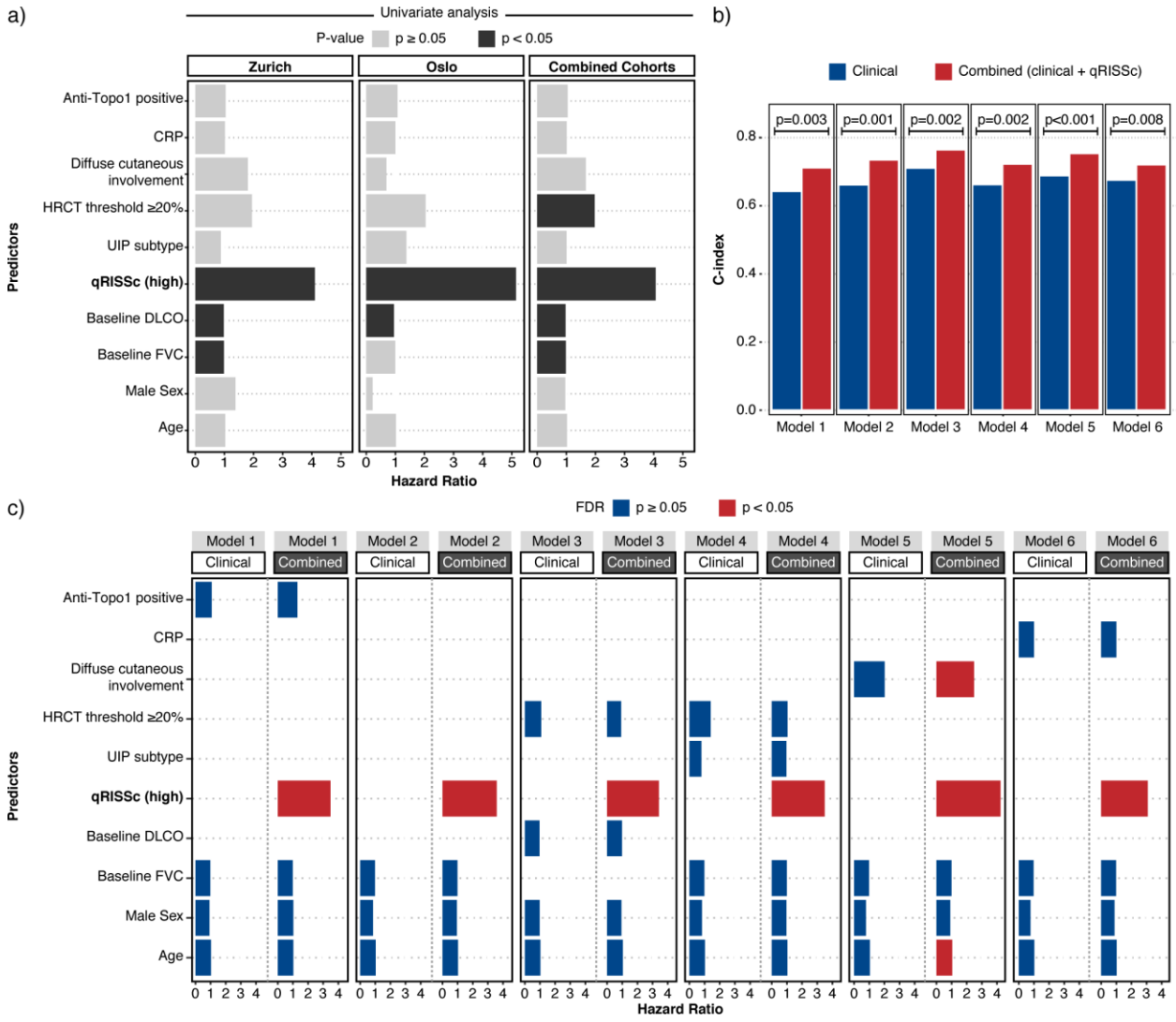

Figure 4: Prognostic performance of qRISSc compared to other risk factors for SSc-ILD progression. (**a**) Bar plot indicating the results of the univariable Cox regression analysis of qRISSc compared to previously proposed clinical risk factors of SSc-ILD progression. (**b**) Bar plot comparing the predictive power (C-index) of the multivariable models composed of the clinical risk factors of SSc-ILD progression alone (clinical models) versus models also incorporating qRISSc (combined models). Two-way ANOVA was used to compare model performances. Model 1: *Age* + *Male Sex* + *Baseline FVC*

(% predicted) + Anti-Topoisomerase 1 ± qRISSc, Model 2: *Age + Male Sex + Baseline FVC (% predicted) ± qRISSc,* Model 3: *Age + Male Sex + Baseline DLCO (% predicted) + HRCT threshold ≥20% ± qRISSc*, Model 4: *Age + Male Sex + Baseline FVC (% predicted) + HRCT threshold ≥20% + UIP subtype ± qRISSc*, Model 5: *Age + Male Sex + Baseline FVC (% predicted) + diffuse cutaneous involvement ± qRISSc*, Model 6: *Age + Male Sex + Baseline FVC (% predicted) + CRP ± qRISSc*. Models 1 and 4 (exclusively composed of clinical covariates) were overall not significant. (**c**) Bar plot summarising the FDR-corrected results of the multivariable Cox regression analysis incorporating qRISSc (combined models) versus multivariable models composed of clinical risk factors alone (clinical models). Bars represent hazard radios for each predictor in each model, whereas colours indicate the p-value of the predictors corrected for multiple testing using false discovery rate (FDR). Covariates for uni- and multivariable Cox regression were selected based on literature evidence [2] and expert opinion.

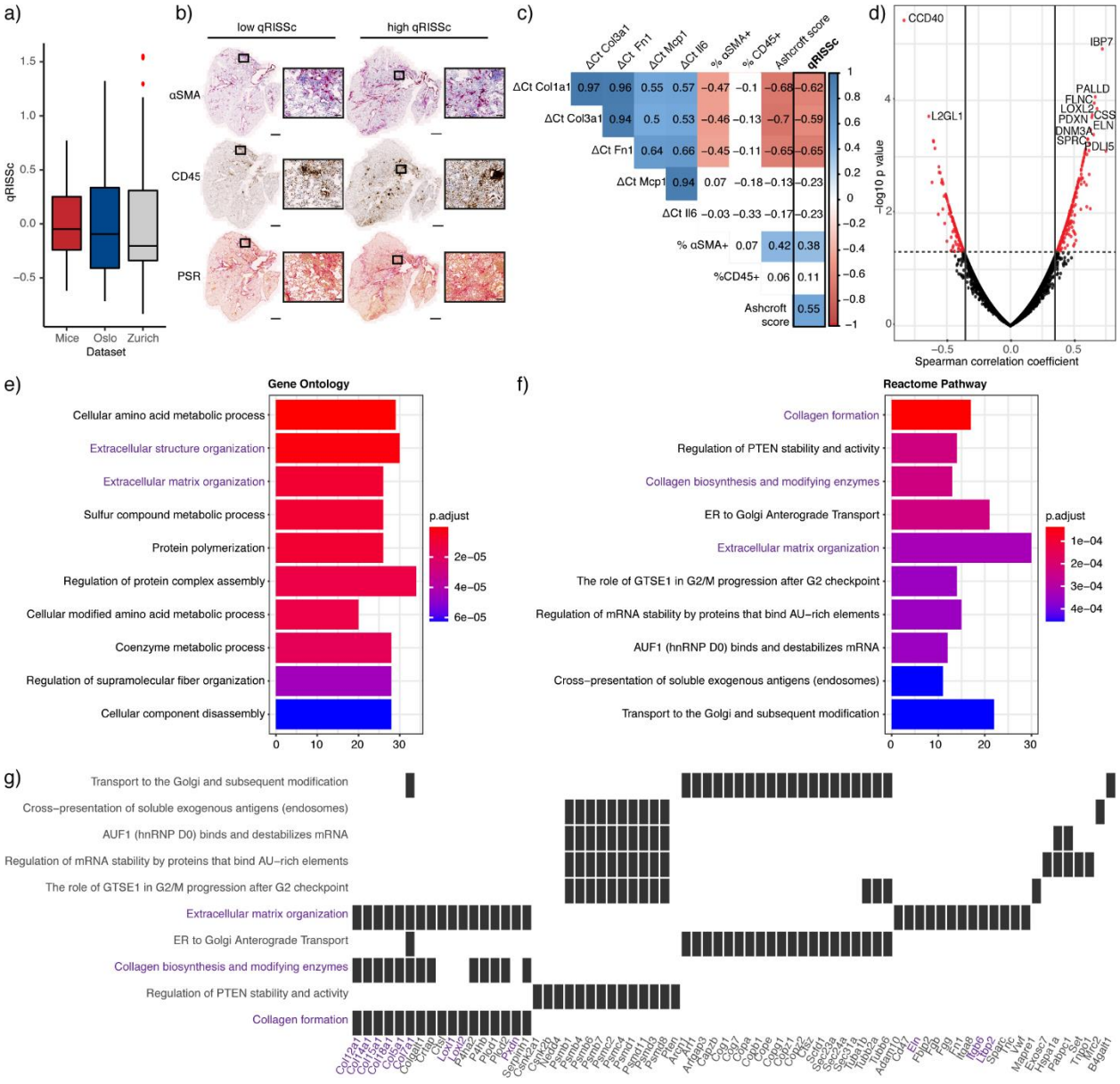

Figure 5: Correlation analysis of qRISSc with molecular data in experimental ILD. (**a**) Score distribution across the three datasets, demonstrating a similar qRISSc distribution between mice of the bleomycin-induced lung fibrosis model (*n*=30) and SSc-ILD patients (Zurich, *n*=75; Oslo, *n*=66). (**b**) Representative histological images of bleomycin-treated mice with low and high qRISSc that were stained for the myofibroblast marker alpha-smooth muscle actin (αSMA, upper panel), the pan-leukocyte marker CD45

(middle panel) and picrosirius red to visualize collagen fibres (PSR, collagen = red, lower panel). Sections of the entire right caudal lobe (scale bar = 1 mm) with higher magnification views (100x magnification, scale bar = 100 µm) are shown. (**c**) Correlation matrix for qRISSc with histological parameters (percentage of αSMA and CD45 positivity, and Ashcroft score), and messenger RNA (mRNA) expression of inflammatory (*Il6*, *Mcp1*) and fibrotic (*Col1a1*, *Col3a1*, *Fn1*) genes. A lower ΔCt value and thus negative correlation indicates higher gene expression. The Spearman correlation coefficient *rho* is shown. Non-significant associations are depicted in white. (**d**) Volcano plot for qRISSc-correlated proteins. Proteins with rho ≥ |0.3| and $p < 0.05$ are highlighted in red. (**e**) Bar plot of the top 10 (based on p-value) biological processes associated with qRISSc. (**f**) Bar plot of the top 10 (based on p-value) pathways associated with qRISSc. (**g**) Heatplot indicating the top enriched proteins per molecular pathway. For (**e-g**), the most important associations are highlighted in purple. For pathway analyses, only proteins with rho ≥ |0.3| and $p < 0.05$ were considered.ss

Data Supplement

Supplementary Methods

Patient Cohorts and Clinical Data

In this study, 90 patients (76.7% female, median age 57.5 years) from the University Hospital Zurich's (derivation cohort) and 66 patients (75.8% female, median age 61.0 years) from the Oslo University Hospital's prospective SSc patient cohorts (external validation cohort) were included. Both centres are part of the EUSTAR (European Scleroderma Trial and Research) network [1]. Patients were retrospectively selected based on the following criteria:

(1) Fulfilment of diagnosis of early/mild SSc according to the Very Early Diagnosis of Systemic Sclerosis (VEDOSS) criteria [2] or established disease according to the 2013 American College of Rheumatology//European league against rheumatism (ACR/EULAR) classification criteria [3],
(2) Presence of ILD on HRCT as determined by a senior radiologist, and
(3) Availability of an HRCT scan with the following settings:
    (a) Slice thickness between 0.6 and 3 mm,
    (b) One of the following lung kernels available (B60f, B70f, Bl64d, LUNG),
    (c) Filtered-back projection as reconstruction algorithm, and
    (d) CT image acquired in full inspiration.

For each patient, demographic and clinical parameters, including age, sex, SSc disease duration and subset, the extent of skin involvement, autoantibody status, CRP levels, presence of pulmonary hypertension according to right heart catheterisation or echocardiography as judged by the local investigators, and pulmonary function test (PFT) parameters were retrieved from the local patients' records. The recorded PFT parameters (expressed as % predicted values) included forced vital capacity (FVC), forced expiratory volume in 1 second (FEV1), and diffusing capacity for carbon monoxide (DLCO). Data from the 6-minute walk test (6-MWT), including walk distance, oxygen saturation (% SpO_2) before and after the test, and Borg scale of perceived exertion (Borg CR-10) [4], were only available for the derivation cohort. Disease duration of SSc was calculated as the difference between the date of first available CT and the date of manifestation of the first non-Raynaud's symptom. The follow-up period was defined as the time interval between the baseline visit and the last available follow-up visit for every patient. The mean follow-up time for the derivation cohort was 66.1 (± 30.1) months and 43.9 (± 30.9) months for the external validation cohort. All outcome events occurring in this period were considered in this study. As outcomes for SSc-ILD, we selected progression-free survival, which was defined as the time from the date of the HRCT to the date of the first occurrence of ILD progression. The primary endpoint for progression-free survival was the progression of ILD defined as a relative decline in FVC% predicted from baseline to follow-up of ≥ 15% based on the criteria recommended for idiopathic pulmonary fibrosis trials by the American Thoracic Society/European Respiratory Society and previous clinical trials in SSc-ILD [5–8]. As a secondary and exploratory endpoint, we used a recently proposed FVC-DLCO composite index, in which progression is defined as either

a relative decrease in FVC% predicted of ≥15% or a relative decline in FVC% predicted of ≥10% combined with DLCO% predicted of ≥15% [9]. As further exploratory and non-lung function-based outcome measures for SSc-ILD, we selected 1) visual ILD progression on HRCT and 2) overall survival, which were defined as the time from the date of the HRCT to the date of the first occurrence of visual ILD progression on HRCT or all-cause death, respectively.

The vital status was determined based on the electronic patients' records.

The local ethics committees approved the study (approval numbers: pre-BASEC-EK-839 (KEK-no.-2016-01515), KEK-ZH-no. 2010-158/5, BASEC-no. 2018-02165, BASEC-no. 2018-01873) and written informed consent was obtained from every patient.

Pulmonary Function Tests

In brief, spirometry, body plethysmography, and DLCO measurements were performed by trained technicians in the Department of Pneumology of the University Hospital Zurich and Oslo. Measures included, among others FVC, FEV1, TLC, VC, and DLCO. The PFTs were performed following established protocols [10–13]. Since the PFTs were performed as part of the routine diagnostics, the respective pulmonologist on call interpreted the results and provided a written report, including the measured values and their interpretation.

HRCT Image Acquisition and Visual CT Analysis

The settings used for the acquisition of HRCT images are summarized in Supplementary Table 9. All HRCT images were assessed for the presence of characteristic visual

features of ILD, including ground glass opacification (GGO), reticular changes, traction bronchiectasis, emphysema, and honeycombing. In addition, the radiological subtype (usual interstitial pneumonia (UIP), nonspecific interstitial pneumonia (NSIP), or diffuse interstitial pneumonia (DIP)) was determined. UIP includes the radiological diagnosis of both, “definite” and “probable” UIP [14, 15]. The extent of lung fibrosis was determined visually by the clinical radiologists in charge of routine diagnostics. All sections from the lung apex to the hemidiaphragm were assessed. All CT scans from both cohorts were re-evaluated by a long-standing expert on chest radiology (T.F.). The extent of lung fibrosis on HRCT, defined as the presence of reticular changes and/or honeycombing, was categorized as either <20% or ≥ 20% in relation to the total lung volume. For visual analysis of ILD progression on HRCT, all available follow-up HRCT scans from every patient were extracted from the electronic patient’s records. Due to the differences in the types of scanners and kernels used, ILD progression on HRCT was visually assessed by a senior radiologist and expert in chest radiology (T.F.). ILD progression was defined as an increase in ground-glass, reticulation or honeycombing including more than a second lobule or the transition of ground-glass into reticulation or honeycombing. All visual analyses were performed using a standard picture archiving and communication system workstation (Impax, Version 6.5.5.1033; Agfa-Gevaert, Mortsel, Belgium) and a high definition liquid crystal display monitor (BARCO; Medical Imaging Systems, Kortrijk, Belgium).

CT Segmentation and Extraction of Radiomic Features

The left and right lung lobes of each patient were semi-automatically segmented by two readers (J.S., M.B.) using the “region grow” function (lower threshold -950 HU, upper threshold: -300 HU) of MIM software (version 6.9.2, MIM Software Inc., Cleveland, Ohio, United States). Manual corrections were applied when computationally defined tissue borders did not coincide with the actual lung borders. In addition, pulmonary hilar vessels and atelectatic lung areas were carefully excluded from the regions of interest.

Radiomic analysis was performed on merged structures of both lung lobes using the in-house developed software Z-Rad based on Python programming language 2.7. For radiomics analysis, CT images were resized to isotropic voxels of 2.75 mm and discretized to a fixed bin size of 50 HU. In total, 1,386 radiomic features were calculated per lung (HU limits: -1000 HU to 200 HU), corresponding to the following radiomic feature classes:

(1) Intensity or histogram features (*n* = 17),

(2) Texture features (*n* = 137) of the *Gray Level Co-occurrence Matrix* (*n* = 52; GLCM), the *Neighborhood Gray Tone Difference Matrix* (*n* = 5; NGTDM), the *Gray Level Run Length Matrix* (*n* = 32); GLRLM), the *Gray Level Size Zone Matrix* (*n* = 16; GLSZM), the *Gray Level Distance Matrix* (*n* = 16; GLDZM) and the *Neighboring Gray Level Dependence Matrix* (*n* = 16; NGLDM), and

(3) Wavelet features (*n* = 1,232).

The first class of radiomic features relates to the histogram or distribution of voxel intensities using first-order statistics (e.g. mean, standard deviation, skewness and kurtosis) and quantifies tissue intensity characteristics. The second category, including the texture features, describes the intra-tissue heterogeneity by calculating the statistical, spatial inter-relationship between neighbouring voxel intensities [16]. The third group of features, the wavelet features, calculates the intensity and texture features after wavelet decompositions of the original image using eight different coiflet filters (high-pass to low-pass filters), thereby focusing the features on different frequency ranges [17].

A list of all radiomic features is provided in Supplementary File 1. Radiomic feature definitions were based on the Imaging Biomarker Standardization Initiative report by Zwanenburg *et al. [18]*.

Assessment of Radiomic Feature Stability

Intraclass correlation (ICC) analysis was performed to assess the stability of radiomic features against intra- and inter-operator variability in the semi-automated segmentation process (Supplementary Figure 1). For inter-operator ICC analysis, three examiners (J.S., M.B., C.B.), and for intra-operator ICC analysis, one examiner (J.S.) twice, independently contoured 15 randomly selected SSc patients from the derivation (Zurich) cohort, and radiomic features were extracted from the multiple delineation structures. The ICC coefficient for every radiomic feature was quantified using two-way mixed effect models and applying the “consistency” method (ICC(3,1)) according to [19] using “irr” package of

R. Only features with good reproducibility defined as ICC ≥ 0.75 [20] were considered in further analyses.

Unsupervised Clustering

Unsupervised clustering was performed to identify groups of patients with similar radiomic feature patterns in the derivation cohort (Zurich; n=90). After confirmation of data clusterability by visual assessment of cluster tendency (VAT) and calculation of the Hopkin's statistic *H* (with *H* > 0.5 indicating clusterability) [21], the *k*-Means clustering algorithm [22] was applied to the z-scored radiomic data. Only robust radiomic features (ICC ≥ 0.75) entered the cluster analyses. The optimal number of clusters was determined by varying the number of k-clusters between 2 and 10 and selecting the optimal k concerning best visual separation and stability as determined by Jaccard bootstrapping (n = 1,000 iterations).

Building a Quantitative Radiomic Risk Score for SSc-ILD

The Zurich cohort was used as a derivation cohort to build and train the radiomic risk score for ILD progression (qRISSc). Patients with no follow-up and survival data available on the electronic patients' records were excluded from the analysis, resulting in a final dataset of 75 patients. For score building, we adapted a recently described approach by Lu et al. [23] for *z*-scored, radiomic features. Following Lu and colleagues, we selected radiomic features in two steps: 1) Cox regression and 2) penalized LASSO regression using "cox" family with 10-fold cross-validation. In the first step, we applied univariate Cox regression per radiomic feature only considering features with FDR of $p<0.005$. Features

selected in step 1) underwent further reduction by LASSO. Only features with non-zero coefficients were retained, thereby removing strongly inter-correlated, redundant features. Since limited by the modest sample size of the derivation cohort, we did not perform weighting of score features according to the coefficients from LASSO regression and assigned the same importance to each feature by dividing each standardized feature by the total number of features *j.* The final radiomic score was constructed as follows: $qRISSc = \sum_{i=1}^{j} \alpha_i f_i$ with $\alpha = \frac{1}{j}$ being the feature weight and *f* being the values of *z*-transformed radiomic features.

After having selected features in steps 1) and 2) we searched for the significant cut-off value for Cox regression by applying the “cox” function from the “cutoff” package of R. Due to the modest sample size, we searched for two groups, i.e. “low” and “high” risk patients composed of at least 25% of subjects for the minority group. We selected the one that was significant after correction for multiple testing from the proposed pairs of cut-offs. Once a score was built, we fitted a univariate Cox regression model on the external validation cohort (Oslo). Kaplan-Meier plots were used to visualize the Cox regression results. As a reference model to qRISSc, we analogously build a radiomic score composed only of less complex, first-order densitometric (intensity) features, which have been previously explored for the quantification of disease extent and progression of SSc-ILD [24–27].

Multivariable Cox regression analyses were applied to analyse the predictive ability of conventional risk factors and qRISSc for progressive ILD in the pooled cohorts (n=156). Ten events per variable were required in the multivariable analyses, and the variables were selected based on literature evidence and expert opinion [28–30]. We reported the

concordance index (C-index) as the general assessment of the quality of the model, the p-value of the whole model, and the hazard ratio (HR) with 95% confidence intervals for the quantitative radiomic risk score. The C-index is equivalent to the area under the curve in ROC analysis and can also be used in Cox regression analysis [31].

Association Analyses with Clinical Characteristics

Association analyses were performed to explore associations of identified patient groups (*k*-Means clusters and risk groups) with clinical parameters.

Fisher's exact test was used to compare categorical, and Mann-Whitney U for comparison of continuous clinical variables, respectively.

Association Analyses with Biological Data

To reveal possible associations of the radiomic risk score with the underlying pathophysiology of ILD, correlation analysis with histological, proteomics and quantitative PCR data was performed. Since lung biopsies are only very rarely performed in SSc-ILD and thus matched patient tissue samples have not been available for molecular analyses, we conducted a cross-species correlation approach, using the mouse model of bleomycin-induced lung fibrosis as a model system for SSc-ILD. For this animal model, we have recently confirmed the transferability of radiomics signatures between mice and humans [32].

Animal Model of Experimental ILD

We applied the well-established preclinical model of bleomycin-induced lung fibrosis to model human SSc-ILD as described previously [33, 34]. In brief, 30 female, 8-week-old C57BL/6J-rj (Janvier Labs, Le Genest-Saint-Isle, France) were randomized and intratracheally instilled with 2 U/kg bleomycin sulfate (BLM, Baxter 15,000 I.U., pharmacy of the canton Zurich, Switzerland) to induce ILD. For molecular and histological analyses, mice were sacrificed with carbon dioxide and subsequently transcardially perfused with ice-cold phosphate-buffered saline (PBS) solution to remove residual blood. All animal experiments were approved by the cantonal veterinary office (approval number ZH235-2018) and performed in strict compliance with the Swiss law for animal protection.

Proteomic Data

For proteomic analyses, frozen left lung lobes (blood-free) collected from PBS-perfused BLM-treated mice were homogenized in 8M urea/100mM Tris (pH 8.0) buffer supplemented with protease inhibitors using the FastPrep system (MP Biomedicals). After reduction and alkylation, and overnight protein precipitation with ice-cold acetone, 10 ug of the cleaned protein mixture were digested into peptides using a two-step digestion protocol (LysC for 2 h at 37 °C followed by Trypsin at room temperature overnight) and then subjected to liquid-chromatography-based tandem mass spectrometric analysis (LC-MS/MS). For LC-MS/MS, mouse samples were randomly allocated to the analysis by loading 800 ng onto a pre-column (C18 PepMap 100, 5 µm, 100 A, 300 µm i.d. x 5 mm length) at a flow rate of 50µL/min with solvent C (0.05% TFA in water/acetonitrile 98:2).

After loading, peptides were eluted in backflush mode onto a home packed analytical Nano-column (Reprosil Pur C18-AQ, 1.9 µm, 120 A, 0.075 mm i.d. x 500 mm length) using an acetonitrile gradient of 5% to 40% solvent B (0.1% Formic Acid in water/acetonitrile 4,9:95) in 180 min at a flow rate of 250 nL/min. The column effluent was directly coupled to a Fusion LUMOS mass spectrometer (Thermo Fisher, Bremen; Germany) via a nano-spray ESI source. Data acquisition was done in data-dependent mode with precursor ion scans recorded in the orbitrap with a resolution of 120’000 (at m/z=250) parallel to top speed HCD fragment spectra of the most intense precursor ions in the Linear trap for a cycle time of 3 seconds. Mass spectrometry data were processed by MaxQuant software, and set parameters are available in Supplementary Table 10. MaxQuant experimental design was such that the two repeated injections were combined, and match between runs allowed between all samples.

Histological and Immunohistochemical Data

Formalin-fixed paraffin-embedded lung sections (4 µm thick) from all BLM-treated mice were stained with Hematoxylin and Eosin (HE) for the examination of the overall tissue architecture, and the presence of cellular infiltrates and stained with Picrosirius Red (PSR) to visualize collagen deposition using standard protocols. Furthermore, specific immunohistochemical stainings for the pan-leukocyte marker CD45 and the myofibroblast marker alpha-smooth muscle actin (αSMA) were performed as described in [33, 34]. Whole slide images of histological and immunohistological stainings were obtained with the AxioScan.Z1 slide scanner (Zeiss, Feldbach, Switzerland) in bright-field mode using a Plan-Apochromat 20x/0.8 M27 objective. Stainings were automatically quantified on

whole slide images using the open-source Orbit Image Analysis software (License: GPLv3; Actelion Pharmaceuticals Ltd) as described in [35, 36]. Furthermore, for histopathological scoring of pulmonary fibrosis, the Ashcroft score [37] was applied on PSR stained lung sections by two experienced blinded examiners (J.S., M.B.) as previously described [38].

Gene Expression Data

Total RNA was isolated from perfused cranial lobes of the right mouse lung with the RNeasy Tissue Mini Kit from Qiagen (Hombrechtikon, Switzerland), reverse-transcribed into complementary DNA, and messenger RNA (mRNA) expressions of inflammatory (*Il6*, *Mcp1*) and fibrotic (*Col1a1*, *Col3a1*, *Fn1*) genes were analyzed by SYBR Green quantitative real-time PCR as described in [33]. mRNA expression was expressed as ΔCt values (Ct (gene-of-interest) - Ct (reference gene)) with 60S acidic ribosomal protein P0 (*Rplp0*) as a reference gene, with a lower ΔCt indicating higher target gene expression. A list of primers used in this study is provided in Supplementary Table 11.

Micro-CT imaging, Radiomics Analysis and Score Calculation in Mice

CT images were acquired in free-breathing mice with prospective respiratory gating on a state-of-the-art micro-CT scanner (Skyscan 1176; Bruker-microCT, Kontich, Belgium) under isoflurane anaesthesia at the following time points: day 0, 7, 14, 21, 28, and 35. The following scan parameters were used: tube voltage 50 kV, tube current 500 µA, filter AI 0.5 mm, averaging (frames) 3, rotation step 0.7 degrees, sync with event 50 ms, X-ray tube rotation 360 degrees, resolution 35 µm, and slice thickness 35 µm. Images were reconstructed with NRecon reconstruction software (v.1.7.4.6; Bruker) using the built-in

filtered-back projection Feldkamp algorithm and applying misalignment compensation, ring artefact reduction, and a beam hardening correction of 10% to the images.

Analogous to the radiomics analysis in patients, mouse lungs were segmented, resized to isotropic voxels (150 µm) and discretized to a fixed bin size of 50 HU, and all 1,386 radiomic features were extracted (HU limits: -1000 HU to 200 HU).

The Hounsfield units depend on the tube voltage, and the Hounsfield scale is normalized for 120 keV for patient diagnostics. Our microCT scanner allows a maximum tube voltage of 80keV. Thus, the Hounsfield units can be transferred to a limited extent. We addressed this by post-processing the microCT scans to adjust the pixel values to match the human patient data. This has been done by plotting the intensity histograms of several mice and patients from the Zurich cohort with the subsequent estimation of optimal parameters for linear transformation based on visual assessment. Specifically, the intercept value has been changed from -1000 to -1024, whereas the slope was changed from 1.0 to 0.6. These parameters were applied to all microCT scans. The choice of 2.75 mm voxel size in patients was dictated by the voxel size in mice and the difference in lung size between mice and humans. Since the voxel size in mice was 0.15 mm and the total lung capacity in humans was estimated to be 6000x greater than in mice [39], a comparable voxel size in patients was set to 2.75 mm.

For calculating the quantitative radiomic ILD risk score, the respective radiomic features were z-transformed and summed up as for patients.

Correlation Analysis and Pathway Enrichment Analysis

Spearman's rank correlation coefficient *rho* was calculated between the quantitative radiomic ILD risk score and the different biological features for correlation analysis with established inflammatory and fibrotic markers on the tissue level.

For pathway enrichment analyses, *rho* was calculated between qRISSc and the LFQ intensity value of every protein identified in at least 50% of mice in the proteomics analyses, and only proteins with $p < 0.05$ and $rho \geq |0.3|$ entered further analyses. The resulting list of proteins, and their coding genes, were used as input for the pathway analysis using the 'ClusterProfiler' package of Bioconductor. Protein names were converted to gene IDs using the UniProt mapping tool (https://www.uniprot.org/uploadlists/). We investigated pathway enrichment searching against "Reactome" and "GO Biological Process" databases and retained results after adjustment ($p < 0.05$).

Statistical Analyses

All statistical analyses were conducted in R using the following packages: "ggplot2", "tidyverse", "ggsci", "corrplot", "readxl", "clusterSim", "dplyr", "readxl", "survival", "glmnet", "cutoff", "survminer", "cluster", "fpc", "factoextra", "clustvarsel", "clustertend". For all analyses, a p-value of < 0.05 was considered statistically significant.

Supplementary Figures

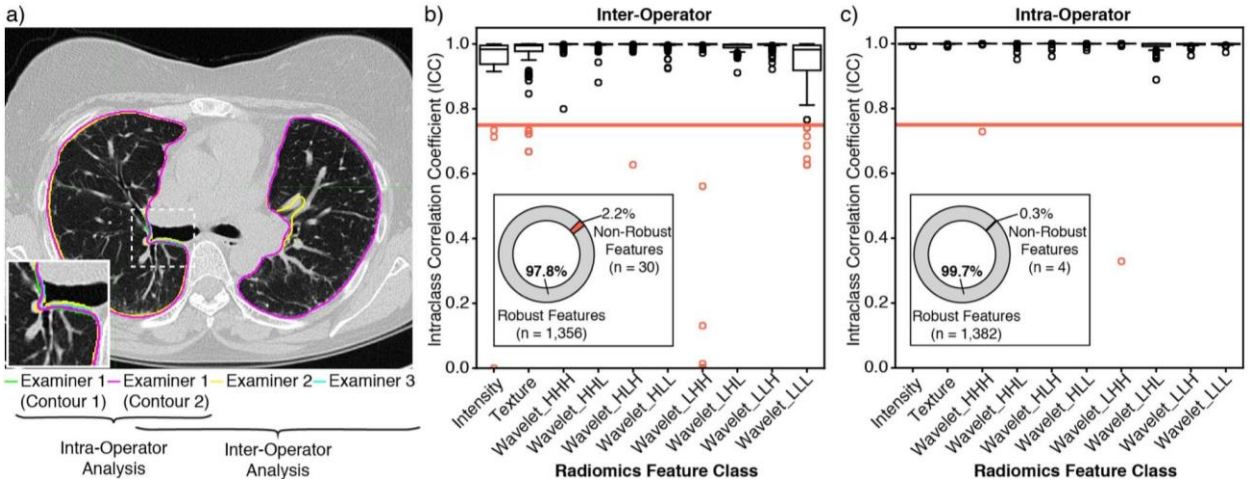

Supplementary Figure 1: Assessment of radiomic feature robustness against inter-and intra-operator variability in the semi-automated lung segmentation process. (a) Representative transversal HRCT image showing excellent agreement and overlap in the semi-automatically delineated lung structures of the three different examiners (examiner 1: green and magenta, examiner 2: yellow, examiner 3: cyan) for the intra- and inter-operator ICC analyses. This confirmed the reproducibility and validity of our lung segmentation protocol. (**b**) Boxplots showing the distribution of the ICC coefficient per radiomic feature category for inter-operator ICC analysis and (**c**) intra-operator ICC analysis. In (b, c), the bright red line indicates the threshold defined for the ICC analyses (ICC = 0.75; corresponding to good reproducibility [20]). The pie charts summarize the respective percentage and total numbers of robust (ICC ≥ 0.75) and non-robust (ICC < 0.75) radiomic features.

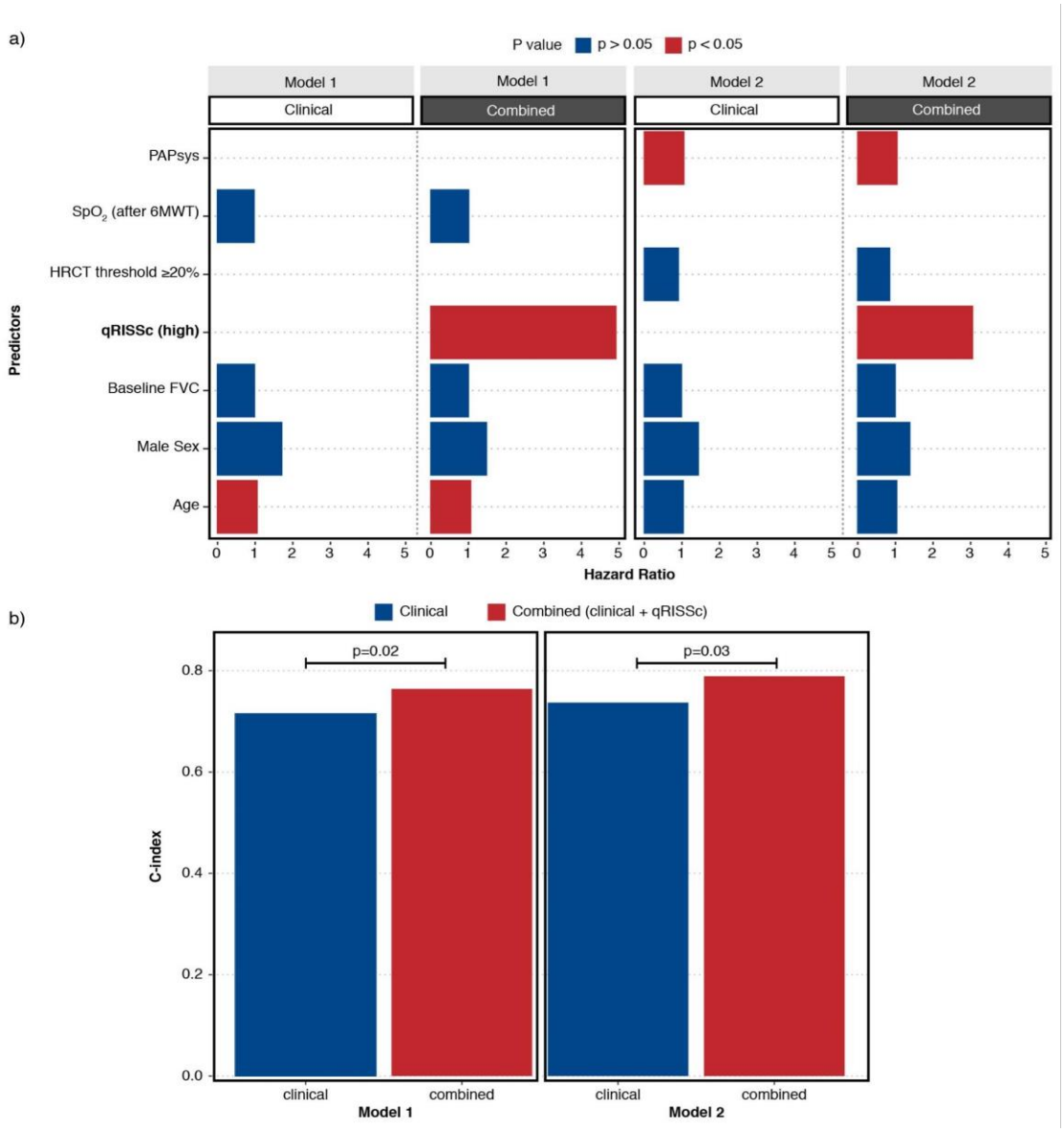

Supplementary Figure 2. Prognostic performance of qRISSc compared to other SSc-ILD risk factors. (**a**) Bar plot indicating the results of the multivariable Cox regression analysis incorporating qRISSc (combined models) versus multivariable models composed of clinical risk factors alone (clinical model). Bars represent hazard radios for each predictor in each model, whereas colours indicate the nominal p-value of the predictors. Covariates for Cox regression were selected based on literature evidence [29] and expert opinion. Due to missing data for the systolic pulmonary artery pressure *(*PAPsys, in mmHg) and the oxygen saturation at the end of the 6-min walk test (SpO_2 after 6MWT, in percent) in the validation cohort from Oslo, we only fitted the multivariable models on the derivation cohort from Zurich. (**b**) Bar plot comparing the predictive power (C-index) of multivariable models composed of clinical risk factors of SSc-ILD progression alone (clinical models) versus models also incorporating qRISSc (combined models). Two-way ANOVA was used to compare model performances.

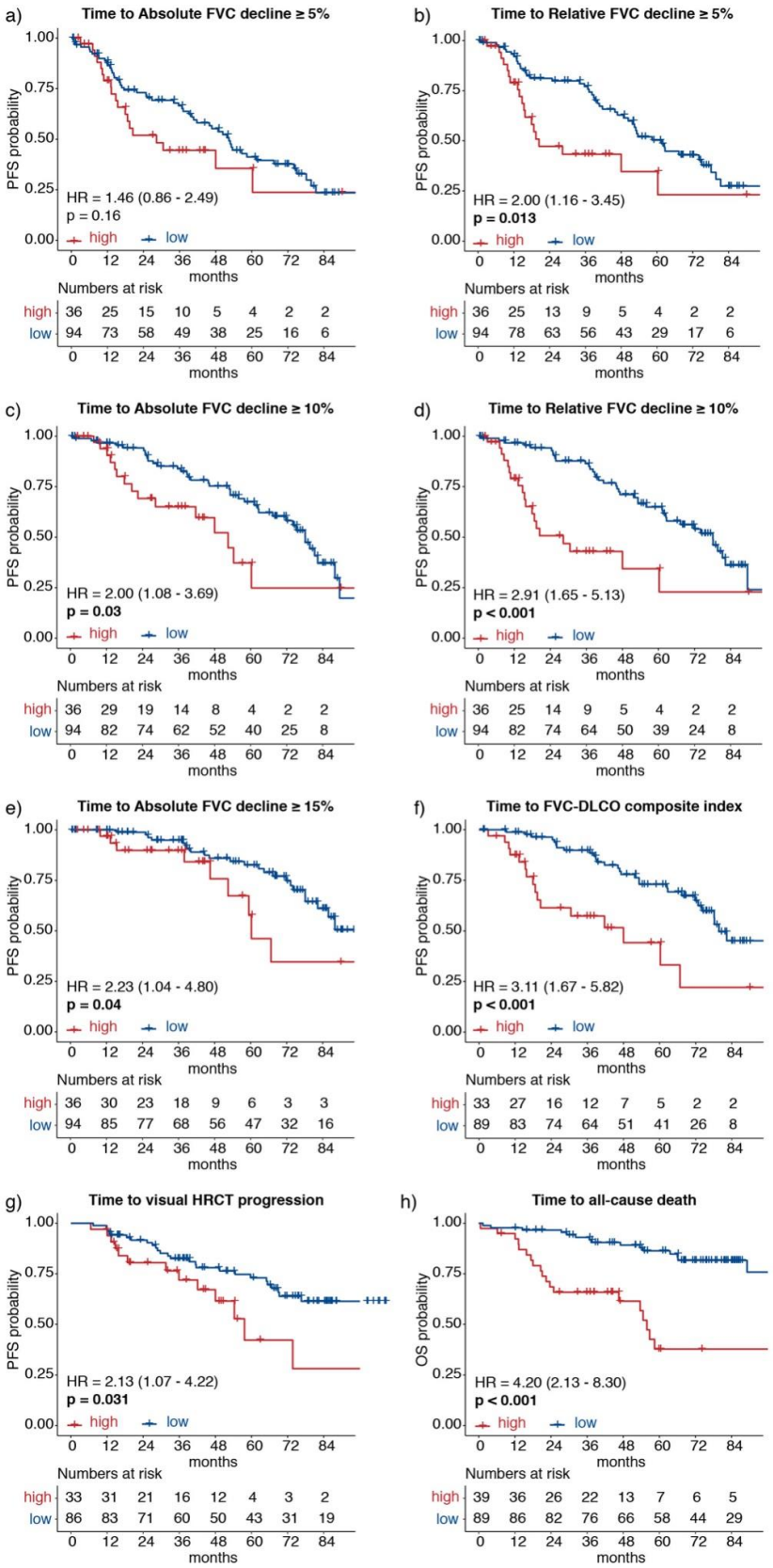

Supplementary Figure 3: Associations of qRISSc-stratified patient groups with different clinical

outcomes. Kaplan Meier curves for progression-free survival (PFS) defined as the time to (**a**) an absolute decline of FVC predicted ≥ 5%, (**b**) a relative decline of FVC predicted ≥ 5%, (**c**) an absolute decline of FVC predicted ≥ 10%, (**d**) a relative decline of FVC predicted ≥ 10%, (**e**) an absolute decline of FVC predicted ≥ 15%, (**f**) the time to the FVC-DLCO composite index (= relative decrease in FVC% predicted of ≥15% or a relative decline in FVC% predicted of ≥10% combined with DLCO% predicted of ≥15% according to [9]), or (**g**) the time to the visual ILD progression on HRCT. (**h**) Kaplan Meier curves for overall survival (OS) defined as the time to all-cause death. The Hazard ratios (HR) with 95% confidence intervals and p-value of the univariate Cox regression for the combined study cohorts are shown.

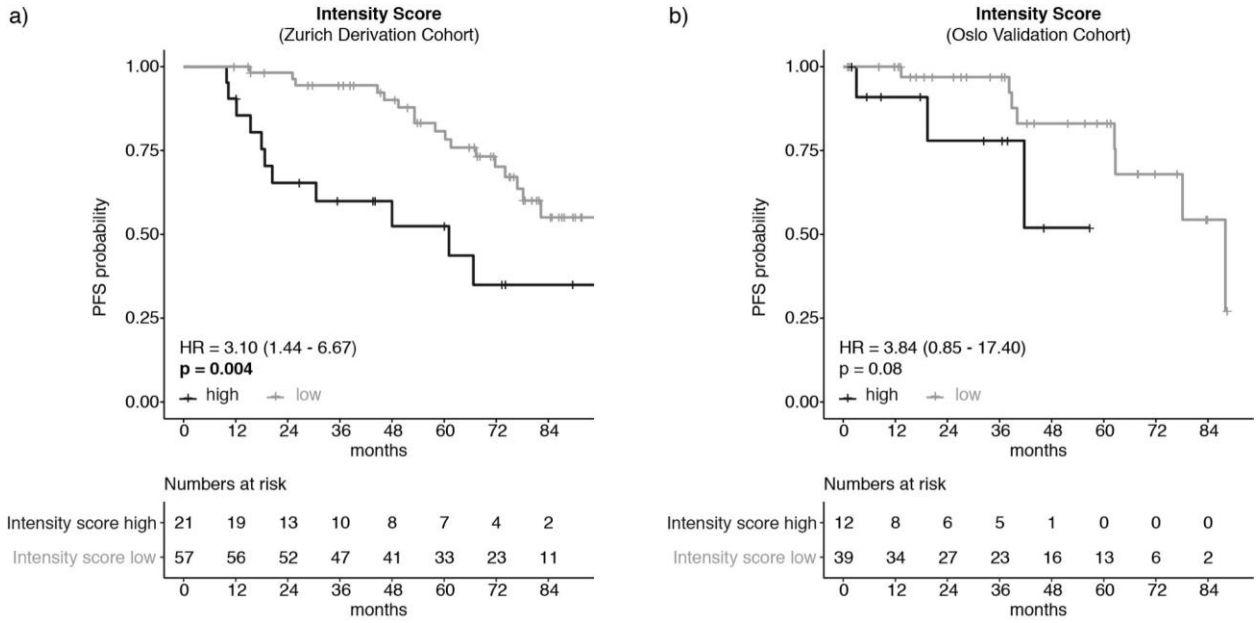

Supplementary Figure 4: Assessment of the prognostic potential of a quantitative radiomics score that is only composed of less complex, first-order intensity features. Kaplan Meier curves of the constructed intensity score for progression-free survival (PFS) defined as the time to relative FVC decline ≥ 15% in (**a**) the derivation cohort from Zurich and (**b**) in the external validation cohort from Oslo. The Hazard ratios (HR) with 95% confidence intervals and p-values of the univariate Cox regression are shown. The intensity score was statistically constructed analogously to qRISSc yet only taking first-order intensity features instead of all radiomic features into consideration.

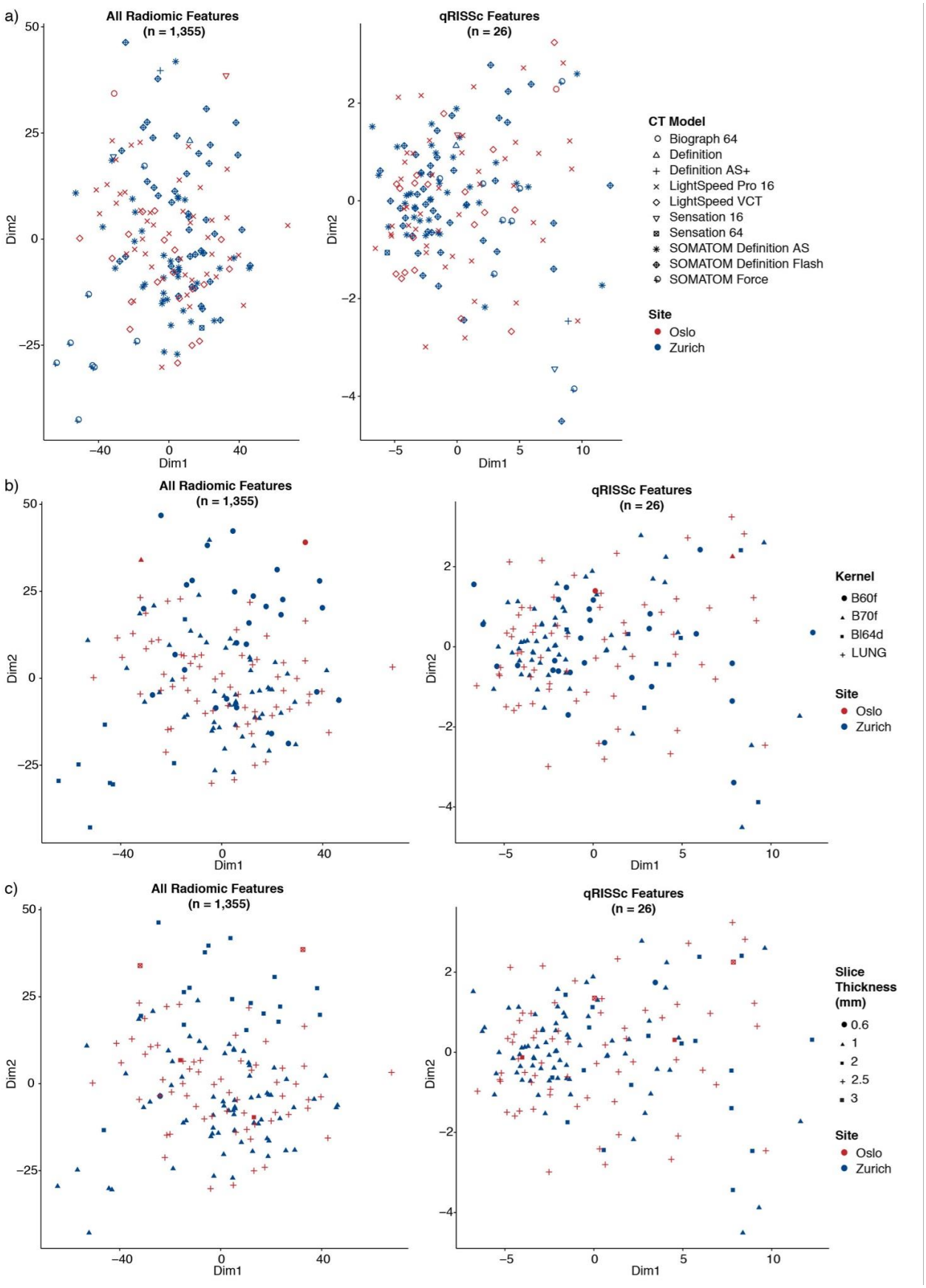
a)
All Radiomic Features
(n = 1,355)
qRISSc Features
(n = 26)
Dim1
Dim2
CT Model
Biograph 64
Definition
Definition AS+
LightSpeed Pro 16
LightSpeed VCT
Sensation 16
Sensation 64
SOMATOM Definition AS
SOMATOM Definition Flash
SOMATOM Force
Site
Oslo
Zurich
b)
All Radiomic Features
(n = 1,355)
qRISSc Features
(n = 26)
Kernel
B60f
B70f
Bl64d
LUNG
Site
Oslo
Zurich
c)
All Radiomic Features
(n = 1,355)
qRISSc Features
(n = 26)
Slice Thickness (mm)
0.6
1
2
2.5
3
Site
Oslo
Zurich

Supplementary Figure 5: Impact of different CT image acquisition and reconstruction settings on radiomic feature values and qRISSc.
Multidimensional scaling of *z*-transformed radiomic profiles of all robust radiomic features (left panel) or only qRISSc features (right panel) combined for all SSc-ILD patients from the Zurich (*n* = 90) and Oslo cohort (*n* = 66) for (**a**) the different CT scanner types, (**b**) different lung reconstruction kernels, and (**c**) different slice thicknesses.

Supplementary Tables

Supplementary Table 1: Associations of the identified patients' clusters based on their radiomic profile with clinical parameters for the Zurich cohort. Continuous variables are described as median ± interquartile range, and categorical variables are presented as absolute values with relative frequencies (percent). P-values of univariate comparisons of baseline characteristics between the two clusters are shown. Fisher's exact test was used to compare categorical, and Mann-Whitney U to compare continuous variables, respectively. *Abbreviations: UIP = usual interstitial pneumonia, NSIP = nonspecific interstitial pneumonia, DIP = diffuse interstitial pneumonia, PAPsys = systolic pulmonary artery pressure, FVC = forced vital capacity, FEV1 = forced expiratory volume in 1 second, DLCO = diffusing capacity for carbon monoxide, 6-MWT = 6-min walk test, CRP = C-reactive protein*

Characteristics	**Cluster 1** (n=59)	**Cluster 2** (n=31)	**P-value**
Age (years)	58.0 ± 17.0	57.0 ± 16.9	0.693
Sex			
Male	14 (23.7%)	7 (22.6%)	1.000
Female	45 (76.3%)	24 (77.4%)	
SSc disease duration (years)*	5.0 ± 8.0	4.3 ± 8.3	0.507
SSc subset (LeRoy 1988)			
Limited cutaneous SSc	30 (50.8%)	11 (35.5%)	0.234
Diffuse cutaneous SSc	26 (44.1%)	16 (51.6%)	
No skin involvement	3 (5.1%)	4 (12.9%)	
Skin involvement			
Limited cutaneous	20 (33.9%)	11 (35.5%)	0.224
Diffuse cutaneous	27 (45.8%)	16 (51.6%)	
No skin involvement	5 (8.5%)	4 (12.9%)	
Only sclerodactyly	7 (11.9%)	0 (0.0%)	
Autoantibodies			
Anti-centromere positive	10 (16.9%)	3 (9.7%)	0.530
Anti-topoisomerase I positive	28 (47.5%)	13 (41.9%)	0.661
Anti-RNA polymerase III positive	4 (6.8%)	3 (9.7%)	0.602
Anti-PMScl positive	14 (23.7%)	4 (12.9%)	0.496
FVC (% predicted)	97.0 ± 26.0	65.5 ± 22.2	
FVC ≥70% predicted	54 (91.5%)	10 (32.3%)	**<0.001**
FVC <70% predicted	4 (6.8%)	20 (64.5%)	
DLCO (% predicted)	75.0 ± 24.0	48.0 ± 25.5	**<0.001**
FEV1 (% predicted)	95.8 ± 19.0	65.5 ± 25.5	**<0.001**
Pulmonary hypertension†	7 (11.9%)	13 (41.9%)	**0.001**
PAPsys (mmHg)‡	25.0 ± 7.0	32.0 ± 18.0	**<0.001**
CRP (mg/l)	2.4 ± 5.6	4.2 ± 6.1	0.071
6 min walk distance (m)	543.5 ± 109.2	407.0 ± 173.0	**<0.001**
SpO_2 before 6-MWT (%)	97.0 ± 1.2	96.0 ± 3.0	**0.011**
SpO_2 after 6-MWT (%)	96.0 ± 3.0	88.5 ± 9.8	**<0.001**
Borg scale (unit; range 0-10)	2.0 ± 2.0	4.0 ± 3.0	**<0.001**

Extent of lung fibrosis on CT			
<20%	40 (67.8%)	10 (32.3%)	**0.002**
≥20%	19 (32.2%)	21 (67.7%)	
Ground glass opacification	30 (50.8%)	15 (48.4%)	1.000
Reticular changes	58 (98.3%)	29 (93.5%)	0.272
Traction bronchiectasis	30 (50.8%)	20 (64.5%)	0.267
Honeycombing	9 (15.3%)	13 (41.9%)	**0.009**
Bullae	1 (1.7%)	2 (6.5%)	0.272
Radiological subtype			
NSIP	33 (55.9%)	16 (51.6%)	0.662
UIP[#]	24 (40.7%)	13 (41.9%)	
DIP	0 (0.0%)	1 (3.2%)	
Unclassifiable	2 (3.4%)	1 (3.2%)	
Immunomodulatory therapy[§]	29 (49.2%)	22 (71.0%)	0.073
Smoking status			
Never	35 (59.3%)	20 (64.5%)	0.868
Former	14 (23.7%)	7 (22.6%)	
Current	9 (15.3%)	3 (9.7%)	

*Disease duration of SSc was calculated as the difference between the date of baseline CT and the date of manifestation of the first non-Raynaud's symptom.

†Pulmonary hypertension was assessed by echocardiography or right heart catheterisation.

‡PAPsys was determined by right heart catheterisation.

#UIP includes the radiological diagnosis of both, "definite" and "probable" UIP.

§Immunomodulatory therapy included prednisone, methotrexate, rituximab, cyclophosphamide, mycophenolate mofetil, hydroxychloroquine, tocilizumab, imatinib, azathioprine, adalimumab, leflunomid, cyclosporine.

Supplementary Table 2: Radiomic features used to construct the quantitative radiomic risk score for SSc-ILD (qRISSc). A complete list of all radiomics features, including standardized feature names is provided in Supplementary File 1. *Abbreviations: GLCM = Gray Level Co-occurrence Matrix, NGTDM = Neighborhood Gray Tone Difference Matrix, GLRLM = Gray Level Run Length Matrix, GLDZM = Gray Level Distance Matrix and NGLDM = Neighboring Gray Level Dependence Matrix*

Feature ID	Feature Name	Feature Class	Feature Subclass	Wavelet Filter	LASSO Coeff.
V3	COV	Intensity	Intensity	Unfiltered	15.14
V10	iqr	Intensity	Intensity	Unfiltered	14.41
V12	mad	Intensity	Intensity	Unfiltered	17.86
V13	rmad	Intensity	Intensity	Unfiltered	-42.79
V26	variance	Texture	GLCM	Unfiltered	-11.36
V29	sum_variance	Texture	GLCM	Unfiltered	0.01
V40	autocorrelation	Texture	GLCM	Unfiltered	-5.41
V41	clust_tendency	Texture	GLCM	Unfiltered	11.66
V66	M_autocorrelation	Texture	mGLCM	Unfiltered	-0.29
V84	len_sshge	Texture	GLRLM	Unfiltered	-9.68
V86	len_lshge	Texture	GLRLM	Unfiltered	-19.25
V102	M_len_lshge	Texture	mGLRLM	Unfiltered	-0.0024
V146	NGLDM_hgse	Texture	NGLDM	Unfiltered	59.55
V588	GLDZM_sizeVar_n.3	Wavelet	GLDZM	HLH	-0.3
V641	idiff_n.4	Wavelet	GLCM	HLL	1.84
V665	M_homogenity_n.4	Wavelet	mGLCM	HLL	-2.79
V686	coarseness.4	Wavelet	NGTDM	HLL	0.96
V687	neighContrast.4	Wavelet	NGTDM	HLL	0.03
V840	coarseness.5	Wavelet	NGTDM	LHH	-0.83
V994	coarseness.6	Wavelet	NGTDM	LHL	1.03
V998	strength6	Wavelet	NGTDM	LHL	1.26
V1082	skewness.7	Wavelet	Intensity	LLH	1.55
V1235	COV.8	Wavelet	Intensity	LLL	6.6
V1236	skewness.8	Wavelet	Intensity	LLL	8.6
V1242	iqr.8	Wavelet	Intensity	LLL	16.99
V1302	coarseness.8	Wavelet	NGTDM	LLL	0.38

Supplementary Table 3: Associations of the patients' risk groups based on qRISSc with clinical parameters for the derivation (Zurich) dataset. Continuous variables are described as median ± interquartile range, and categorical variables are presented as absolute values with relative frequencies (percent). P-values of univariate comparisons of baseline characteristics between the two risk groups are shown. Fisher's exact test was used to compare categorical, and Mann-Whitney U to compare continuous variables, respectively. *Abbreviations: UIP = usual interstitial pneumonia, NSIP = nonspecific interstitial pneumonia, DIP = diffuse interstitial pneumonia, PAPsys = systolic pulmonary artery pressure, FVC = forced vital capacity, FEV1 = forced expiratory volume in 1 second, DLCO = diffusing capacity for carbon monoxide, 6-MWT = 6-min walk test, CRP = C-reactive protein*

Characteristics	**Low risk** (n=54)	**High risk** (n=21)	**P-value**
Age (years)	56.5 ± 16.8	56.0 ± 18.0	0.939
Sex			
Male	14 (25.9%)	5 (23.8%)	1.000
Female	40 (74.1%)	16 (76.2%)	
SSc disease duration (years)*	4.3 ± 6.6	5.0 ± 9.3	0.915
SSc subset (LeRoy 1988)			
Limited cutaneous SSc	27 (50.0%)	9 (42.9%)	
Diffuse cutaneous SSc	23 (42.6%)	10 (47.6%)	0.797
No skin involvement	4 (7.4%)	2 (9.5%)	
Skin involvement			
Limited cutaneous	18 (33.3%)	9 (42.9%)	
Diffuse cutaneous	24 (44.4%)	10 (47.6%)	0.481
No skin involvement	6 (11.1%)	2 (9.5%)	
Only sclerodactyly	6 (11.1%)	0 (0.0%)	
Autoantibodies			
Anti-Centromere positive	12 (22.2%)	0 (0.0%)	**0.016**
Anti-Topoisomerase I positive	28 (51.9%)	9 (42.9%)	0.609
Anti-RNA polymerase III positive	3 (5.6%)	3 (14.3%)	0.343
Anti-PMScl positive	12 (22.2%)	4 (19.0%)	1.000
FVC (% predicted)	97.4 ± 28.5	65.0 ± 18.0	
FVC ≥70% predicted	48 (88.9%)	6 (28.6%)	**<0.001**
FVC <70% predicted	6 (11.1%)	15 (71.4%)	
DLCO (% predicted)	74.4 ± 24.2	51.0 ± 25.0	**<0.001**
FEV1 (% predicted)	95.8 ± 21.0	65.0 ± 27.0	**<0.001**
Pulmonary hypertension†	3 (5.6%)	10 (47.6%)	**<0.001**
PAPsys (mmHg)‡	24.0 ± 7.0	31.0 ± 12.5	**<0.001**
CRP (mg/l)	2.4 ± 5.4	6.1 ± 6.8	**0.006**
6 min walk distance (m)	543.0 ± 118.0	421.0 ± 126.5	**<0.001**
SpO_2 before 6MWT (%)	97.0 ± 1.0	96.0 ± 3.2	0.087
SpO_2 after 6MWT (%)	96.0 ± 3.0	85.5 ± 5.2	**<0.001**
Borg (unit; range 0-10)	2.0 ± 2.0	5.5 ± 3.2	**<0.001**
Extent of lung fibrosis on CT			
<20%	40 (74.1%)	5 (23.8%)	**<0.001**

≥20%	14 (25.9%)	16 (76.2%)	
Ground glass opacification	25 (46.3%)	11 (52.4%)	0.797
Reticular changes	52 (96.3%)	20 (95.2%)	1.000
Traction bronchiectasis	21 (38.9%)	17 (81.0%)	**0.002**
Honeycombing	5 (9.3%)	11 (52.4%)	**<0.001**
Bullae	2 (3.7%)	1 (4.8%)	1.000
Radiological subtype			
NSIP	29 (53.7%)	12 (57.1%)	**0.461**
UIP[#]	23 (42.6%)	8 (38.1%)	
DIP	0 (0.0%)	1 (4.8%)	
Unclassifiable	2 (3.7%)	0 (0.0%)	
Immunomodulatory therapy[§]	30 (55.6%)	14 (66.7%)	0.441
Smoking status			
Never	35 (64.8%)	13 (61.9%)	
Former	12 (22.2%)	5 (23.8%)	1.000
Current	7 (13.0%)	2 (9.5%)	

*Disease duration of SSc was calculated as the difference between the date of baseline CT and the date of manifestation of the first non-Raynaud's symptom.

[†]Pulmonary hypertension was assessed by echocardiography or right heart catheterisation.

[‡]PAP sys was determined by right heart catheterisation.

[#]UIP includes the radiological diagnosis of both, "definite" and "probable" UIP.

[§]Immunomodulatory therapy included prednisone, methotrexate, rituximab, cyclophosphamide, mycophenolate mofetil, hydroxychloroquine, tocilizumab, imatinib, azathioprine, adalimumab, leflunomid, cyclosporine.

Supplementary Table 4: Associations of the patients' risk groups based on qRISSc with clinical parameters for the external and independent validation (Oslo) cohort. Continuous variables are described as median ± interquartile range, and categorical variables are presented as absolute values with relative frequencies (percent). P-values of univariate comparisons of baseline characteristics between the two risk groups are shown. Fisher's exact test was used to compare categorical, and Mann-Whitney U to compare continuous variables, respectively. *Abbreviations: UIP = usual interstitial pneumonia, NSIP = nonspecific interstitial pneumonia, DIP = diffuse interstitial pneumonia, PAPsys = systolic pulmonary artery pressure, FVC = forced vital capacity, FEV1 = forced expiratory volume in 1 second, DLCO = diffusing capacity for carbon monoxide, 6-MWT = 6-min walk test, CRP = C-reactive protein*

Characteristics	**Low risk** (n=47)	**High risk** (n=19)	***p* value**
Age (years)	58.0 ± 22.0	64.0 ± 19.0	0.311
Sex			
Male	12 (25.5%)	4 (21.1%)	1.000
Female	35 (74.5%)	15 (78.9%)	
SSc disease duration (years)*	4.3 ± 9.1	6.1 ± 9.1	0.325
SSc subset (LeRoy 1988)			
Limited cutaneous SSc	26 (55.3%)	11 (57.9%)	
Diffuse cutaneous SSc	21 (44.7%)	8 (42.1%)	1.000
No skin involvement	0 (0.0%)	0 (0.0%)	
Skin involvement			
Limited cutaneous	26 (55.3%)	11 (57.9%)	
Diffuse cutaneous	21 (44.7%)	8 (42.1%)	1.000
No skin involvement	0 (0.0%)	0 (0.0%)	
Only sclerodactyly	0 (0.0%)	0 (0.0%)	
Autoantibodies			
Anti-Centromere positive	5 (10.6%)	2 (10.5%)	1.000
Anti-Topoisomerase I positive	17 (36.2%)	7 (36.8%)	1.000
Anti-RNA polymerase III positive	8 (17.0%)	0 (0.0%)	**0.046**
Anti-PMScl positive	3 (6.4%)	1 (5.3%)	1.000
FVC (% predicted)	92.0 ± 25.5	60.0 ± 20.0	
FVC ≥70% predicted	36 (76.6%)	8 (42.1%)	**<0.001**
FVC <70% predicted	6 (12.8%)	9 (47.4%)	
DLCO (% predicted)	66.0 ± 17.5	35.0 ± 20.0	**<0.001**
FEV1 (% predicted)	82.0 ± 22.0	64.0 ± 18.0	**<0.001**
Pulmonary hypertension†	1 (2.1%)	5 (26.3%)	**0.008**
PAPsys (mmHg)‡	15.0 ± 10.0	35.0 ± 18.8	0.054
CRP (mg/l)	2.9 ± 5.7	5.4 ± 9.0	0.121
6 min walk distance (m)	n/a	n/a	n/a
SpO_2 before 6MWT (%)	n/a	n/a	n/a
SpO_2 after 6MWT (%)	n/a	n/a	n/a
Borg (unit; range 0-10))	n/a	n/a	n/a
Extent of lung fibrosis on CT			
<20%	30 (63.8%)	0 (0.0%)	**<0.001**

≥20%	17 (36.2%)	19 (100.0%)	
Ground glass opacification	33 (70.2%)	9 (47.4%)	0.097
Reticular changes	34 (72.3%)	17 (89.5%)	0.198
Traction bronchiectasis	12 (25.5%)	15 (78.9%)	**<0.001**
Honeycombing	6 (12.8%)	10 (52.6%)	**0.001**
Bullae	2 (4.3%)	2 (10.5%)	0.573
Radiological subtype			
NSIP	27 (57.4%)	7 (36.8%)	0.175
UIP[#]	16 (34.0%)	11 (57.9%)	
DIP	0 (0.0%)	0 (0.0%)	
Unclassifiable	4 (8.5%)	1 (5.3%)	
Immunomodulatory therapy[§]	16 (34.0%)	12 (63.2%)	0.053
Smoking status			
Never	16 (34.0%)	8 (42.1%)	0.578
Former	17 (36.2%)	8 (42.1%)	
Current	5 (10.6%)	0 (0.0%)	

*Disease duration of SSc was calculated as the difference between the date of baseline CT and the date of manifestation of the first non-Raynaud's symptom.

[†]Pulmonary hypertension was assessed by echocardiography or right heart catheterisation.

[‡]PAP sys was determined by right heart catheterisation.

[#]UIP includes the radiological diagnosis of both, "definite" and "probable" UIP.

[§]Immunomodulatory therapy included prednisone, methotrexate, rituximab, cyclophosphamide, mycophenolate mofetil, hydroxychloroquine, tocilizumab, imatinib, azathioprine, adalimumab, leflunomid, cyclosporine.

Supplementary Table 5: Summary of the univariable Cox regression analysis for qRISSc and the previously proposed clinical risk factors for SSc-ILD progression. Covariates for univariable Cox regression were selected based on literature evidence [29] and expert opinion.

Predictor	HR (95% CI)	P-value	C-Index (SE), p-value
Zurich			
Age	1.03 (0.99, 1.06)	0.17	0.59 (0.06), p=0.17
Male Sex	1.38 (0.60, 3.16)	0.45	0.53 (0.05), p=0.46
Anti-Topoisomerase 1 positive	1.04 (0.49, 2.22)	0.92	0.46 (0.05), p=0.92
Baseline FVC (% predicted)	0.98 (0.96, 1.00)	**0.04**	0.62 (0.07), **p=0.04**
Baseline DLCO (% predicted)	0.98 (0.96, 1.00)	**0.02**	0.69 (0.05), **p=0.02**
HRCT Threshold (≥20%)	1.94 (0.90, 4.19)	0.09	0.61 (0.05), p=0.10
UIP Subtype*	0.88 (0.40, 1.92)	0.74	0.49 (0.05), p=0.74
Diffuse cutaneous skin involvement	1.81 (0.84, 3.89)	0.13	0.56 (0.05), **p=0.13**
CRP	1.01 (0.99, 1.04)	0.31	0.63 (0.06), p=0.35
qRISSc (high)	4.10 (1.87, 9.03)	**<0.001**	0.67 (0.05), **p=0.001**
Oslo			
Age	1.02 (0.97, 1.07)	0.45	0.61 (0.11), p=0.44
Male Sex	0.22 (0.03, 1.71)	0.15	0.61 (0.04), p=0.08
Anti-Topoisomerase 1 positive	1.07 (0.25, 4.55)	0.93	0.48 (0.10), p=0.93
Baseline FVC (% predicted)	1.00 (0.97, 1.03)	0.87	0.60 (0.12), p=0.87
Baseline DLCO (% predicted)	0.95 (0.92, 0.99)	**0.01**	0.85 (0.06), **p=0.008**
HRCT Threshold (≥20%)	2.04 (0.52, 8.00)	0.31	0.65 (0.06), p=0.29
UIP Subtype*	1.38 (0.42, 4.55)	0.60	0.55 (0.09), p=0.60
Diffuse cutaneous skin involvement	0.69 (0.19, 2.59)	0.58	0.48 (0.09), p=0.59
CRP	1.00 (0.94, 1.07)	0.98	0.52 (0.10), p=0.98
qRISSc (high)	5.14 (1.14, 23.2)	**0.03**	0.71 (0.07), **p=0.04**
Combined Cohorts			
Age	1.02 (1.00, 1.05)	0.11	0.59 (0.05), p=0.10
Male Sex	0.96 (0.46, 2.04)	0.92	0.50 (0.04), p=0.92
Anti-Topoisomerase 1 positive	1.05 (0.54, 2.02)	0.89	0.47 (0.05), p=0.89
Baseline FVC (% predicted)	0.98 (0.97, 1.00)	**0.04**	0.62 (0.06), **p=0.04**
Baseline DLCO (% predicted)	0.97 (0.96, 0.99)	**0.001**	0.72 (0.04), **p=0.001**
HRCT Threshold (≥20%)	1.98 (1.04, 3.76)	**0.04**	0.62 (0.04), **p=0.04**
UIP Subtype*	1.01 (0.53, 1.94)	0.98	0.53 (0.05), p=0.98
Diffuse cutaneous skin involvement	1.67 (0.88, 3.17)	0.12	0.54 (0.05), p=0.12
CRP	1.01 (0.99, 1.04)	0.40	0.60 (0.05), p=0.43
qRISSc (high)	4.07 (2.07, 8.00)	**<0.001**	0.68 (0.04), **p<0.001**

*UIP includes the radiological diagnosis of both, “definite” and “probable” UIP.

Supplementary Table 6: Summary of the multivariable Cox regression analysis of the clinical models composed of previously proposed risk factors for SSc-ILD progression. Covariates for multivariable Cox regression were selected based on literature evidence [29] and expert opinion.

Predictor	HR (95% CI)	P-value	FDR	C-Index (SE), p-value
Model 1				
Age	1.03 (1.00, 1.06)	0.09	0.18	0.64 (0.05) p=0.16
Male Sex	0.92 (0.42, 2.03)	0.84	0.88	
Baseline FVC (% predicted)	0.98 (0.97, 1.00)	**0.04**	0.15	
Anti-Topoisomerase 1 positive	1.07 (0.55, 2.11)	0.84	0.88	
Model 2				
Age	1.03 (1.00, 1.06)	0.06	0.15	0.66 (0.05) **p=0.04**
Male Sex	0.85 (0.39, 1.86)	0.69	0.83	
Baseline FVC (% predicted)	0.98 (0.96, 1.00)	**0.02**	0.12	
Model 3				
Age	1.03 (1.00, 1.06)	0.09	0.18	0.71 (0.04) **p=0.006**
Male Sex	0.98 (0.45, 2.11)	0.96	0.96	
Baseline DLCO (% predicted)	0.97 (0.95, 0.99)	**0.003**	0.06	
HRCT Threshold (≥20%)	1.08 (0.52, 2.25)	0.84	0.88	
Model 4				
Age	1.02 (0.99, 1.05)	0.15	0.28	0.66 (0.05) p=0.12
Male Sex	0.83 (0.38, 1.82)	0.64	0.83	
Baseline FVC (% predicted)	0.98 (0.97, 1.00)	0.06	0.15	
HRCT Threshold (≥20%)	1.40 (0.68, 2.90)	0.36	0.62	
UIP Subtype*	0.79 (0.39, 1.59)	0.50	0.77	
Model 5				
Age	1.04 (1.01, 1.07)	**0.02**	0.12	0.69 (0.04) **p=0.02**
Male Sex	0.78 (0.36, 1.73)	0.54	0.77	
Baseline FVC (% predicted)	0.98 (0.97, 1.00)	**0.03**	0.15	
Diffuse cutaneous skin involvement	2.01 (1.00, 4.04)	**0.05**	0.15	
Model 6				
Age	1.03 (1.00, 1.06)	0.06	0.15	0.68 (0.06) **p=0.03**
Male Sex	0.77 (0.35, 1.72)	0.53	0.77	
Baseline FVC (% predicted)	0.98 (0.96, 0.99)	**0.005**	0.06	
CRP (mg/l)	1.01 (0.98, 1.04)	0.67	0.83	

*UIP includes the radiological diagnosis of both, “definite” and “probable” UIP.

Supplementary Table 7: Summary of the multivariable Cox regression analysis of the combined models, i.e. incorporating qRISSc and the previously proposed clinical risk factors for SSc-ILD progression. Covariates for multivariable Cox regression were selected based on literature evidence [29] and expert opinion.

Predictor	HR (95% CI)	p-value	FDR	C-Index (SE), p-value
Model 1				
Age	1.03 (1.00, 1.06)	0.06	0.15	0.71 (0.05), **p=0.009**
Male Sex	1.03 (0.46, 2.30)	0.95	0.95	
Baseline FVC (% predicted)	0.99 (0.97, 1.01)	0.37	0.58	
Anti-Topoisomerase 1 positive	1.29 (0.65, 2.56)	0.46	0.70	
qRISSc (high)	3.48 (1.60, 7.55)	**0.002**	**0.01**	
Model 2				
Age	1.03 (1.00, 1.06)	0.06	0.15	0.74 (0.04), **p=0.001**
Male Sex	0.96 (0.43, 2.13)	0.92	0.95	
Baseline FVC (% predicted)	0.99 (0.97, 1.01)	0.30	0.56	
qRISSc (high)	3.59 (1.72, 7.50)	**0.001**	**0.01**	
Model 3				
Age	1.03 (1.00, 1.07)	**0.04**	0.15	0.77 (0.04), **p=2.72E-04**
Male Sex	0.95 (0.43, 2.10)	0.90	0.95	
Baseline DLCO (% predicted)	0.98 (0.96, 1.00)	**0.05**	0.15	
HRCT Threshold (≥20%)	0.92 (0.44, 1.93)	0.83	0.95	
qRISSc (high)	3.42 (1.58, 7.41)	**0.002**	**0.01**	
Model 4				
Age	1.03 (0.99, 1.06)	0.12	0.25	0.72 (0.05), **p=0.006**
Male Sex	0.96 (0.42, 2.19)	0.92	0.95	
Baseline FVC (% predicted)	0.99 (0.97, 1.01)	0.33	0.56	
HRCT Threshold (≥20%)	1.04 (0.48, 2.25)	0.92	0.95	
UIP Subtype*	0.96 (0.47, 1.98)	0.91	0.95	
qRISSc (high)	3.49 (1.60, 7.61)	**0.002**	**0.01**	
Model 5				
Age	1.04 (1.01, 1.07)	**0.01**	**0.05**	0.75 (0.04) **p<0.001**
Male Sex	0.91 (0.41, 2.03)	0.81	0.95	
Baseline FVC (% predicted)	0.99 (0.98, 1.01)	0.33	0.56	
Diffuse cutaneous skin involvement	2.48 (1.23, 5.01)	**0.01**	**0.05**	
qRISSc (high)	4.23 (2.03, 8.83)	**<0.001**	**0.001**	
Model 6				
Age	1.03 (1.00, 1.06)	0.07	0.16	0.72 (0.05) **p=0.003**
Male Sex	0.89 (0.39, 1.99)	0.77	0.95	
Baseline FVC (% predicted)	0.99 (0.97, 1.01)	0.18	0.35	
CRP (mg/l)	1.01 (0.98, 1.04)	0.69	0.95	
qRISSc (high)	3.07 (1.38, 6.85)	**0.006**	**0.03**	

*UIP includes the radiological diagnosis of both, “definite” and “probable” UIP.

Supplementary Table 8. Summary of the multivariable Cox regression analysis for the clinical and combined models, incorporating systolic pulmonary artery pressure or oxygen saturation at the end of the 6-min walk test as previously proposed risk factors for SSc-ILD progression, respectively. Covariates for multivariable Cox regression were selected based on literature evidence [29] and expert opinion. Due to missing data for the systolic pulmonary artery pressure (PAPsys, in mmHg) and the oxygen saturation at the end of the 6-min walk test (SpO_2 after 6MWT, in percent) in the validation cohort from Oslo, we only fitted the multivariable models on the derivation cohort from Zurich.

Predictor	HR (95% CI)	p-value	C-Index (SE), p-value
Clinical 1			
Age	1.05 (1.00, 1.10)	**0.05**	0.72 (0.05), p=0.06
Male Sex	1.70 (0.58, 5.01)	0.33	
Baseline FVC (% predicted.)	0.98 (0.96, 1.01)	0.15	
SpO_2 after 6-MWT (%)	0.97 (0.91, 1.03)	0.34	
Clinical 2			
Age	1.03 (0.99, 1.08)	0.13	0.74 (0.05), **p=0.006**
Male Sex	1.43 (0.49, 4.16)	0.51	
Baseline FVC (% predicted)	0.98 (0.96, 1.00)	0.10	
HRCT Threshold (≥20%)	0.90 (0.37, 2.22)	0.82	
PAPsys (mmHg)*	1.05 (1.02, 1.08)	**0.003**	
Combined 1			
Age	1.05 (1.00, 1.10)	**0.04**	0.76 (0.06), **p=0.01**
Male Sex	1.47 (0.52, 4.18)	0.47	
Baseline FVC (% predicted)	0.99 (0.96, 1.02)	0.67	
SpO_2 after 6-MWT (%)	1.00 (0.92, 1.10)	0.96	
qRISSc (high)	4.91 (1.19, 20.26)	**0.03**	
Combined 2			
Age	1.03 (0.99, 1.08)	0.13	0.79 (0.05), **p=0.002**
Male Sex	1.38 (0.46, 4.15)	0.56	
Baseline FVC (% predicted)	0.99 (0.97, 1.02)	0.47	
HRCT Threshold (≥20%)	0.85 (0.35, 2.06)	0.71	
PAPsys (mmHg)*	1.04 (1.01, 1.08)	**0.008**	
qRISSc (high)	3.05 (1.13, 8.20)	**0.03**	

*PAPsys was determined by right heart catheterization

Supplementary Table 9: Summary of HRCT image acquisition parameters for the two study cohorts. For slice thickness and tube voltage, data are presented as median and range of minimal and maximal values.

CT parameter	**Discovery (Zurich) cohort** (n=90)	**Validation (Oslo) cohort** (n=66)
Manufacturer*	Siemens	Siemens, GE Medical Systems
Acquisition Model	Inspiration (breath hold)	Inspiration (breath hold)
Slice thickness (mm)	1 (range 0.6 - 2)	2.5 (range 2 - 3)
Reconstruction kernels	B60f, B70f, Bl64	B60f, B70f, LUNG
Tube voltage (kVP)	120 (range 80 - 150)	120

*HRCT scanners included SOMATOM Definition AS, SOMATOM Definition Flash, SOMATOM Force, SOMATOM Sensation 64, SOMATOM Sensation 16, Biograph 64, LightSpeed Pro 16, LightSpeed VCT.

Supplementary Table 10: Parameter settings for MaxQuant analysis.

Parameter	Value
Version	1.6.6.0
Machine name	PROXMOX-W10
PSM FDR	0.01
PSM FDR Crosslink	0.01
Protein FDR	0.01
Site FDR	0.01
Use Normalized Ratios For Occupancy	TRUE
Min. peptide Length	7
Min. score for unmodified peptides	0
Min. score for modified peptides	40
Min. delta score for unmodified peptides	0
Min. delta score for modified peptides	6
Min. unique peptides	0
Min. razor peptides	2
Min. peptides	2
Use only unmodified peptides and	FALSE
Peptides used for protein quantification	Razor
Discard unmodified counterpart peptides	TRUE
Label min. ratio count	2
Use delta score	FALSE
iBAQ	TRUE
iBAQ log fit	TRUE
Match between runs	TRUE
Matching time window [min]	0.7
Match ion mobility window [indices]	0.05
Alignment time window [min]	20
Alignment ion mobility window [indices]	1
Find dependent peptides	FALSE
Fasta file	MusMusculus_SP_2019_10.fasta
Decoy mode	revert
Include contaminants	TRUE
Fixed modification	Carbamidomethylation of Cys
Variable modifications	Oxidation on Met; Acetyl on protein N-term
Advanced ratios	FALSE
Second peptides	TRUE
Stabilize large LFQ ratios	TRUE
Separate LFQ in parameter groups	FALSE
Require MS/MS for LFQ comparisons	TRUE
Calculate peak properties	FALSE
Main search max. combinations	200
Advanced site intensities	FALSE
Write msScans table	FALSE

Write msmsScans table	FALSE
Write ms3Scans table	FALSE
Write allPeptides table	FALSE
Write mzRange table	FALSE
Write pasefMsmsScans table	FALSE
Write accumulatedPasefMsmsScans table	FALSE
Max. peptide mass [Da]	5500
Min. peptide length for unspecific search	8
Max. peptide length for unspecific search	25
Razor protein FDR	TRUE
Max mods in site table	3
Match unidentified features	FALSE
Evaluate variant peptides separately	TRUE
Variation mode	None
MS/MS tol. (FTMS)	20 ppm
Top MS/MS peaks per Da interval. (FTMS)	6
Da interval. (FTMS)	20
MS/MS deisotoping (FTMS)	TRUE
MS/MS deisotoping tolerance (FTMS)	7
MS/MS deisotoping tolerance unit (FTMS)	ppm
MS/MS higher charges (FTMS)	TRUE
MS/MS water loss (FTMS)	TRUE
MS/MS ammonia loss (FTMS)	TRUE
MS/MS dependent losses (FTMS)	TRUE
MS/MS recalibration (FTMS)	FALSE
MS/MS tol. (ITMS)	0.4 Da
Top MS/MS peaks per Da interval. (ITMS)	12
Da interval. (ITMS)	100
MS/MS deisotoping (ITMS)	FALSE
MS/MS deisotoping tolerance (ITMS)	0.15
MS/MS deisotoping tolerance unit (ITMS)	Da
MS/MS higher charges (ITMS)	TRUE
MS/MS water loss (ITMS)	TRUE
MS/MS ammonia loss (ITMS)	TRUE
MS/MS dependent losses (ITMS)	TRUE
MS/MS recalibration (ITMS)	FALSE
MS/MS deisotoping (Unknown)	FALSE
MS/MS deisotoping tolerance (Unknown)	0.15
MS/MS deisotoping tolerance unit (Unknown)	Da
MS/MS higher charges (Unknown)	TRUE
MS/MS water loss (Unknown)	TRUE
MS/MS ammonia loss (Unknown)	TRUE
MS/MS dependent losses (Unknown)	TRUE
MS/MS recalibration (Unknown)	FALSE

Supplementary Table 11: Murine primer sequences used for qRT-PCR.

Gene	Forward primer (5' - 3')	Reverse primer (5' - 3')
Collagen 1 alpha 1 (*Col1a1*)	GAT GAC GTG CAA TGC AAT GAA	CCC TCG ACT CCT ACA TCT TCT GA
Collagen 3 alpha 1 (*Col3a1*)	AGC TTT GTG CAA AGT GGA ACC	ATA GGA CTG ACC AAG GTG GC
Fibronectin 1 (*Fn1*)	ATG TGG ACC CCT CCT GAT AGT	GCC CAG TGA TTT CAG CAA AGG
Interleukin 6 (*Il6*)	TGA TGG ATG CTA CCA AAC TGG	GGT ACT CCA GAA GAC CAG AG
Monocyte chemoattractant protein 1 (*Mcp-1*)	CCA CTC ACC TGC TGC TAC TCA T	TGG TGA TCC TCT TGT AGC TCT CC
60S acidic ribosomal protein P0 (*Rplp0*)	GCA GGT GTT TGA CAA CGG CAG	GAT GAT GGA GTG TGG CAC CGA

Supplementary References

1. Tyndall A, Ladner UM, Matucci-Cerinic M. The EULAR Scleroderma Trials And Research group (EUSTAR): an international framework for accelerating scleroderma research [Internet]. Current Opinion in Rheumatology 2008. p. 703–706Available from: http://dx.doi.org/10.1097/bor.0b013e328311f841.

2. Minier T, Guiducci S, Bellando-Randone S, Bruni C, Lepri G, Czirják L, Distler O, Walker UA, Fransen J, Allanore Y, Denton C, Cutolo M, Tyndall A, Müller-Ladner U, Matucci-Cerinic M, EUSTAR co-workers, EUSTAR co-workers. Preliminary analysis of the very early diagnosis of systemic sclerosis (VEDOSS) EUSTAR multicentre study: evidence for puffy fingers as a pivotal sign for suspicion of systemic sclerosis. *Ann. Rheum. Dis.* 2014; 73: 2087–2093.

3. van den Hoogen F, Khanna D, Fransen J, Johnson SR, Baron M, Tyndall A, Matucci-Cerinic M, Naden RP, Medsger TA Jr, Carreira PE, Riemekasten G, Clements PJ, Denton CP, Distler O, Allanore Y, Furst DE, Gabrielli A, Mayes MD, van Laar JM, Seibold JR, Czirjak L, Steen VD, Inanc M, Kowal-Bielecka O, Müller-Ladner U, Valentini G, Veale DJ, Vonk MC, Walker UA, Chung L, et al. 2013 classification criteria for systemic sclerosis: an American College of Rheumatology/European League against Rheumatism collaborative initiative. *Arthritis Rheum.* 2013; 65: 2737–2747.

4. Borg G. Borg's Perceived Exertion and Pain Scales. Human Kinetics 1; 1998.

5. Tashkin DP, Elashoff R, Clements PJ, Goldin J, Roth MD, Furst DE, Arriola E, Silver R, Strange C, Bolster M, Seibold JR, Riley DJ, Hsu VM, Varga J, Schraufnagel DE, Theodore A, Simms R, Wise R, Wigley F, White B, Steen V, Read C, Mayes M, Parsley E, Mubarak K, Connolly MK, Golden J, Olman M, Fessler B, Rothfield N, et al. Cyclophosphamide versus placebo in scleroderma lung disease. *N. Engl. J. Med.* 2006; 354: 2655–2666.

6. Tashkin DP, Roth MD, Clements PJ, Furst DE, Khanna D, Kleerup EC, Goldin J, Arriola E, Volkmann ER, Kafaja S, Silver R, Steen V, Strange C, Wise R, Wigley F, Mayes M, Riley DJ, Hussain S, Assassi S, Hsu VM, Patel B, Phillips K, Martinez F, Golden J, Connolly MK, Varga J, Dematte J, Hinchcliff ME, Fischer A, Swigris J, et al. Mycophenolate mofetil versus oral cyclophosphamide in scleroderma-related interstitial lung disease (SLS II): a randomised controlled, double-blind, parallel group trial. *Lancet Respir. Med.* Elsevier BV; 2016; 4: 708–719.

7. American Thoracic Society. Idiopathic pulmonary fibrosis: diagnosis and treatment. International consensus statement. American Thoracic Society (ATS), and the European Respiratory Society (ERS). *Am. J. Respir. Crit. Care Med.* 2000; 161: 646–664.

8. Wu W, Jordan S, Becker MO, Dobrota R, Maurer B, Fretheim H, Ye S, Siegert E, Allanore Y, Hoffmann-Vold A-M, Distler O. Prediction of progression of interstitial

lung disease in patients with systemic sclerosis: the SPAR model. *Ann. Rheum. Dis.* 2018; 77: 1326–1332.

9. Wu W, Jordan S, Becker MO, Dobrota R, Maurer B, Fretheim H, Ye S, Siegert E, Allanore Y, Hoffmann-Vold A-M, Distler O. Prediction of progression of interstitial lung disease in patients with systemic sclerosis: the SPAR model. *Ann. Rheum. Dis.* 2018; 77: 1326–1332.

10. Graham BL, Steenbruggen I, Miller MR, Barjaktarevic IZ, Cooper BG, Hall GL, Hallstrand TS, Kaminsky DA, McCarthy K, McCormack MC, Oropez CE, Rosenfeld M, Stanojevic S, Swanney MP, Thompson BR. Standardization of Spirometry 2019 Update. An Official American Thoracic Society and European Respiratory Society Technical Statement. *Am. J. Respir. Crit. Care Med.* 2019; 200: e70–e88.

11. Graham BL, Brusasco V, Burgos F, Cooper BG, Jensen R, Kendrick A, MacIntyre NR, Thompson BR, Wanger J. 2017 ERS/ATS standards for single-breath carbon monoxide uptake in the lung. *Eur. Respir. J.* [Internet] 2017; 49Available from: http://dx.doi.org/10.1183/13993003.00016-2016.

12. Holland AE, Spruit MA, Troosters T, Puhan MA, Pepin V, Saey D, McCormack MC, Carlin BW, Sciurba FC, Pitta F, Wanger J, MacIntyre N, Kaminsky DA, Culver BH, Revill SM, Hernandes NA, Andrianopoulos V, Camillo CA, Mitchell KE, Lee AL, Hill CJ, Singh SJ. An official European Respiratory Society/American Thoracic Society technical standard: field walking tests in chronic respiratory disease. *Eur. Respir. J.* 2014; 44: 1428–1446.

13. Wanger J, Clausen JL, Coates A, Pedersen OF, Brusasco V, Burgos F, Casaburi R, Crapo R, Enright P, van der Grinten CPM, Gustafsson P, Hankinson J, Jensen R, Johnson D, Macintyre N, McKay R, Miller MR, Navajas D, Pellegrino R, Viegi G. Standardisation of the measurement of lung volumes. *Eur. Respir. J.* 2005; 26: 511–522.

14. Raghu G, Remy-Jardin M, Myers JL, Richeldi L, Ryerson CJ, Lederer DJ, Behr J, Cottin V, Danoff SK, Morell F, Flaherty KR, Wells A, Martinez FJ, Azuma A, Bice TJ, Bouros D, Brown KK, Collard HR, Duggal A, Galvin L, Inoue Y, Jenkins RG, Johkoh T, Kazerooni EA, Kitaichi M, Knight SL, Mansour G, Nicholson AG, Pipavath SNJ, Buendía-Roldán I, et al. Diagnosis of Idiopathic Pulmonary Fibrosis. An Official ATS/ERS/JRS/ALAT Clinical Practice Guideline. *Am. J. Respir. Crit. Care Med.* 2018; 198: e44–e68.

15. Lynch DA, Sverzellati N, Travis WD, Brown KK, Colby TV, Galvin JR, Goldin JG, Hansell DM, Inoue Y, Johkoh T, Nicholson AG, Knight SL, Raoof S, Richeldi L, Ryerson CJ, Ryu JH, Wells AU. Diagnostic criteria for idiopathic pulmonary fibrosis: a Fleischner Society White Paper. *Lancet Respir Med* 2018; 6: 138–153.

16. Rizzo S, Botta F, Raimondi S, Origgi D, Fanciullo C, Morganti AG, Bellomi M. Radiomics: the facts and the challenges of image analysis. *Eur Radiol Exp* 2018; 2: 36.

17. Aerts HJWL, Velazquez ER, Leijenaar RTH, Parmar C, Grossmann P, Carvalho S, Bussink J, Monshouwer R, Haibe-Kains B, Rietveld D, Hoebers F, Rietbergen MM, Leemans CR, Dekker A, Quackenbush J, Gillies RJ, Lambin P. Decoding tumour phenotype by noninvasive imaging using a quantitative radiomics approach. *Nat. Commun.* 2014; 5: 4006.

18. Zwanenburg A, Vallières M, Abdalah MA, Aerts HJWL, Andrearczyk V, Apte A, Ashrafinia S, Bakas S, Beukinga RJ, Boellaard R, Bogowicz M, Boldrini L, Buvat I, Cook GJR, Davatzikos C, Depeursinge A, Desseroit M-C, Dinapoli N, Dinh CV, Echegaray S, El Naqa I, Fedorov AY, Gatta R, Gillies RJ, Goh V, Götz M, Guckenberger M, Ha SM, Hatt M, Isensee F, et al. The Image Biomarker Standardization Initiative: Standardized Quantitative Radiomics for High-Throughput Image-based Phenotyping. *Radiology* 2020; : 191145.

19. Shrout PE, Fleiss JL. Intraclass correlations: Uses in assessing rater reliability [Internet]. Psychological Bulletin 1979. p. 420–428Available from: http://dx.doi.org/10.1037/0033-2909.86.2.420.

20. Koo TK, Li MY. A Guideline of Selecting and Reporting Intraclass Correlation Coefficients for Reliability Research. *J. Chiropr. Med.* 2016; 15: 155–163.

21. Lawson RG, Jurs PC. New index for clustering tendency and its application to chemical problems [Internet]. Journal of Chemical Information and Modeling 1990. p. 36–41Available from: http://dx.doi.org/10.1021/ci00065a010.

22. Hartigan JA, Wong MA. Algorithm AS 136: A K-Means Clustering Algorithm [Internet]. Applied Statistics 1979. p. 100Available from: http://dx.doi.org/10.2307/2346830.

23. Lu H, Arshad M, Thornton A, Avesani G, Cunnea P, Curry E, Kanavati F, Liang J, Nixon K, Williams ST, Hassan MA, Bowtell DDL, Gabra H, Fotopoulou C, Rockall A, Aboagye EO. A mathematical-descriptor of tumor-mesoscopic-structure from computed-tomography images annotates prognostic- and molecular-phenotypes of epithelial ovarian cancer. *Nat. Commun.* 2019; 10: 764.

24. Ufuk F, Demirci M, Altinisik G. Quantitative computed tomography assessment for systemic sclerosis-related interstitial lung disease: comparison of different methods. *Eur. Radiol.* 2020; 30: 4369–4380.

25. Bocchino M, Bruzzese D, D'Alto M, Argiento P, Borgia A, Capaccio A, Romeo E, Russo B, Sanduzzi A, Valente T, Sverzellati N, Rea G, Vettori S. Performance of a new quantitative computed tomography index for interstitial lung disease assessment in systemic sclerosis. *Sci. Rep.* 2019; 9: 9468.

26. Saldana DC, Hague CJ, Murphy D, Coxson HO, Tschirren J, Peterson S, Sieren JP, Kirby M, Ryerson CJ. Association of Computed Tomography Densitometry with Disease Severity, Functional Decline, and Survival in Systemic Sclerosis-associated Interstitial Lung Disease. *Ann. Am. Thorac. Soc.* 2020; 17: 813–820.

27. Ariani A, Silva M, Seletti V, Bravi E, Saracco M, Parisi S, De Gennaro F, Idolazzi L, Caramaschi P, Benini C, Bodini FC, Scirè CA, Carrara G, Lumetti F, Alfieri V, Bonati E, Lucchini G, Aiello M, Santilli D, Mozzani F, Imberti D, Michieletti E, Arrigoni E, Delsante G, Pellerito R, Fusaro E, Chetta A, Sverzellati N. Quantitative chest computed tomography is associated with two prediction models of mortality in interstitial lung disease related to systemic sclerosis. *Rheumatology* 2017; 56: 922–927.

28. Lydersen S. Statistical review: frequently given comments. *Ann. Rheum. Dis.* BMJ; 2015; 74: 323–325.

29. Distler O, Assassi S, Cottin V, Cutolo M, Danoff SK, Denton CP, Distler JHW, Hoffmann-Vold A-M, Johnson SR, Müller Ladner U, Smith V, Volkmann ER, Maher TM. Predictors of progression in systemic sclerosis patients with interstitial lung disease. *Eur. Respir. J.* [Internet] 2020; 55Available from: http://dx.doi.org/10.1183/13993003.02026-2019.

30. Heinze G, Dunkler D. Five myths about variable selection. *Transpl. Int.* 2017; 30: 6–10.

31. Harrell FE. Regression Modeling Strategies: With Applications to Linear Models, Logistic and Ordinal Regression, and Survival Analysis. Cham: Springer International Publishing; 2015.

32. Schniering J, Gabrys H, Brunner M, Distler O, Guckenberger M, Bogowicz M, Vuong D, Karava K, Müller C, Frauenfelder T, Tanadini-Lang S, Maurer B. Computed-tomography-based radiomics features for staging of interstitial lung disease – transferability from experimental to human lung fibrosis - a proof-of-concept study [Internet]. Imaging 2019.Available from: http://dx.doi.org/10.1183/13993003.congress-2019.pa4806.

33. Schniering J, Benešová M, Brunner M, Haller S, Cohrs S, Frauenfelder T, Vrugt B, Feghali-Bostwick C, Schibli R, Distler O, Müller C, Maurer B. F-AzaFol for Detection of Folate Receptor-β Positive Macrophages in Experimental Interstitial Lung Disease-A Proof-of-Concept Study. *Front. Immunol.* 2019; 10: 2724.

34. Schniering J, Benešová M, Brunner M, Haller S, Cohrs S, Frauenfelder T, Vrugt B, Feghali-Bostwick CA, Schibli R, Distler O, Mueller C, Maurer B. Visualisation of interstitial lung disease by molecular imaging of integrin αvβ3 and somatostatin receptor 2. *Ann. Rheum. Dis.* 2019; 78: 218–227.

35. Stritt M, Stalder AK, Vezzali E. Orbit Image Analysis: An open-source whole slide image analysis tool. *PLoS Comput. Biol.* 2020; 16: e1007313.

36. Seger S, Stritt M, Vezzali E, Nayler O, Hess P, Groenen PMA, Stalder AK. A fully automated image analysis method to quantify lung fibrosis in the bleomycin-induced rat model. *PLoS One* 2018; 13: e0193057.

37. Ashcroft T, Simpson JM, Timbrell V. Simple method of estimating severity of pulmonary fibrosis on a numerical scale. *J. Clin. Pathol.* 1988; 41: 467–470.

38. Schniering J, Guo L, Brunner M, Schibli R, Ye S, Distler O, Béhé M, Maurer B. Evaluation of Tc-rhAnnexin V-128 SPECT/CT as a diagnostic tool for early stages of interstitial lung disease associated with systemic sclerosis. *Arthritis Res. Ther.* 2018; 20: 183.

39. Irvin CG, Bates JHT. Measuring the lung function in the mouse: the challenge of size. *Respir. Res.* 2003; 4: 4.

Index	Feature Number	full name	Standardization Name
1	V1	Mean	mean
2	V2	SD	standard deviation
3	V3	COV	coefficient of variation
4	V4	skewness	skewness
5	V5	kurtosis	kurtosis
6	V6	var	variance
7	V7	median	median
8	V8	percentile10	percentile 10th
9	V9	percentile90	percentile 90th
10	V10	iqr	interquartile range
11	V11	Hrange	range
12	V12	mad	mean absolut deviation
13	V13	rmad	robust mean absolut deviation
14	V14	H_energy	energy
15	V15	H_entropy	entropy
16	V16	rms	root mean square
17	V17	H_uniformity	uniformity
18	V18	energy	energy
19	V19	entropy	entropy
20	V20	contrast	contrast
21	V21	correlation	correlation
22	V22	homogenity	homogeneity
23	V23	homogenity_n	homogeneity normalized
24	V24	idiff	inverese difference
25	V25	idiff_n	inverese difference normalized
26	V26	variance	variance
27	V27	sum_average	sum of average
28	V28	sum_entropy	sum of entropy
29	V29	sum_variance	sum of variance
30	V30	diff_entropy	difference entropy
31	V31	diff_variance	difference variance
32	V32	IMC1	information measures of correlation 1
33	V33	IMC2	information measures of correlation 2
34	V34	MCC	maximal correlation coefficient
35	V35	joint_max	joint maximum
36	V36	joint_average	joint average
37	V37	diff_average	difference average
38	V38	dissimilarity	dissimilarity
39	V39	inverse_variance	inverse variance
40	V40	autocorrelation	autocorrelation
41	V41	clust_tendency	cluster tendency
42	V42	clust_shade	cluster shade
43	V43	clust_prominence	cluster prominence
44	V44	M_energy	energy
45	V45	M_entropy	entropy
46	V46	M_contrast	contrast
47	V47	M_correlation	correlation

48	V48	M_homogenity	homogeneity
49	V49	M_homogenity_n	homogeneity normalized
50	V50	M_idiff	inverese difference
51	V51	M_idiff_n	inverese difference normalized
52	V52	M_variance	variance
53	V53	M_sum_average	sum of average
54	V54	M_sum_entropy	sum of entropy
55	V55	M_sum_variance	sum of variance
56	V56	M_diff_entropy	difference entropy
57	V57	M_diff_variance	difference variance
58	V58	M_IMC1	information measures of correlation 1
59	V59	M_IMC2	information measures of correlation 2
60	V60	M_MCC	maximal correlation coefficient
61	V61	M_joint_max	joint maximum
62	V62	M_joint_average	joint average
63	V63	M_diff_average	difference average
64	V64	M_dissimilarity	dissimilarity
65	V65	M_inverse_variance	inverse variance
66	V66	M_autocorrelation	autocorrelation
67	V67	M_clust_tendency	cluster tendency
68	V68	M_clust_shade	cluster shade
69	V69	M_clust_prominence	cluster prominence
70	V70	coarseness	coarseness
71	V71	neighContrast	contrast
72	V72	busyness	busyness
73	V73	complexity	complexity
74	V74	strength	strength
75	V75	len_intensityVar	grey level non-uniformity
76	V76	len_intensityVar_n	grey level non-uniformity normalized
77	V77	len_sizeVar	zone size non-uniformity
78	V78	len_sizeVar_n	zone size non-uniformity normalized
79	V79	len_sse	short runs emphasis
80	V80	len_lse	long runs emphasis
81	V81	len_lgse	low grey level run emphasis
82	V82	len_hgse	high grey level run emphasis
83	V83	len_sslge	short run low grey level emphasis
84	V84	len_sshge	short run high grey level emphasis
85	V85	len_lslge	long run low grey level emphasis
86	V86	len_lshge	long run high grey level emphasis
87	V87	len_rpc	run percentage
88	V88	len_grey_lev_var	grey level variance
89	V89	len_zone_size_var	run length variance
90	V90	len_size_entropy	run entropy
91	V91	M_len_intensityVar	grey level non-uniformity
92	V92	M_len_intensityVar_n	grey level non-uniformity normalized
93	V93	M_len_sizeVar	zone size non-uniformity
94	V94	M_len_sizeVar_n	zone size non-uniformity normalized
95	V95	M_len_sse	short runs emphasis
96	V96	M_len_lse	long runs emphasis
97	V97	M_len_lgse	low grey level run emphasis

98	V98	M_len_hgse	high grey level run emphasis
99	V99	M_len_sslge	short run low grey level emphasis
100	V100	M_len_sshge	short run high grey level emphasis
101	V101	M_len_lslge	long run low grey level emphasis
102	V102	M_len_lshge	long run high grey level emphasis
103	V103	M_len_rpc	run percentage
104	V104	M_len_grey_lev_var	grey level variance
105	V105	M_len_zone_size_var	run length variance
106	V106	M_len_size_entropy	run entropy
107	V107	intensityVar	grey level non-uniformity
108	V108	intensityVar_n	grey level non-uniformity normalized
109	V109	sizeVar	zone size non-uniformity
110	V110	sizeVar_n	zone size non-uniformity normalized
111	V111	sse	small zone emphasis
112	V112	lse	large zone emphasis
113	V113	lgse	low grey level zone emphasis
114	V114	hgse	high grey level zone emphasis
115	V115	sslge	small zone low grey level emphasis
116	V116	sshge	small zone high grey level emphasis
117	V117	lslge	large zone low grey level emphasis
118	V118	lshge	large zone high grey level emphasis
119	V119	rpc	zone percentage
120	V120	grey_lev_var	grey level variance
121	V121	zone_size_var	zone size variance
122	V122	size_entropy	zone size entropy
123	V123	GLDZM_intensityVar	grey level non-uniformity
124	V124	GLDZM_intensityVar_n	grey level non-uniformity normalized
125	V125	GLDZM_sizeVar	zone size non-uniformity
126	V126	GLDZM_sizeVar_n	zone size non-uniformity normalized
127	V127	GLDZM_sse	small distance emphasis
128	V128	GLDZM_lse	large distance emphasis
129	V129	GLDZM_lgse	low grey level zone emphasis
130	V130	GLDZM_hgse	high grey level zone emphasis
131	V131	GLDZM_sslge	small distance low grey level emphasis
132	V132	GLDZM_sshge	small distance high grey level emphasis
133	V133	GLDZM_lslge	large distance low grey level emphasis
134	V134	GLDZM_lshge	large distance high grey level emphasis
135	V135	GLDZM_rpc	zone percentage
136	V136	GLDZM_grey_lev_var	grey level variance
137	V137	GLDZM_zone_size_var	zone distance variance
138	V138	GLDZM_size_entropy	zone distance entropy
139	V139	NGLDM_intensityVar	grey level non-uniformity
140	V140	NGLDM_intensityVar_n	grey level non-uniformity normalized
141	V141	NGLDM_sizeVar	dependence count non-uniformity
142	V142	NGLDM_sizeVar_n	dependence count non-uniformity normalized
143	V143	NGLDM_sse	low dependence emphasis
144	V144	NGLDM_lse	high dependence emphasis
145	V145	NGLDM_lgse	low grey level count emphasis
146	V146	NGLDM_hgse	high grey level count emphasis
147	V147	NGLDM_sslge	low dependence low grey level emphasis

148	V148	NGLDM_sshge	low dependence high grey level emphasis
149	V149	NGLDM_lslge	high dependence low grey level emphasis
150	V150	NGLDM_lshge	high dependence high grey level emphasis
151	V151	NGLDM_grey_lev_var	grey level variance
152	V152	NGLDM_zone_size_var	dependence count variance
153	V153	NGLDM_size_entropy	dependence count entropy
154	V154	NGLDM_energy	dependence count energy
155	V155	Mean	mean
156	V156	SD	standard deviation
157	V157	COV	coefficient of variation
158	V158	skewness	skewness
159	V159	kurtosis	kurtosis
160	V160	var	variance
161	V161	median	median
162	V162	percentile10	percentile 10th
163	V163	percentile90	percentile 90th
164	V164	iqr	interquartile range
165	V165	Hrange	range
166	V166	mad	mean absolut deviation
167	V167	rmad	robust mean absolut deviation
168	V168	H_energy	energy
169	V169	H_entropy	entropy
170	V170	rms	root mean square
171	V171	H_uniformity	uniformity
172	V172	energy	energy
173	V173	entropy	entropy
174	V174	contrast	contrast
175	V175	correlation	correlation
176	V176	homogenity	homogeneity
177	V177	homogenity_n	homogeneity normalized
178	V178	idiff	inverese difference
179	V179	idiff_n	inverese difference normalized
180	V180	variance	variance
181	V181	sum_average	sum of average
182	V182	sum_entropy	sum of entropy
183	V183	sum_variance	sum of variance
184	V184	diff_entropy	difference entropy
185	V185	diff_variance	difference variance
186	V186	IMC1	information measures of correlation 1
187	V187	IMC2	information measures of correlation 2
188	V188	MCC	maximal correlation coefficient
189	V189	joint_max	joint maximum
190	V190	joint_average	joint average
191	V191	diff_average	difference average
192	V192	dissimilarity	dissimilarity
193	V193	inverse_variance	inverse variance
194	V194	autocorrelation	autocorrelation
195	V195	clust_tendency	cluster tendency
196	V196	clust_shade	cluster shade
197	V197	clust_prominence	cluster prominence

198	V198	M_energy	energy
199	V199	M_entropy	entropy
200	V200	M_contrast	contrast
201	V201	M_correlation	correlation
202	V202	M_homogenity	homogeneity
203	V203	M_homogenity_n	homogeneity normalized
204	V204	M_idiff	inverese difference
205	V205	M_idiff_n	inverese difference normalized
206	V206	M_variance	variance
207	V207	M_sum_average	sum of average
208	V208	M_sum_entropy	sum of entropy
209	V209	M_sum_variance	sum of variance
210	V210	M_diff_entropy	difference entropy
211	V211	M_diff_variance	difference variance
212	V212	M_IMC1	information measures of correlation 1
213	V213	M_IMC2	information measures of correlation 2
214	V214	M_MCC	maximal correlation coefficient
215	V215	M_joint_max	joint maximum
216	V216	M_joint_average	joint average
217	V217	M_diff_average	difference average
218	V218	M_dissimilarity	dissimilarity
219	V219	M_inverse_variance	inverse variance
220	V220	M_autocorrelation	autocorrelation
221	V221	M_clust_tendency	cluster tendency
222	V222	M_clust_shade	cluster shade
223	V223	M_clust_prominence	cluster prominence
224	V224	coarseness	coarseness
225	V225	neighContrast	contrast
226	V226	busyness	busyness
227	V227	complexity	complexity
228	V228	strength	strength
229	V229	len_intensityVar	grey level non-uniformity
230	V230	len_intensityVar_n	grey level non-uniformity normalized
231	V231	len_sizeVar	zone size non-uniformity
232	V232	len_sizeVar_n	zone size non-uniformity normalized
233	V233	len_sse	short runs emphasis
234	V234	len_lse	long runs emphasis
235	V235	len_lgse	low grey level run emphasis
236	V236	len_hgse	high grey level run emphasis
237	V237	len_sslge	short run low grey level emphasis
238	V238	len_sshge	short run high grey level emphasis
239	V239	len_lslge	long run low grey level emphasis
240	V240	len_lshge	long run high grey level emphasis
241	V241	len_rpc	run percentage
242	V242	len_grey_lev_var	grey level variance
243	V243	len_zone_size_var	run length variance
244	V244	len_size_entropy	run entropy
245	V245	M_len_intensityVar	grey level non-uniformity
246	V246	M_len_intensityVar_n	grey level non-uniformity normalized
247	V247	M_len_sizeVar	zone size non-uniformity

248	V248	M_len_sizeVar_n	zone size non-uniformity normalized
249	V249	M_len_sse	short runs emphasis
250	V250	M_len_lse	long runs emphasis
251	V251	M_len_lgse	low grey level run emphasis
252	V252	M_len_hgse	high grey level run emphasis
253	V253	M_len_sslge	short run low grey level emphasis
254	V254	M_len_sshge	short run high grey level emphasis
255	V255	M_len_lslge	long run low grey level emphasis
256	V256	M_len_lshge	long run high grey level emphasis
257	V257	M_len_rpc	run percentage
258	V258	M_len_grey_lev_var	grey level variance
259	V259	M_len_zone_size_var	run length variance
260	V260	M_len_size_entropy	run entropy
261	V261	intensityVar	grey level non-uniformity
262	V262	intensityVar_n	grey level non-uniformity normalized
263	V263	sizeVar	zone size non-uniformity
264	V264	sizeVar_n	zone size non-uniformity normalized
265	V265	sse	small zone emphasis
266	V266	lse	large zone emphasis
267	V267	lgse	low grey level zone emphasis
268	V268	hgse	high grey level zone emphasis
269	V269	sslge	small zone low grey level emphasis
270	V270	sshge	small zone high grey level emphasis
271	V271	lslge	large zone low grey level emphasis
272	V272	lshge	large zone high grey level emphasis
273	V273	rpc	zone percentage
274	V274	grey_lev_var	grey level variance
275	V275	zone_size_var	zone size variance
276	V276	size_entropy	zone size entropy
277	V277	GLDZM_intensityVar	grey level non-uniformity
278	V278	GLDZM_intensityVar_n	grey level non-uniformity normalized
279	V279	GLDZM_sizeVar	zone size non-uniformity
280	V280	GLDZM_sizeVar_n	zone size non-uniformity normalized
281	V281	GLDZM_sse	small distance emphasis
282	V282	GLDZM_lse	large distance emphasis
283	V283	GLDZM_lgse	low grey level zone emphasis
284	V284	GLDZM_hgse	high grey level zone emphasis
285	V285	GLDZM_sslge	small distance low grey level emphasis
286	V286	GLDZM_sshge	small distance high grey level emphasis
287	V287	GLDZM_lslge	large distance low grey level emphasis
288	V288	GLDZM_lshge	large distance high grey level emphasis
289	V289	GLDZM_rpc	zone percentage
290	V290	GLDZM_grey_lev_var	grey level variance
291	V291	GLDZM_zone_size_var	zone distance variance
292	V292	GLDZM_size_entropy	zone distance entropy
293	V293	NGLDM_intensityVar	grey level non-uniformity
294	V294	NGLDM_intensityVar_n	grey level non-uniformity normalized
295	V295	NGLDM_sizeVar	dependence count non-uniformity
296	V296	NGLDM_sizeVar_n	dependence count non-uniformity normalized
297	V297	NGLDM_sse	low dependence emphasis

298	V298	NGLDM_lse	high dependence emphasis
299	V299	NGLDM_lgse	low grey level count emphasis
300	V300	NGLDM_hgse	high grey level count emphasis
301	V301	NGLDM_sslge	low dependence low grey level emphasis
302	V302	NGLDM_sshge	low dependence high grey level emphasis
303	V303	NGLDM_lslge	high dependence low grey level emphasis
304	V304	NGLDM_lshge	high dependence high grey level emphasis
305	V305	NGLDM_grey_lev_var	grey level variance
306	V306	NGLDM_zone_size_var	dependence count variance
307	V307	NGLDM_size_entropy	dependence count entropy
308	V308	NGLDM_energy	dependence count energy
309	V309	Mean	mean
310	V310	SD	standard deviation
311	V311	COV	coefficient of variation
312	V312	skewness	skewness
313	V313	kurtosis	kurtosis
314	V314	var	variance
315	V315	median	median
316	V316	percentile10	percentile 10th
317	V317	percentile90	percentile 90th
318	V318	iqr	interquartile range
319	V319	Hrange	range
320	V320	mad	mean absolut deviation
321	V321	rmad	robust mean absolut deviation
322	V322	H_energy	energy
323	V323	H_entropy	entropy
324	V324	rms	root mean square
325	V325	H_uniformity	uniformity
326	V326	energy	energy
327	V327	entropy	entropy
328	V328	contrast	contrast
329	V329	correlation	correlation
330	V330	homogenity	homogeneity
331	V331	homogenity_n	homogeneity normalized
332	V332	idiff	inverese difference
333	V333	idiff_n	inverese difference normalized
334	V334	variance	variance
335	V335	sum_average	sum of average
336	V336	sum_entropy	sum of entropy
337	V337	sum_variance	sum of variance
338	V338	diff_entropy	difference entropy
339	V339	diff_variance	difference variance
340	V340	IMC1	information measures of correlation 1
341	V341	IMC2	information measures of correlation 2
342	V342	MCC	maximal correlation coefficient
343	V343	joint_max	joint maximum
344	V344	joint_average	joint average
345	V345	diff_average	difference average
346	V346	dissimilarity	dissimilarity
347	V347	inverse_variance	inverse variance

348	V348	autocorrelation	autocorrelation
349	V349	clust_tendency	cluster tendency
350	V350	clust_shade	cluster shade
351	V351	clust_prominence	cluster prominence
352	V352	M_energy	energy
353	V353	M_entropy	entropy
354	V354	M_contrast	contrast
355	V355	M_correlation	correlation
356	V356	M_homogenity	homogeneity
357	V357	M_homogenity_n	homogeneity normalized
358	V358	M_idiff	inverese difference
359	V359	M_idiff_n	inverese difference normalized
360	V360	M_variance	variance
361	V361	M_sum_average	sum of average
362	V362	M_sum_entropy	sum of entropy
363	V363	M_sum_variance	sum of variance
364	V364	M_diff_entropy	difference entropy
365	V365	M_diff_variance	difference variance
366	V366	M_IMC1	information measures of correlation 1
367	V367	M_IMC2	information measures of correlation 2
368	V368	M_MCC	maximal correlation coefficient
369	V369	M_joint_max	joint maximum
370	V370	M_joint_average	joint average
371	V371	M_diff_average	difference average
372	V372	M_dissimilarity	dissimilarity
373	V373	M_inverse_variance	inverse variance
374	V374	M_autocorrelation	autocorrelation
375	V375	M_clust_tendency	cluster tendency
376	V376	M_clust_shade	cluster shade
377	V377	M_clust_prominence	cluster prominence
378	V378	coarseness	coarseness
379	V379	neighContrast	contrast
380	V380	busyness	busyness
381	V381	complexity	complexity
382	V382	strength	strength
383	V383	len_intensityVar	grey level non-uniformity
384	V384	len_intensityVar_n	grey level non-uniformity normalized
385	V385	len_sizeVar	zone size non-uniformity
386	V386	len_sizeVar_n	zone size non-uniformity normalized
387	V387	len_sse	short runs emphasis
388	V388	len_lse	long runs emphasis
389	V389	len_lgse	low grey level run emphasis
390	V390	len_hgse	high grey level run emphasis
391	V391	len_sslge	short run low grey level emphasis
392	V392	len_sshge	short run high grey level emphasis
393	V393	len_lslge	long run low grey level emphasis
394	V394	len_lshge	long run high grey level emphasis
395	V395	len_rpc	run percentage
396	V396	len_grey_lev_var	grey level variance
397	V397	len_zone_size_var	run length variance

398	V398	len_size_entropy	run entropy
399	V399	M_len_intensityVar	grey level non-uniformity
400	V400	M_len_intensityVar_n	grey level non-uniformity normalized
401	V401	M_len_sizeVar	zone size non-uniformity
402	V402	M_len_sizeVar_n	zone size non-uniformity normalized
403	V403	M_len_sse	short runs emphasis
404	V404	M_len_lse	long runs emphasis
405	V405	M_len_lgse	low grey level run emphasis
406	V406	M_len_hgse	high grey level run emphasis
407	V407	M_len_sslge	short run low grey level emphasis
408	V408	M_len_sshge	short run high grey level emphasis
409	V409	M_len_lslge	long run low grey level emphasis
410	V410	M_len_lshge	long run high grey level emphasis
411	V411	M_len_rpc	run percentage
412	V412	M_len_grey_lev_var	grey level variance
413	V413	M_len_zone_size_var	run length variance
414	V414	M_len_size_entropy	run entropy
415	V415	intensityVar	grey level non-uniformity
416	V416	intensityVar_n	grey level non-uniformity normalized
417	V417	sizeVar	zone size non-uniformity
418	V418	sizeVar_n	zone size non-uniformity normalized
419	V419	sse	small zone emphasis
420	V420	lse	large zone emphasis
421	V421	lgse	low grey level zone emphasis
422	V422	hgse	high grey level zone emphasis
423	V423	sslge	small zone low grey level emphasis
424	V424	sshge	small zone high grey level emphasis
425	V425	lslge	large zone low grey level emphasis
426	V426	lshge	large zone high grey level emphasis
427	V427	rpc	zone percentage
428	V428	grey_lev_var	grey level variance
429	V429	zone_size_var	zone size variance
430	V430	size_entropy	zone size entropy
431	V431	GLDZM_intensityVar	grey level non-uniformity
432	V432	GLDZM_intensityVar_n	grey level non-uniformity normalized
433	V433	GLDZM_sizeVar	zone size non-uniformity
434	V434	GLDZM_sizeVar_n	zone size non-uniformity normalized
435	V435	GLDZM_sse	small distance emphasis
436	V436	GLDZM_lse	large distance emphasis
437	V437	GLDZM_lgse	low grey level zone emphasis
438	V438	GLDZM_hgse	high grey level zone emphasis
439	V439	GLDZM_sslge	small distance low grey level emphasis
440	V440	GLDZM_sshge	small distance high grey level emphasis
441	V441	GLDZM_lslge	large distance low grey level emphasis
442	V442	GLDZM_lshge	large distance high grey level emphasis
443	V443	GLDZM_rpc	zone percentage
444	V444	GLDZM_grey_lev_var	grey level variance
445	V445	GLDZM_zone_size_var	zone distance variance
446	V446	GLDZM_size_entropy	zone distance entropy
447	V447	NGLDM_intensityVar	grey level non-uniformity

448	V448	NGLDM_intensityVar_n	grey level non-uniformity normalized
449	V449	NGLDM_sizeVar	dependence count non-uniformity
450	V450	NGLDM_sizeVar_n	dependence count non-uniformity normalized
451	V451	NGLDM_sse	low dependence emphasis
452	V452	NGLDM_lse	high dependence emphasis
453	V453	NGLDM_lgse	low grey level count emphasis
454	V454	NGLDM_hgse	high grey level count emphasis
455	V455	NGLDM_sslge	low dependence low grey level emphasis
456	V456	NGLDM_sshge	low dependence high grey level emphasis
457	V457	NGLDM_lslge	high dependence low grey level emphasis
458	V458	NGLDM_lshge	high dependence high grey level emphasis
459	V459	NGLDM_grey_lev_var	grey level variance
460	V460	NGLDM_zone_size_var	dependence count variance
461	V461	NGLDM_size_entropy	dependence count entropy
462	V462	NGLDM_energy	dependence count energy
463	V463	Mean	mean
464	V464	SD	standard deviation
465	V465	COV	coefficient of variation
466	V466	skewness	skewness
467	V467	kurtosis	kurtosis
468	V468	var	variance
469	V469	median	median
470	V470	percentile10	percentile 10th
471	V471	percentile90	percentile 90th
472	V472	iqr	interquartile range
473	V473	Hrange	range
474	V474	mad	mean absolut deviation
475	V475	rmad	robust mean absolut deviation
476	V476	H_energy	energy
477	V477	H_entropy	entropy
478	V478	rms	root mean square
479	V479	H_uniformity	uniformity
480	V480	energy	energy
481	V481	entropy	entropy
482	V482	contrast	contrast
483	V483	correlation	correlation
484	V484	homogenity	homogeneity
485	V485	homogenity_n	homogeneity normalized
486	V486	idiff	inverese difference
487	V487	idiff_n	inverese difference normalized
488	V488	variance	variance
489	V489	sum_average	sum of average
490	V490	sum_entropy	sum of entropy
491	V491	sum_variance	sum of variance
492	V492	diff_entropy	difference entropy
493	V493	diff_variance	difference variance
494	V494	IMC1	information measures of correlation 1
495	V495	IMC2	information measures of correlation 2
496	V496	MCC	maximal correlation coefficient
497	V497	joint_max	joint maximum

498	V498	joint_average	joint average
499	V499	diff_average	difference average
500	V500	dissimilarity	dissimilarity
501	V501	inverse_variance	inverse variance
502	V502	autocorrelation	autocorrelation
503	V503	clust_tendency	cluster tendency
504	V504	clust_shade	cluster shade
505	V505	clust_prominence	cluster prominence
506	V506	M_energy	energy
507	V507	M_entropy	entropy
508	V508	M_contrast	contrast
509	V509	M_correlation	correlation
510	V510	M_homogenity	homogeneity
511	V511	M_homogenity_n	homogeneity normalized
512	V512	M_idiff	inverese difference
513	V513	M_idiff_n	inverese difference normalized
514	V514	M_variance	variance
515	V515	M_sum_average	sum of average
516	V516	M_sum_entropy	sum of entropy
517	V517	M_sum_variance	sum of variance
518	V518	M_diff_entropy	difference entropy
519	V519	M_diff_variance	difference variance
520	V520	M_IMC1	information measures of correlation 1
521	V521	M_IMC2	information measures of correlation 2
522	V522	M_MCC	maximal correlation coefficient
523	V523	M_joint_max	joint maximum
524	V524	M_joint_average	joint average
525	V525	M_diff_average	difference average
526	V526	M_dissimilarity	dissimilarity
527	V527	M_inverse_variance	inverse variance
528	V528	M_autocorrelation	autocorrelation
529	V529	M_clust_tendency	cluster tendency
530	V530	M_clust_shade	cluster shade
531	V531	M_clust_prominence	cluster prominence
532	V532	coarseness	coarseness
533	V533	neighContrast	contrast
534	V534	busyness	busyness
535	V535	complexity	complexity
536	V536	strength	strength
537	V537	len_intensityVar	grey level non-uniformity
538	V538	len_intensityVar_n	grey level non-uniformity normalized
539	V539	len_sizeVar	zone size non-uniformity
540	V540	len_sizeVar_n	zone size non-uniformity normalized
541	V541	len_sse	short runs emphasis
542	V542	len_lse	long runs emphasis
543	V543	len_lgse	low grey level run emphasis
544	V544	len_hgse	high grey level run emphasis
545	V545	len_sslge	short run low grey level emphasis
546	V546	len_sshge	short run high grey level emphasis
547	V547	len_lslge	long run low grey level emphasis

548	V548	len_lshge	long run high grey level emphasis
549	V549	len_rpc	run percentage
550	V550	len_grey_lev_var	grey level variance
551	V551	len_zone_size_var	run length variance
552	V552	len_size_entropy	run entropy
553	V553	M_len_intensityVar	grey level non-uniformity
554	V554	M_len_intensityVar_n	grey level non-uniformity normalized
555	V555	M_len_sizeVar	zone size non-uniformity
556	V556	M_len_sizeVar_n	zone size non-uniformity normalized
557	V557	M_len_sse	short runs emphasis
558	V558	M_len_lse	long runs emphasis
559	V559	M_len_lgse	low grey level run emphasis
560	V560	M_len_hgse	high grey level run emphasis
561	V561	M_len_sslge	short run low grey level emphasis
562	V562	M_len_sshge	short run high grey level emphasis
563	V563	M_len_lslge	long run low grey level emphasis
564	V564	M_len_lshge	long run high grey level emphasis
565	V565	M_len_rpc	run percentage
566	V566	M_len_grey_lev_var	grey level variance
567	V567	M_len_zone_size_var	run length variance
568	V568	M_len_size_entropy	run entropy
569	V569	intensityVar	grey level non-uniformity
570	V570	intensityVar_n	grey level non-uniformity normalized
571	V571	sizeVar	zone size non-uniformity
572	V572	sizeVar_n	zone size non-uniformity normalized
573	V573	sse	small zone emphasis
574	V574	lse	large zone emphasis
575	V575	lgse	low grey level zone emphasis
576	V576	hgse	high grey level zone emphasis
577	V577	sslge	small zone low grey level emphasis
578	V578	sshge	small zone high grey level emphasis
579	V579	lslge	large zone low grey level emphasis
580	V580	lshge	large zone high grey level emphasis
581	V581	rpc	zone percentage
582	V582	grey_lev_var	grey level variance
583	V583	zone_size_var	zone size variance
584	V584	size_entropy	zone size entropy
585	V585	GLDZM_intensityVar	grey level non-uniformity
586	V586	GLDZM_intensityVar_n	grey level non-uniformity normalized
587	V587	GLDZM_sizeVar	zone size non-uniformity
588	V588	GLDZM_sizeVar_n	zone size non-uniformity normalized
589	V589	GLDZM_sse	small distance emphasis
590	V590	GLDZM_lse	large distance emphasis
591	V591	GLDZM_lgse	low grey level zone emphasis
592	V592	GLDZM_hgse	high grey level zone emphasis
593	V593	GLDZM_sslge	small distance low grey level emphasis
594	V594	GLDZM_sshge	small distance high grey level emphasis
595	V595	GLDZM_lslge	large distance low grey level emphasis
596	V596	GLDZM_lshge	large distance high grey level emphasis
597	V597	GLDZM_rpc	zone percentage

598	V598	GLDZM_grey_lev_var	grey level variance
599	V599	GLDZM_zone_size_var	zone distance variance
600	V600	GLDZM_size_entropy	zone distance entropy
601	V601	NGLDM_intensityVar	grey level non-uniformity
602	V602	NGLDM_intensityVar_n	grey level non-uniformity normalized
603	V603	NGLDM_sizeVar	dependence count non-uniformity
604	V604	NGLDM_sizeVar_n	dependence count non-uniformity normalized
605	V605	NGLDM_sse	low dependence emphasis
606	V606	NGLDM_lse	high dependence emphasis
607	V607	NGLDM_lgse	low grey level count emphasis
608	V608	NGLDM_hgse	high grey level count emphasis
609	V609	NGLDM_sslge	low dependence low grey level emphasis
610	V610	NGLDM_sshge	low dependence high grey level emphasis
611	V611	NGLDM_lslge	high dependence low grey level emphasis
612	V612	NGLDM_lshge	high dependence high grey level emphasis
613	V613	NGLDM_grey_lev_var	grey level variance
614	V614	NGLDM_zone_size_var	dependence count variance
615	V615	NGLDM_size_entropy	dependence count entropy
616	V616	NGLDM_energy	dependence count energy
617	V617	Mean	mean
618	V618	SD	standard deviation
619	V619	COV	coefficient of variation
620	V620	skewness	skewness
621	V621	kurtosis	kurtosis
622	V622	var	variance
623	V623	median	median
624	V624	percentile10	percentile 10th
625	V625	percentile90	percentile 90th
626	V626	iqr	interquartile range
627	V627	Hrange	range
628	V628	mad	mean absolut deviation
629	V629	rmad	robust mean absolut deviation
630	V630	H_energy	energy
631	V631	H_entropy	entropy
632	V632	rms	root mean square
633	V633	H_uniformity	uniformity
634	V634	energy	energy
635	V635	entropy	entropy
636	V636	contrast	contrast
637	V637	correlation	correlation
638	V638	homogenity	homogeneity
639	V639	homogenity_n	homogeneity normalized
640	V640	idiff	inverese difference
641	V641	idiff_n	inverese difference normalized
642	V642	variance	variance
643	V643	sum_average	sum of average
644	V644	sum_entropy	sum of entropy
645	V645	sum_variance	sum of variance
646	V646	diff_entropy	difference entropy
647	V647	diff_variance	difference variance

648	V648	IMC1	information measures of correlation 1
649	V649	IMC2	information measures of correlation 2
650	V650	MCC	maximal correlation coefficient
651	V651	joint_max	joint maximum
652	V652	joint_average	joint average
653	V653	diff_average	difference average
654	V654	dissimilarity	dissimilarity
655	V655	inverse_variance	inverse variance
656	V656	autocorrelation	autocorrelation
657	V657	clust_tendency	cluster tendency
658	V658	clust_shade	cluster shade
659	V659	clust_prominence	cluster prominence
660	V660	M_energy	energy
661	V661	M_entropy	entropy
662	V662	M_contrast	contrast
663	V663	M_correlation	correlation
664	V664	M_homogenity	homogeneity
665	V665	M_homogenity_n	homogeneity normalized
666	V666	M_idiff	inverese difference
667	V667	M_idiff_n	inverese difference normalized
668	V668	M_variance	variance
669	V669	M_sum_average	sum of average
670	V670	M_sum_entropy	sum of entropy
671	V671	M_sum_variance	sum of variance
672	V672	M_diff_entropy	difference entropy
673	V673	M_diff_variance	difference variance
674	V674	M_IMC1	information measures of correlation 1
675	V675	M_IMC2	information measures of correlation 2
676	V676	M_MCC	maximal correlation coefficient
677	V677	M_joint_max	joint maximum
678	V678	M_joint_average	joint average
679	V679	M_diff_average	difference average
680	V680	M_dissimilarity	dissimilarity
681	V681	M_inverse_variance	inverse variance
682	V682	M_autocorrelation	autocorrelation
683	V683	M_clust_tendency	cluster tendency
684	V684	M_clust_shade	cluster shade
685	V685	M_clust_prominence	cluster prominence
686	V686	coarseness	coarseness
687	V687	neighContrast	contrast
688	V688	busyness	busyness
689	V689	complexity	complexity
690	V690	strength	strength
691	V691	len_intensityVar	grey level non-uniformity
692	V692	len_intensityVar_n	grey level non-uniformity normalized
693	V693	len_sizeVar	zone size non-uniformity
694	V694	len_sizeVar_n	zone size non-uniformity normalized
695	V695	len_sse	short runs emphasis
696	V696	len_lse	long runs emphasis
697	V697	len_lgse	low grey level run emphasis

698	V698	len_hgse	high grey level run emphasis
699	V699	len_sslge	short run low grey level emphasis
700	V700	len_sshge	short run high grey level emphasis
701	V701	len_lslge	long run low grey level emphasis
702	V702	len_lshge	long run high grey level emphasis
703	V703	len_rpc	run percentage
704	V704	len_grey_lev_var	grey level variance
705	V705	len_zone_size_var	run length variance
706	V706	len_size_entropy	run entropy
707	V707	M_len_intensityVar	grey level non-uniformity
708	V708	M_len_intensityVar_n	grey level non-uniformity normalized
709	V709	M_len_sizeVar	zone size non-uniformity
710	V710	M_len_sizeVar_n	zone size non-uniformity normalized
711	V711	M_len_sse	short runs emphasis
712	V712	M_len_lse	long runs emphasis
713	V713	M_len_lgse	low grey level run emphasis
714	V714	M_len_hgse	high grey level run emphasis
715	V715	M_len_sslge	short run low grey level emphasis
716	V716	M_len_sshge	short run high grey level emphasis
717	V717	M_len_lslge	long run low grey level emphasis
718	V718	M_len_lshge	long run high grey level emphasis
719	V719	M_len_rpc	run percentage
720	V720	M_len_grey_lev_var	grey level variance
721	V721	M_len_zone_size_var	run length variance
722	V722	M_len_size_entropy	run entropy
723	V723	intensityVar	grey level non-uniformity
724	V724	intensityVar_n	grey level non-uniformity normalized
725	V725	sizeVar	zone size non-uniformity
726	V726	sizeVar_n	zone size non-uniformity normalized
727	V727	sse	small zone emphasis
728	V728	lse	large zone emphasis
729	V729	lgse	low grey level zone emphasis
730	V730	hgse	high grey level zone emphasis
731	V731	sslge	small zone low grey level emphasis
732	V732	sshge	small zone high grey level emphasis
733	V733	lslge	large zone low grey level emphasis
734	V734	lshge	large zone high grey level emphasis
735	V735	rpc	zone percentage
736	V736	grey_lev_var	grey level variance
737	V737	zone_size_var	zone size variance
738	V738	size_entropy	zone size entropy
739	V739	GLDZM_intensityVar	grey level non-uniformity
740	V740	GLDZM_intensityVar_n	grey level non-uniformity normalized
741	V741	GLDZM_sizeVar	zone size non-uniformity
742	V742	GLDZM_sizeVar_n	zone size non-uniformity normalized
743	V743	GLDZM_sse	small distance emphasis
744	V744	GLDZM_lse	large distance emphasis
745	V745	GLDZM_lgse	low grey level zone emphasis
746	V746	GLDZM_hgse	high grey level zone emphasis
747	V747	GLDZM_sslge	small distance low grey level emphasis

748	V748	GLDZM_sshge	small distance high grey level emphasis
749	V749	GLDZM_lslge	large distance low grey level emphasis
750	V750	GLDZM_lshge	large distance high grey level emphasis
751	V751	GLDZM_rpc	zone percentage
752	V752	GLDZM_grey_lev_var	grey level variance
753	V753	GLDZM_zone_size_var	zone distance variance
754	V754	GLDZM_size_entropy	zone distance entropy
755	V755	NGLDM_intensityVar	grey level non-uniformity
756	V756	NGLDM_intensityVar_n	grey level non-uniformity normalized
757	V757	NGLDM_sizeVar	dependence count non-uniformity
758	V758	NGLDM_sizeVar_n	dependence count non-uniformity normalized
759	V759	NGLDM_sse	low dependence emphasis
760	V760	NGLDM_lse	high dependence emphasis
761	V761	NGLDM_lgse	low grey level count emphasis
762	V762	NGLDM_hgse	high grey level count emphasis
763	V763	NGLDM_sslge	low dependence low grey level emphasis
764	V764	NGLDM_sshge	low dependence high grey level emphasis
765	V765	NGLDM_lslge	high dependence low grey level emphasis
766	V766	NGLDM_lshge	high dependence high grey level emphasis
767	V767	NGLDM_grey_lev_var	grey level variance
768	V768	NGLDM_zone_size_var	dependence count variance
769	V769	NGLDM_size_entropy	dependence count entropy
770	V770	NGLDM_energy	dependence count energy
771	V771	Mean	mean
772	V772	SD	standard deviation
773	V773	COV	coefficient of variation
774	V774	skewness	skewness
775	V775	kurtosis	kurtosis
776	V776	var	variance
777	V777	median	median
778	V778	percentile10	percentile 10th
779	V779	percentile90	percentile 90th
780	V780	iqr	interquartile range
781	V781	Hrange	range
782	V782	mad	mean absolut deviation
783	V783	rmad	robust mean absolut deviation
784	V784	H_energy	energy
785	V785	H_entropy	entropy
786	V786	rms	root mean square
787	V787	H_uniformity	uniformity
788	V788	energy	energy
789	V789	entropy	entropy
790	V790	contrast	contrast
791	V791	correlation	correlation
792	V792	homogenity	homogeneity
793	V793	homogenity_n	homogeneity normalized
794	V794	idiff	inverese difference
795	V795	idiff_n	inverese difference normalized
796	V796	variance	variance
797	V797	sum_average	sum of average

798	V798	sum_entropy	sum of entropy
799	V799	sum_variance	sum of variance
800	V800	diff_entropy	difference entropy
801	V801	diff_variance	difference variance
802	V802	IMC1	information measures of correlation 1
803	V803	IMC2	information measures of correlation 2
804	V804	MCC	maximal correlation coefficient
805	V805	joint_max	joint maximum
806	V806	joint_average	joint average
807	V807	diff_average	difference average
808	V808	dissimilarity	dissimilarity
809	V809	inverse_variance	inverse variance
810	V810	autocorrelation	autocorrelation
811	V811	clust_tendency	cluster tendency
812	V812	clust_shade	cluster shade
813	V813	clust_prominence	cluster prominence
814	V814	M_energy	energy
815	V815	M_entropy	entropy
816	V816	M_contrast	contrast
817	V817	M_correlation	correlation
818	V818	M_homogenity	homogeneity
819	V819	M_homogenity_n	homogeneity normalized
820	V820	M_idiff	inverese difference
821	V821	M_idiff_n	inverese difference normalized
822	V822	M_variance	variance
823	V823	M_sum_average	sum of average
824	V824	M_sum_entropy	sum of entropy
825	V825	M_sum_variance	sum of variance
826	V826	M_diff_entropy	difference entropy
827	V827	M_diff_variance	difference variance
828	V828	M_IMC1	information measures of correlation 1
829	V829	M_IMC2	information measures of correlation 2
830	V830	M_MCC	maximal correlation coefficient
831	V831	M_joint_max	joint maximum
832	V832	M_joint_average	joint average
833	V833	M_diff_average	difference average
834	V834	M_dissimilarity	dissimilarity
835	V835	M_inverse_variance	inverse variance
836	V836	M_autocorrelation	autocorrelation
837	V837	M_clust_tendency	cluster tendency
838	V838	M_clust_shade	cluster shade
839	V839	M_clust_prominence	cluster prominence
840	V840	coarseness	coarseness
841	V841	neighContrast	contrast
842	V842	busyness	busyness
843	V843	complexity	complexity
844	V844	strength	strength
845	V845	len_intensityVar	grey level non-uniformity
846	V846	len_intensityVar_n	grey level non-uniformity normalized
847	V847	len_sizeVar	zone size non-uniformity

848	V848	len_sizeVar_n	zone size non-uniformity normalized
849	V849	len_sse	short runs emphasis
850	V850	len_lse	long runs emphasis
851	V851	len_lgse	low grey level run emphasis
852	V852	len_hgse	high grey level run emphasis
853	V853	len_sslge	short run low grey level emphasis
854	V854	len_sshge	short run high grey level emphasis
855	V855	len_lslge	long run low grey level emphasis
856	V856	len_lshge	long run high grey level emphasis
857	V857	len_rpc	run percentage
858	V858	len_grey_lev_var	grey level variance
859	V859	len_zone_size_var	run length variance
860	V860	len_size_entropy	run entropy
861	V861	M_len_intensityVar	grey level non-uniformity
862	V862	M_len_intensityVar_n	grey level non-uniformity normalized
863	V863	M_len_sizeVar	zone size non-uniformity
864	V864	M_len_sizeVar_n	zone size non-uniformity normalized
865	V865	M_len_sse	short runs emphasis
866	V866	M_len_lse	long runs emphasis
867	V867	M_len_lgse	low grey level run emphasis
868	V868	M_len_hgse	high grey level run emphasis
869	V869	M_len_sslge	short run low grey level emphasis
870	V870	M_len_sshge	short run high grey level emphasis
871	V871	M_len_lslge	long run low grey level emphasis
872	V872	M_len_lshge	long run high grey level emphasis
873	V873	M_len_rpc	run percentage
874	V874	M_len_grey_lev_var	grey level variance
875	V875	M_len_zone_size_var	run length variance
876	V876	M_len_size_entropy	run entropy
877	V877	intensityVar	grey level non-uniformity
878	V878	intensityVar_n	grey level non-uniformity normalized
879	V879	sizeVar	zone size non-uniformity
880	V880	sizeVar_n	zone size non-uniformity normalized
881	V881	sse	small zone emphasis
882	V882	lse	large zone emphasis
883	V883	lgse	low grey level zone emphasis
884	V884	hgse	high grey level zone emphasis
885	V885	sslge	small zone low grey level emphasis
886	V886	sshge	small zone high grey level emphasis
887	V887	lslge	large zone low grey level emphasis
888	V888	lshge	large zone high grey level emphasis
889	V889	rpc	zone percentage
890	V890	grey_lev_var	grey level variance
891	V891	zone_size_var	zone size variance
892	V892	size_entropy	zone size entropy
893	V893	GLDZM_intensityVar	grey level non-uniformity
894	V894	GLDZM_intensityVar_n	grey level non-uniformity normalized
895	V895	GLDZM_sizeVar	zone size non-uniformity
896	V896	GLDZM_sizeVar_n	zone size non-uniformity normalized
897	V897	GLDZM_sse	small distance emphasis

898	V898	GLDZM_lse	large distance emphasis
899	V899	GLDZM_lgse	low grey level zone emphasis
900	V900	GLDZM_hgse	high grey level zone emphasis
901	V901	GLDZM_sslge	small distance low grey level emphasis
902	V902	GLDZM_sshge	small distance high grey level emphasis
903	V903	GLDZM_lslge	large distance low grey level emphasis
904	V904	GLDZM_lshge	large distance high grey level emphasis
905	V905	GLDZM_rpc	zone percentage
906	V906	GLDZM_grey_lev_var	grey level variance
907	V907	GLDZM_zone_size_var	zone distance variance
908	V908	GLDZM_size_entropy	zone distance entropy
909	V909	NGLDM_intensityVar	grey level non-uniformity
910	V910	NGLDM_intensityVar_n	grey level non-uniformity normalized
911	V911	NGLDM_sizeVar	dependence count non-uniformity
912	V912	NGLDM_sizeVar_n	dependence count non-uniformity normalized
913	V913	NGLDM_sse	low dependence emphasis
914	V914	NGLDM_lse	high dependence emphasis
915	V915	NGLDM_lgse	low grey level count emphasis
916	V916	NGLDM_hgse	high grey level count emphasis
917	V917	NGLDM_sslge	low dependence low grey level emphasis
918	V918	NGLDM_sshge	low dependence high grey level emphasis
919	V919	NGLDM_lslge	high dependence low grey level emphasis
920	V920	NGLDM_lshge	high dependence high grey level emphasis
921	V921	NGLDM_grey_lev_var	grey level variance
922	V922	NGLDM_zone_size_var	dependence count variance
923	V923	NGLDM_size_entropy	dependence count entropy
924	V924	NGLDM_energy	dependence count energy
925	V925	Mean	mean
926	V926	SD	standard deviation
927	V927	COV	coefficient of variation
928	V928	skewness	skewness
929	V929	kurtosis	kurtosis
930	V930	var	variance
931	V931	median	median
932	V932	percentile10	percentile 10th
933	V933	percentile90	percentile 90th
934	V934	iqr	interquartile range
935	V935	Hrange	range
936	V936	mad	mean absolut deviation
937	V937	rmad	robust mean absolut deviation
938	V938	H_energy	energy
939	V939	H_entropy	entropy
940	V940	rms	root mean square
941	V941	H_uniformity	uniformity
942	V942	energy	energy
943	V943	entropy	entropy
944	V944	contrast	contrast
945	V945	correlation	correlation
946	V946	homogenity	homogeneity
947	V947	homogenity_n	homogeneity normalized

948	V948	idiff	inverese difference
949	V949	idiff_n	inverese difference normalized
950	V950	variance	variance
951	V951	sum_average	sum of average
952	V952	sum_entropy	sum of entropy
953	V953	sum_variance	sum of variance
954	V954	diff_entropy	difference entropy
955	V955	diff_variance	difference variance
956	V956	IMC1	information measures of correlation 1
957	V957	IMC2	information measures of correlation 2
958	V958	MCC	maximal correlation coefficient
959	V959	joint_max	joint maximum
960	V960	joint_average	joint average
961	V961	diff_average	difference average
962	V962	dissimilarity	dissimilarity
963	V963	inverse_variance	inverse variance
964	V964	autocorrelation	autocorrelation
965	V965	clust_tendency	cluster tendency
966	V966	clust_shade	cluster shade
967	V967	clust_prominence	cluster prominence
968	V968	M_energy	energy
969	V969	M_entropy	entropy
970	V970	M_contrast	contrast
971	V971	M_correlation	correlation
972	V972	M_homogenity	homogeneity
973	V973	M_homogenity_n	homogeneity normalized
974	V974	M_idiff	inverese difference
975	V975	M_idiff_n	inverese difference normalized
976	V976	M_variance	variance
977	V977	M_sum_average	sum of average
978	V978	M_sum_entropy	sum of entropy
979	V979	M_sum_variance	sum of variance
980	V980	M_diff_entropy	difference entropy
981	V981	M_diff_variance	difference variance
982	V982	M_IMC1	information measures of correlation 1
983	V983	M_IMC2	information measures of correlation 2
984	V984	M_MCC	maximal correlation coefficient
985	V985	M_joint_max	joint maximum
986	V986	M_joint_average	joint average
987	V987	M_diff_average	difference average
988	V988	M_dissimilarity	dissimilarity
989	V989	M_inverse_variance	inverse variance
990	V990	M_autocorrelation	autocorrelation
991	V991	M_clust_tendency	cluster tendency
992	V992	M_clust_shade	cluster shade
993	V993	M_clust_prominence	cluster prominence
994	V994	coarseness	coarseness
995	V995	neighContrast	contrast
996	V996	busyness	busyness
997	V997	complexity	complexity

998	V998	strength	strength
999	V999	len_intensityVar	grey level non-uniformity
1000	V1000	len_intensityVar_n	grey level non-uniformity normalized
1001	V1001	len_sizeVar	zone size non-uniformity
1002	V1002	len_sizeVar_n	zone size non-uniformity normalized
1003	V1003	len_sse	short runs emphasis
1004	V1004	len_lse	long runs emphasis
1005	V1005	len_lgse	low grey level run emphasis
1006	V1006	len_hgse	high grey level run emphasis
1007	V1007	len_sslge	short run low grey level emphasis
1008	V1008	len_sshge	short run high grey level emphasis
1009	V1009	len_lslge	long run low grey level emphasis
1010	V1010	len_lshge	long run high grey level emphasis
1011	V1011	len_rpc	run percentage
1012	V1012	len_grey_lev_var	grey level variance
1013	V1013	len_zone_size_var	run length variance
1014	V1014	len_size_entropy	run entropy
1015	V1015	M_len_intensityVar	grey level non-uniformity
1016	V1016	M_len_intensityVar_n	grey level non-uniformity normalized
1017	V1017	M_len_sizeVar	zone size non-uniformity
1018	V1018	M_len_sizeVar_n	zone size non-uniformity normalized
1019	V1019	M_len_sse	short runs emphasis
1020	V1020	M_len_lse	long runs emphasis
1021	V1021	M_len_lgse	low grey level run emphasis
1022	V1022	M_len_hgse	high grey level run emphasis
1023	V1023	M_len_sslge	short run low grey level emphasis
1024	V1024	M_len_sshge	short run high grey level emphasis
1025	V1025	M_len_lslge	long run low grey level emphasis
1026	V1026	M_len_lshge	long run high grey level emphasis
1027	V1027	M_len_rpc	run percentage
1028	V1028	M_len_grey_lev_var	grey level variance
1029	V1029	M_len_zone_size_var	run length variance
1030	V1030	M_len_size_entropy	run entropy
1031	V1031	intensityVar	grey level non-uniformity
1032	V1032	intensityVar_n	grey level non-uniformity normalized
1033	V1033	sizeVar	zone size non-uniformity
1034	V1034	sizeVar_n	zone size non-uniformity normalized
1035	V1035	sse	small zone emphasis
1036	V1036	lse	large zone emphasis
1037	V1037	lgse	low grey level zone emphasis
1038	V1038	hgse	high grey level zone emphasis
1039	V1039	sslge	small zone low grey level emphasis
1040	V1040	sshge	small zone high grey level emphasis
1041	V1041	lslge	large zone low grey level emphasis
1042	V1042	lshge	large zone high grey level emphasis
1043	V1043	rpc	zone percentage
1044	V1044	grey_lev_var	grey level variance
1045	V1045	zone_size_var	zone size variance
1046	V1046	size_entropy	zone size entropy
1047	V1047	GLDZM_intensityVar	grey level non-uniformity

1048	V1048	GLDZM_intensityVar_n	grey level non-uniformity normalized
1049	V1049	GLDZM_sizeVar	zone size non-uniformity
1050	V1050	GLDZM_sizeVar_n	zone size non-uniformity normalized
1051	V1051	GLDZM_sse	small distance emphasis
1052	V1052	GLDZM_lse	large distance emphasis
1053	V1053	GLDZM_lgse	low grey level zone emphasis
1054	V1054	GLDZM_hgse	high grey level zone emphasis
1055	V1055	GLDZM_sslge	small distance low grey level emphasis
1056	V1056	GLDZM_sshge	small distance high grey level emphasis
1057	V1057	GLDZM_lslge	large distance low grey level emphasis
1058	V1058	GLDZM_lshge	large distance high grey level emphasis
1059	V1059	GLDZM_rpc	zone percentage
1060	V1060	GLDZM_grey_lev_var	grey level variance
1061	V1061	GLDZM_zone_size_var	zone distance variance
1062	V1062	GLDZM_size_entropy	zone distance entropy
1063	V1063	NGLDM_intensityVar	grey level non-uniformity
1064	V1064	NGLDM_intensityVar_n	grey level non-uniformity normalized
1065	V1065	NGLDM_sizeVar	dependence count non-uniformity
1066	V1066	NGLDM_sizeVar_n	dependence count non-uniformity normalized
1067	V1067	NGLDM_sse	low dependence emphasis
1068	V1068	NGLDM_lse	high dependence emphasis
1069	V1069	NGLDM_lgse	low grey level count emphasis
1070	V1070	NGLDM_hgse	high grey level count emphasis
1071	V1071	NGLDM_sslge	low dependence low grey level emphasis
1072	V1072	NGLDM_sshge	low dependence high grey level emphasis
1073	V1073	NGLDM_lslge	high dependence low grey level emphasis
1074	V1074	NGLDM_lshge	high dependence high grey level emphasis
1075	V1075	NGLDM_grey_lev_var	grey level variance
1076	V1076	NGLDM_zone_size_var	dependence count variance
1077	V1077	NGLDM_size_entropy	dependence count entropy
1078	V1078	NGLDM_energy	dependence count energy
1079	V1079	Mean	mean
1080	V1080	SD	standard deviation
1081	V1081	COV	coefficient of variation
1082	V1082	skewness	skewness
1083	V1083	kurtosis	kurtosis
1084	V1084	var	variance
1085	V1085	median	median
1086	V1086	percentile10	percentile 10th
1087	V1087	percentile90	percentile 90th
1088	V1088	iqr	interquartile range
1089	V1089	Hrange	range
1090	V1090	mad	mean absolut deviation
1091	V1091	rmad	robust mean absolut deviation
1092	V1092	H_energy	energy
1093	V1093	H_entropy	entropy
1094	V1094	rms	root mean square
1095	V1095	H_uniformity	uniformity
1096	V1096	energy	energy
1097	V1097	entropy	entropy

1098	V1098	contrast	contrast
1099	V1099	correlation	correlation
1100	V1100	homogenity	homogeneity
1101	V1101	homogenity_n	homogeneity normalized
1102	V1102	idiff	inverese difference
1103	V1103	idiff_n	inverese difference normalized
1104	V1104	variance	variance
1105	V1105	sum_average	sum of average
1106	V1106	sum_entropy	sum of entropy
1107	V1107	sum_variance	sum of variance
1108	V1108	diff_entropy	difference entropy
1109	V1109	diff_variance	difference variance
1110	V1110	IMC1	information measures of correlation 1
1111	V1111	IMC2	information measures of correlation 2
1112	V1112	MCC	maximal correlation coefficient
1113	V1113	joint_max	joint maximum
1114	V1114	joint_average	joint average
1115	V1115	diff_average	difference average
1116	V1116	dissimilarity	dissimilarity
1117	V1117	inverse_variance	inverse variance
1118	V1118	autocorrelation	autocorrelation
1119	V1119	clust_tendency	cluster tendency
1120	V1120	clust_shade	cluster shade
1121	V1121	clust_prominence	cluster prominence
1122	V1122	M_energy	energy
1123	V1123	M_entropy	entropy
1124	V1124	M_contrast	contrast
1125	V1125	M_correlation	correlation
1126	V1126	M_homogenity	homogeneity
1127	V1127	M_homogenity_n	homogeneity normalized
1128	V1128	M_idiff	inverese difference
1129	V1129	M_idiff_n	inverese difference normalized
1130	V1130	M_variance	variance
1131	V1131	M_sum_average	sum of average
1132	V1132	M_sum_entropy	sum of entropy
1133	V1133	M_sum_variance	sum of variance
1134	V1134	M_diff_entropy	difference entropy
1135	V1135	M_diff_variance	difference variance
1136	V1136	M_IMC1	information measures of correlation 1
1137	V1137	M_IMC2	information measures of correlation 2
1138	V1138	M_MCC	maximal correlation coefficient
1139	V1139	M_joint_max	joint maximum
1140	V1140	M_joint_average	joint average
1141	V1141	M_diff_average	difference average
1142	V1142	M_dissimilarity	dissimilarity
1143	V1143	M_inverse_variance	inverse variance
1144	V1144	M_autocorrelation	autocorrelation
1145	V1145	M_clust_tendency	cluster tendency
1146	V1146	M_clust_shade	cluster shade
1147	V1147	M_clust_prominence	cluster prominence

1148	V1148	coarseness	coarseness
1149	V1149	neighContrast	contrast
1150	V1150	busyness	busyness
1151	V1151	complexity	complexity
1152	V1152	strength	strength
1153	V1153	len_intensityVar	grey level non-uniformity
1154	V1154	len_intensityVar_n	grey level non-uniformity normalized
1155	V1155	len_sizeVar	zone size non-uniformity
1156	V1156	len_sizeVar_n	zone size non-uniformity normalized
1157	V1157	len_sse	short runs emphasis
1158	V1158	len_lse	long runs emphasis
1159	V1159	len_lgse	low grey level run emphasis
1160	V1160	len_hgse	high grey level run emphasis
1161	V1161	len_sslge	short run low grey level emphasis
1162	V1162	len_sshge	short run high grey level emphasis
1163	V1163	len_lslge	long run low grey level emphasis
1164	V1164	len_lshge	long run high grey level emphasis
1165	V1165	len_rpc	run percentage
1166	V1166	len_grey_lev_var	grey level variance
1167	V1167	len_zone_size_var	run length variance
1168	V1168	len_size_entropy	run entropy
1169	V1169	M_len_intensityVar	grey level non-uniformity
1170	V1170	M_len_intensityVar_n	grey level non-uniformity normalized
1171	V1171	M_len_sizeVar	zone size non-uniformity
1172	V1172	M_len_sizeVar_n	zone size non-uniformity normalized
1173	V1173	M_len_sse	short runs emphasis
1174	V1174	M_len_lse	long runs emphasis
1175	V1175	M_len_lgse	low grey level run emphasis
1176	V1176	M_len_hgse	high grey level run emphasis
1177	V1177	M_len_sslge	short run low grey level emphasis
1178	V1178	M_len_sshge	short run high grey level emphasis
1179	V1179	M_len_lslge	long run low grey level emphasis
1180	V1180	M_len_lshge	long run high grey level emphasis
1181	V1181	M_len_rpc	run percentage
1182	V1182	M_len_grey_lev_var	grey level variance
1183	V1183	M_len_zone_size_var	run length variance
1184	V1184	M_len_size_entropy	run entropy
1185	V1185	intensityVar	grey level non-uniformity
1186	V1186	intensityVar_n	grey level non-uniformity normalized
1187	V1187	sizeVar	zone size non-uniformity
1188	V1188	sizeVar_n	zone size non-uniformity normalized
1189	V1189	sse	small zone emphasis
1190	V1190	lse	large zone emphasis
1191	V1191	lgse	low grey level zone emphasis
1192	V1192	hgse	high grey level zone emphasis
1193	V1193	sslge	small zone low grey level emphasis
1194	V1194	sshge	small zone high grey level emphasis
1195	V1195	lslge	large zone low grey level emphasis
1196	V1196	lshge	large zone high grey level emphasis
1197	V1197	rpc	zone percentage

1198	V1198	grey_lev_var	grey level variance
1199	V1199	zone_size_var	zone size variance
1200	V1200	size_entropy	zone size entropy
1201	V1201	GLDZM_intensityVar	grey level non-uniformity
1202	V1202	GLDZM_intensityVar_n	grey level non-uniformity normalized
1203	V1203	GLDZM_sizeVar	zone size non-uniformity
1204	V1204	GLDZM_sizeVar_n	zone size non-uniformity normalized
1205	V1205	GLDZM_sse	small distance emphasis
1206	V1206	GLDZM_lse	large distance emphasis
1207	V1207	GLDZM_lgse	low grey level zone emphasis
1208	V1208	GLDZM_hgse	high grey level zone emphasis
1209	V1209	GLDZM_sslge	small distance low grey level emphasis
1210	V1210	GLDZM_sshge	small distance high grey level emphasis
1211	V1211	GLDZM_lslge	large distance low grey level emphasis
1212	V1212	GLDZM_lshge	large distance high grey level emphasis
1213	V1213	GLDZM_rpc	zone percentage
1214	V1214	GLDZM_grey_lev_var	grey level variance
1215	V1215	GLDZM_zone_size_var	zone distance variance
1216	V1216	GLDZM_size_entropy	zone distance entropy
1217	V1217	NGLDM_intensityVar	grey level non-uniformity
1218	V1218	NGLDM_intensityVar_n	grey level non-uniformity normalized
1219	V1219	NGLDM_sizeVar	dependence count non-uniformity
1220	V1220	NGLDM_sizeVar_n	dependence count non-uniformity normalized
1221	V1221	NGLDM_sse	low dependence emphasis
1222	V1222	NGLDM_lse	high dependence emphasis
1223	V1223	NGLDM_lgse	low grey level count emphasis
1224	V1224	NGLDM_hgse	high grey level count emphasis
1225	V1225	NGLDM_sslge	low dependence low grey level emphasis
1226	V1226	NGLDM_sshge	low dependence high grey level emphasis
1227	V1227	NGLDM_lslge	high dependence low grey level emphasis
1228	V1228	NGLDM_lshge	high dependence high grey level emphasis
1229	V1229	NGLDM_grey_lev_var	grey level variance
1230	V1230	NGLDM_zone_size_var	dependence count variance
1231	V1231	NGLDM_size_entropy	dependence count entropy
1232	V1232	NGLDM_energy	dependence count energy
1233	V1233	Mean	mean
1234	V1234	SD	standard deviation
1235	V1235	COV	coefficient of variation
1236	V1236	skewness	skewness
1237	V1237	kurtosis	kurtosis
1238	V1238	var	variance
1239	V1239	median	median
1240	V1240	percentile10	percentile 10th
1241	V1241	percentile90	percentile 90th
1242	V1242	iqr	interquartile range
1243	V1243	Hrange	range
1244	V1244	mad	mean absolut deviation
1245	V1245	rmad	robust mean absolut deviation
1246	V1246	H_energy	energy
1247	V1247	H_entropy	entropy

1248	V1248	rms	root mean square
1249	V1249	H_uniformity	uniformity
1250	V1250	energy	energy
1251	V1251	entropy	entropy
1252	V1252	contrast	contrast
1253	V1253	correlation	correlation
1254	V1254	homogenity	homogeneity
1255	V1255	homogenity_n	homogeneity normalized
1256	V1256	idiff	inverese difference
1257	V1257	idiff_n	inverese difference normalized
1258	V1258	variance	variance
1259	V1259	sum_average	sum of average
1260	V1260	sum_entropy	sum of entropy
1261	V1261	sum_variance	sum of variance
1262	V1262	diff_entropy	difference entropy
1263	V1263	diff_variance	difference variance
1264	V1264	IMC1	information measures of correlation 1
1265	V1265	IMC2	information measures of correlation 2
1266	V1266	MCC	maximal correlation coefficient
1267	V1267	joint_max	joint maximum
1268	V1268	joint_average	joint average
1269	V1269	diff_average	difference average
1270	V1270	dissimilarity	dissimilarity
1271	V1271	inverse_variance	inverse variance
1272	V1272	autocorrelation	autocorrelation
1273	V1273	clust_tendency	cluster tendency
1274	V1274	clust_shade	cluster shade
1275	V1275	clust_prominence	cluster prominence
1276	V1276	M_energy	energy
1277	V1277	M_entropy	entropy
1278	V1278	M_contrast	contrast
1279	V1279	M_correlation	correlation
1280	V1280	M_homogenity	homogeneity
1281	V1281	M_homogenity_n	homogeneity normalized
1282	V1282	M_idiff	inverese difference
1283	V1283	M_idiff_n	inverese difference normalized
1284	V1284	M_variance	variance
1285	V1285	M_sum_average	sum of average
1286	V1286	M_sum_entropy	sum of entropy
1287	V1287	M_sum_variance	sum of variance
1288	V1288	M_diff_entropy	difference entropy
1289	V1289	M_diff_variance	difference variance
1290	V1290	M_IMC1	information measures of correlation 1
1291	V1291	M_IMC2	information measures of correlation 2
1292	V1292	M_MCC	maximal correlation coefficient
1293	V1293	M_joint_max	joint maximum
1294	V1294	M_joint_average	joint average
1295	V1295	M_diff_average	difference average
1296	V1296	M_dissimilarity	dissimilarity
1297	V1297	M_inverse_variance	inverse variance

1298	V1298	M_autocorrelation	autocorrelation
1299	V1299	M_clust_tendency	cluster tendency
1300	V1300	M_clust_shade	cluster shade
1301	V1301	M_clust_prominence	cluster prominence
1302	V1302	coarseness	coarseness
1303	V1303	neighContrast	contrast
1304	V1304	busyness	busyness
1305	V1305	complexity	complexity
1306	V1306	strength	strength
1307	V1307	len_intensityVar	grey level non-uniformity
1308	V1308	len_intensityVar_n	grey level non-uniformity normalized
1309	V1309	len_sizeVar	zone size non-uniformity
1310	V1310	len_sizeVar_n	zone size non-uniformity normalized
1311	V1311	len_sse	short runs emphasis
1312	V1312	len_lse	long runs emphasis
1313	V1313	len_lgse	low grey level run emphasis
1314	V1314	len_hgse	high grey level run emphasis
1315	V1315	len_sslge	short run low grey level emphasis
1316	V1316	len_sshge	short run high grey level emphasis
1317	V1317	len_lslge	long run low grey level emphasis
1318	V1318	len_lshge	long run high grey level emphasis
1319	V1319	len_rpc	run percentage
1320	V1320	len_grey_lev_var	grey level variance
1321	V1321	len_zone_size_var	run length variance
1322	V1322	len_size_entropy	run entropy
1323	V1323	M_len_intensityVar	grey level non-uniformity
1324	V1324	M_len_intensityVar_n	grey level non-uniformity normalized
1325	V1325	M_len_sizeVar	zone size non-uniformity
1326	V1326	M_len_sizeVar_n	zone size non-uniformity normalized
1327	V1327	M_len_sse	short runs emphasis
1328	V1328	M_len_lse	long runs emphasis
1329	V1329	M_len_lgse	low grey level run emphasis
1330	V1330	M_len_hgse	high grey level run emphasis
1331	V1331	M_len_sslge	short run low grey level emphasis
1332	V1332	M_len_sshge	short run high grey level emphasis
1333	V1333	M_len_lslge	long run low grey level emphasis
1334	V1334	M_len_lshge	long run high grey level emphasis
1335	V1335	M_len_rpc	run percentage
1336	V1336	M_len_grey_lev_var	grey level variance
1337	V1337	M_len_zone_size_var	run length variance
1338	V1338	M_len_size_entropy	run entropy
1339	V1339	intensityVar	grey level non-uniformity
1340	V1340	intensityVar_n	grey level non-uniformity normalized
1341	V1341	sizeVar	zone size non-uniformity
1342	V1342	sizeVar_n	zone size non-uniformity normalized
1343	V1343	sse	small zone emphasis
1344	V1344	lse	large zone emphasis
1345	V1345	lgse	low grey level zone emphasis
1346	V1346	hgse	high grey level zone emphasis
1347	V1347	sslge	small zone low grey level emphasis

1348	V1348	sshge	small zone high grey level emphasis
1349	V1349	lslge	large zone low grey level emphasis
1350	V1350	lshge	large zone high grey level emphasis
1351	V1351	rpc	zone percentage
1352	V1352	grey_lev_var	grey level variance
1353	V1353	zone_size_var	zone size variance
1354	V1354	size_entropy	zone size entropy
1355	V1355	GLDZM_intensityVar	grey level non-uniformity
1356	V1356	GLDZM_intensityVar_n	grey level non-uniformity normalized
1357	V1357	GLDZM_sizeVar	zone size non-uniformity
1358	V1358	GLDZM_sizeVar_n	zone size non-uniformity normalized
1359	V1359	GLDZM_sse	small distance emphasis
1360	V1360	GLDZM_lse	large distance emphasis
1361	V1361	GLDZM_lgse	low grey level zone emphasis
1362	V1362	GLDZM_hgse	high grey level zone emphasis
1363	V1363	GLDZM_sslge	small distance low grey level emphasis
1364	V1364	GLDZM_sshge	small distance high grey level emphasis
1365	V1365	GLDZM_lslge	large distance low grey level emphasis
1366	V1366	GLDZM_lshge	large distance high grey level emphasis
1367	V1367	GLDZM_rpc	zone percentage
1368	V1368	GLDZM_grey_lev_var	grey level variance
1369	V1369	GLDZM_zone_size_var	zone distance variance
1370	V1370	GLDZM_size_entropy	zone distance entropy
1371	V1371	NGLDM_intensityVar	grey level non-uniformity
1372	V1372	NGLDM_intensityVar_n	grey level non-uniformity normalized
1373	V1373	NGLDM_sizeVar	dependence count non-uniformity
1374	V1374	NGLDM_sizeVar_n	dependence count non-uniformity normalized
1375	V1375	NGLDM_sse	low dependence emphasis
1376	V1376	NGLDM_lse	high dependence emphasis
1377	V1377	NGLDM_lgse	low grey level count emphasis
1378	V1378	NGLDM_hgse	high grey level count emphasis
1379	V1379	NGLDM_sslge	low dependence low grey level emphasis
1380	V1380	NGLDM_sshge	low dependence high grey level emphasis
1381	V1381	NGLDM_lslge	high dependence low grey level emphasis
1382	V1382	NGLDM_lshge	high dependence high grey level emphasis
1383	V1383	NGLDM_grey_lev_var	grey level variance
1384	V1384	NGLDM_zone_size_var	dependence count variance
1385	V1385	NGLDM_size_entropy	dependence count entropy
1386	V1386	NGLDM_energy	dependence count energy
1387			
1388			
1389			
1390			
1391			
1392			
1393			
1394			
1395			
1396			
1397			

General Type	SubType	FeatureType
Intensity	Intensity	Unfiltered
Intensity	Intensity	Unfiltered
Intensity	Intensity	Unfiltered
Intensity	Intensity	Unfiltered
Intensity	Intensity	Unfiltered
Intensity	Intensity	Unfiltered
Intensity	Intensity	Unfiltered
Intensity	Intensity	Unfiltered
Intensity	Intensity	Unfiltered
Intensity	Intensity	Unfiltered
Intensity	Intensity	Unfiltered
Intensity	Intensity	Unfiltered
Intensity	Intensity	Unfiltered
Intensity	Intensity	Unfiltered
Intensity	Intensity	Unfiltered
Intensity	Intensity	Unfiltered
Intensity	Intensity	Unfiltered
Texture	GLCM	Unfiltered
Texture	GLCM	Unfiltered
Texture	GLCM	Unfiltered
Texture	GLCM	Unfiltered
Texture	GLCM	Unfiltered
Texture	GLCM	Unfiltered
Texture	GLCM	Unfiltered
Texture	GLCM	Unfiltered
Texture	GLCM	Unfiltered
Texture	GLCM	Unfiltered
Texture	GLCM	Unfiltered
Texture	GLCM	Unfiltered
Texture	GLCM	Unfiltered
Texture	GLCM	Unfiltered
Texture	GLCM	Unfiltered
Texture	GLCM	Unfiltered
Texture	GLCM	Unfiltered
Texture	GLCM	Unfiltered
Texture	GLCM	Unfiltered
Texture	GLCM	Unfiltered
Texture	GLCM	Unfiltered
Texture	GLCM	Unfiltered
Texture	GLCM	Unfiltered
Texture	GLCM	Unfiltered
Texture	GLCM	Unfiltered
Texture	GLCM	Unfiltered
Texture	mGLCM	Unfiltered
Texture	mGLCM	Unfiltered
Texture	mGLCM	Unfiltered
Texture	mGLCM	Unfiltered

Texture	mGLCM	Unfiltered
Texture	mGLCM	Unfiltered
Texture	mGLCM	Unfiltered
Texture	mGLCM	Unfiltered
Texture	mGLCM	Unfiltered
Texture	mGLCM	Unfiltered
Texture	mGLCM	Unfiltered
Texture	mGLCM	Unfiltered
Texture	mGLCM	Unfiltered
Texture	mGLCM	Unfiltered
Texture	mGLCM	Unfiltered
Texture	mGLCM	Unfiltered
Texture	mGLCM	Unfiltered
Texture	mGLCM	Unfiltered
Texture	mGLCM	Unfiltered
Texture	mGLCM	Unfiltered
Texture	mGLCM	Unfiltered
Texture	mGLCM	Unfiltered
Texture	mGLCM	Unfiltered
Texture	mGLCM	Unfiltered
Texture	mGLCM	Unfiltered
Texture	mGLCM	Unfiltered
Texture	NGTDM	Unfiltered
Texture	NGTDM	Unfiltered
Texture	NGTDM	Unfiltered
Texture	NGTDM	Unfiltered
Texture	NGTDM	Unfiltered
Texture	GLRLM	Unfiltered
Texture	GLRLM	Unfiltered
Texture	GLRLM	Unfiltered
Texture	GLRLM	Unfiltered
Texture	GLRLM	Unfiltered
Texture	GLRLM	Unfiltered
Texture	GLRLM	Unfiltered
Texture	GLRLM	Unfiltered
Texture	GLRLM	Unfiltered
Texture	GLRLM	Unfiltered
Texture	GLRLM	Unfiltered
Texture	GLRLM	Unfiltered
Texture	GLRLM	Unfiltered
Texture	GLRLM	Unfiltered
Texture	GLRLM	Unfiltered
Texture	GLRLM	Unfiltered
Texture	mGLRLM	Unfiltered
Texture	mGLRLM	Unfiltered
Texture	mGLRLM	Unfiltered
Texture	mGLRLM	Unfiltered
Texture	mGLRLM	Unfiltered
Texture	mGLRLM	Unfiltered
Texture	mGLRLM	Unfiltered

Texture	mGLRLM	Unfiltered
Texture	mGLRLM	Unfiltered
Texture	mGLRLM	Unfiltered
Texture	mGLRLM	Unfiltered
Texture	mGLRLM	Unfiltered
Texture	mGLRLM	Unfiltered
Texture	mGLRLM	Unfiltered
Texture	mGLRLM	Unfiltered
Texture	mGLRLM	Unfiltered
Texture	GLSZM	Unfiltered
Texture	GLSZM	Unfiltered
Texture	GLSZM	Unfiltered
Texture	GLSZM	Unfiltered
Texture	GLSZM	Unfiltered
Texture	GLSZM	Unfiltered
Texture	GLSZM	Unfiltered
Texture	GLSZM	Unfiltered
Texture	GLSZM	Unfiltered
Texture	GLSZM	Unfiltered
Texture	GLSZM	Unfiltered
Texture	GLSZM	Unfiltered
Texture	GLSZM	Unfiltered
Texture	GLSZM	Unfiltered
Texture	GLSZM	Unfiltered
Texture	GLSZM	Unfiltered
Texture	GLSZM	Unfiltered
Texture	GLDZM	Unfiltered
Texture	GLDZM	Unfiltered
Texture	GLDZM	Unfiltered
Texture	GLDZM	Unfiltered
Texture	GLDZM	Unfiltered
Texture	GLDZM	Unfiltered
Texture	GLDZM	Unfiltered
Texture	GLDZM	Unfiltered
Texture	GLDZM	Unfiltered
Texture	GLDZM	Unfiltered
Texture	GLDZM	Unfiltered
Texture	GLDZM	Unfiltered
Texture	GLDZM	Unfiltered
Texture	GLDZM	Unfiltered
Texture	GLDZM	Unfiltered
Texture	GLDZM	Unfiltered
Texture	GLDZM	Unfiltered
Texture	NGLDM	Unfiltered
Texture	NGLDM	Unfiltered
Texture	NGLDM	Unfiltered
Texture	NGLDM	Unfiltered
Texture	NGLDM	Unfiltered
Texture	NGLDM	Unfiltered
Texture	NGLDM	Unfiltered
Texture	NGLDM	Unfiltered
Texture	NGLDM	Unfiltered

Texture	NGLDM	Unfiltered
Texture	NGLDM	Unfiltered
Texture	NGLDM	Unfiltered
Texture	NGLDM	Unfiltered
Texture	NGLDM	Unfiltered
Texture	NGLDM	Unfiltered
Texture	NGLDM	Unfiltered
Wavelet	intensity	HHH
Wavelet	intensity	HHH
Wavelet	intensity	HHH
Wavelet	intensity	HHH
Wavelet	intensity	HHH
Wavelet	intensity	HHH
Wavelet	intensity	HHH
Wavelet	intensity	HHH
Wavelet	intensity	HHH
Wavelet	intensity	HHH
Wavelet	intensity	HHH
Wavelet	intensity	HHH
Wavelet	intensity	HHH
Wavelet	intensity	HHH
Wavelet	intensity	HHH
Wavelet	intensity	HHH
Wavelet	intensity	HHH
Wavelet	GLCM	HHH
Wavelet	GLCM	HHH
Wavelet	GLCM	HHH
Wavelet	GLCM	HHH
Wavelet	GLCM	HHH
Wavelet	GLCM	HHH
Wavelet	GLCM	HHH
Wavelet	GLCM	HHH
Wavelet	GLCM	HHH
Wavelet	GLCM	HHH
Wavelet	GLCM	HHH
Wavelet	GLCM	HHH
Wavelet	GLCM	HHH
Wavelet	GLCM	HHH
Wavelet	GLCM	HHH
Wavelet	GLCM	HHH
Wavelet	GLCM	HHH
Wavelet	GLCM	HHH
Wavelet	GLCM	HHH
Wavelet	GLCM	HHH
Wavelet	GLCM	HHH
Wavelet	GLCM	HHH
Wavelet	GLCM	HHH
Wavelet	GLCM	HHH
Wavelet	GLCM	HHH
Wavelet	GLCM	HHH

Wavelet	mGLCM	HHH
Wavelet	mGLCM	HHH
Wavelet	mGLCM	HHH
Wavelet	mGLCM	HHH
Wavelet	mGLCM	HHH
Wavelet	mGLCM	HHH
Wavelet	mGLCM	HHH
Wavelet	mGLCM	HHH
Wavelet	mGLCM	HHH
Wavelet	mGLCM	HHH
Wavelet	mGLCM	HHH
Wavelet	mGLCM	HHH
Wavelet	mGLCM	HHH
Wavelet	mGLCM	HHH
Wavelet	mGLCM	HHH
Wavelet	mGLCM	HHH
Wavelet	mGLCM	HHH
Wavelet	mGLCM	HHH
Wavelet	mGLCM	HHH
Wavelet	mGLCM	HHH
Wavelet	mGLCM	HHH
Wavelet	mGLCM	HHH
Wavelet	mGLCM	HHH
Wavelet	mGLCM	HHH
Wavelet	mGLCM	HHH
Wavelet	mGLCM	HHH
Wavelet	NGTDM	HHH
Wavelet	NGTDM	HHH
Wavelet	NGTDM	HHH
Wavelet	NGTDM	HHH
Wavelet	NGTDM	HHH
Wavelet	GLRLM	HHH
Wavelet	GLRLM	HHH
Wavelet	GLRLM	HHH
Wavelet	GLRLM	HHH
Wavelet	GLRLM	HHH
Wavelet	GLRLM	HHH
Wavelet	GLRLM	HHH
Wavelet	GLRLM	HHH
Wavelet	GLRLM	HHH
Wavelet	GLRLM	HHH
Wavelet	GLRLM	HHH
Wavelet	GLRLM	HHH
Wavelet	GLRLM	HHH
Wavelet	GLRLM	HHH
Wavelet	GLRLM	HHH
Wavelet	GLRLM	HHH
Wavelet	mGLRLM	HHH
Wavelet	mGLRLM	HHH
Wavelet	mGLRLM	HHH

Wavelet	mGLRLM	HHH
Wavelet	mGLRLM	HHH
Wavelet	mGLRLM	HHH
Wavelet	mGLRLM	HHH
Wavelet	mGLRLM	HHH
Wavelet	mGLRLM	HHH
Wavelet	mGLRLM	HHH
Wavelet	mGLRLM	HHH
Wavelet	mGLRLM	HHH
Wavelet	mGLRLM	HHH
Wavelet	mGLRLM	HHH
Wavelet	mGLRLM	HHH
Wavelet	mGLRLM	HHH
Wavelet	GLSZM	HHH
Wavelet	GLSZM	HHH
Wavelet	GLSZM	HHH
Wavelet	GLSZM	HHH
Wavelet	GLSZM	HHH
Wavelet	GLSZM	HHH
Wavelet	GLSZM	HHH
Wavelet	GLSZM	HHH
Wavelet	GLSZM	HHH
Wavelet	GLSZM	HHH
Wavelet	GLSZM	HHH
Wavelet	GLSZM	HHH
Wavelet	GLSZM	HHH
Wavelet	GLSZM	HHH
Wavelet	GLSZM	HHH
Wavelet	GLSZM	HHH
Wavelet	GLDZM	HHH
Wavelet	GLDZM	HHH
Wavelet	GLDZM	HHH
Wavelet	GLDZM	HHH
Wavelet	GLDZM	HHH
Wavelet	GLDZM	HHH
Wavelet	GLDZM	HHH
Wavelet	GLDZM	HHH
Wavelet	GLDZM	HHH
Wavelet	GLDZM	HHH
Wavelet	GLDZM	HHH
Wavelet	GLDZM	HHH
Wavelet	GLDZM	HHH
Wavelet	GLDZM	HHH
Wavelet	GLDZM	HHH
Wavelet	GLDZM	HHH
Wavelet	GLDZM	HHH
Wavelet	NGLDM	HHH
Wavelet	NGLDM	HHH
Wavelet	NGLDM	HHH
Wavelet	NGLDM	HHH
Wavelet	NGLDM	HHH

Wavelet	NGLDM	HHH
Wavelet	NGLDM	HHH
Wavelet	NGLDM	HHH
Wavelet	NGLDM	HHH
Wavelet	NGLDM	HHH
Wavelet	NGLDM	HHH
Wavelet	NGLDM	HHH
Wavelet	NGLDM	HHH
Wavelet	NGLDM	HHH
Wavelet	NGLDM	HHH
Wavelet	NGLDM	HHH
Wavelet	intensity	HHL
Wavelet	intensity	HHL
Wavelet	intensity	HHL
Wavelet	intensity	HHL
Wavelet	intensity	HHL
Wavelet	intensity	HHL
Wavelet	intensity	HHL
Wavelet	intensity	HHL
Wavelet	intensity	HHL
Wavelet	intensity	HHL
Wavelet	intensity	HHL
Wavelet	intensity	HHL
Wavelet	intensity	HHL
Wavelet	intensity	HHL
Wavelet	intensity	HHL
Wavelet	intensity	HHL
Wavelet	intensity	HHL
Wavelet	GLCM	HHL
Wavelet	GLCM	HHL
Wavelet	GLCM	HHL
Wavelet	GLCM	HHL
Wavelet	GLCM	HHL
Wavelet	GLCM	HHL
Wavelet	GLCM	HHL
Wavelet	GLCM	HHL
Wavelet	GLCM	HHL
Wavelet	GLCM	HHL
Wavelet	GLCM	HHL
Wavelet	GLCM	HHL
Wavelet	GLCM	HHL
Wavelet	GLCM	HHL
Wavelet	GLCM	HHL
Wavelet	GLCM	HHL
Wavelet	GLCM	HHL
Wavelet	GLCM	HHL
Wavelet	GLCM	HHL
Wavelet	GLCM	HHL
Wavelet	GLCM	HHL
Wavelet	GLCM	HHL

Wavelet	GLCM	HHL
Wavelet	GLCM	HHL
Wavelet	GLCM	HHL
Wavelet	GLCM	HHL
Wavelet	mGLCM	HHL
Wavelet	mGLCM	HHL
Wavelet	mGLCM	HHL
Wavelet	mGLCM	HHL
Wavelet	mGLCM	HHL
Wavelet	mGLCM	HHL
Wavelet	mGLCM	HHL
Wavelet	mGLCM	HHL
Wavelet	mGLCM	HHL
Wavelet	mGLCM	HHL
Wavelet	mGLCM	HHL
Wavelet	mGLCM	HHL
Wavelet	mGLCM	HHL
Wavelet	mGLCM	HHL
Wavelet	mGLCM	HHL
Wavelet	mGLCM	HHL
Wavelet	mGLCM	HHL
Wavelet	mGLCM	HHL
Wavelet	mGLCM	HHL
Wavelet	mGLCM	HHL
Wavelet	mGLCM	HHL
Wavelet	mGLCM	HHL
Wavelet	mGLCM	HHL
Wavelet	mGLCM	HHL
Wavelet	mGLCM	HHL
Wavelet	mGLCM	HHL
Wavelet	NGTDM	HHL
Wavelet	NGTDM	HHL
Wavelet	NGTDM	HHL
Wavelet	NGTDM	HHL
Wavelet	NGTDM	HHL
Wavelet	GLRLM	HHL
Wavelet	GLRLM	HHL
Wavelet	GLRLM	HHL
Wavelet	GLRLM	HHL
Wavelet	GLRLM	HHL
Wavelet	GLRLM	HHL
Wavelet	GLRLM	HHL
Wavelet	GLRLM	HHL
Wavelet	GLRLM	HHL
Wavelet	GLRLM	HHL
Wavelet	GLRLM	HHL
Wavelet	GLRLM	HHL
Wavelet	GLRLM	HHL
Wavelet	GLRLM	HHL
Wavelet	GLRLM	HHL

Wavelet	GLRLM	HHL
Wavelet	mGLRLM	HHL
Wavelet	mGLRLM	HHL
Wavelet	mGLRLM	HHL
Wavelet	mGLRLM	HHL
Wavelet	mGLRLM	HHL
Wavelet	mGLRLM	HHL
Wavelet	mGLRLM	HHL
Wavelet	mGLRLM	HHL
Wavelet	mGLRLM	HHL
Wavelet	mGLRLM	HHL
Wavelet	mGLRLM	HHL
Wavelet	mGLRLM	HHL
Wavelet	mGLRLM	HHL
Wavelet	mGLRLM	HHL
Wavelet	mGLRLM	HHL
Wavelet	mGLRLM	HHL
Wavelet	GLSZM	HHL
Wavelet	GLSZM	HHL
Wavelet	GLSZM	HHL
Wavelet	GLSZM	HHL
Wavelet	GLSZM	HHL
Wavelet	GLSZM	HHL
Wavelet	GLSZM	HHL
Wavelet	GLSZM	HHL
Wavelet	GLSZM	HHL
Wavelet	GLSZM	HHL
Wavelet	GLSZM	HHL
Wavelet	GLSZM	HHL
Wavelet	GLSZM	HHL
Wavelet	GLSZM	HHL
Wavelet	GLSZM	HHL
Wavelet	GLSZM	HHL
Wavelet	GLDZM	HHL
Wavelet	GLDZM	HHL
Wavelet	GLDZM	HHL
Wavelet	GLDZM	HHL
Wavelet	GLDZM	HHL
Wavelet	GLDZM	HHL
Wavelet	GLDZM	HHL
Wavelet	GLDZM	HHL
Wavelet	GLDZM	HHL
Wavelet	GLDZM	HHL
Wavelet	GLDZM	HHL
Wavelet	GLDZM	HHL
Wavelet	GLDZM	HHL
Wavelet	GLDZM	HHL
Wavelet	GLDZM	HHL
Wavelet	GLDZM	HHL
Wavelet	GLDZM	HHL
Wavelet	NGLDM	HHL

Wavelet	NGLDM	HHL
Wavelet	NGLDM	HHL
Wavelet	NGLDM	HHL
Wavelet	NGLDM	HHL
Wavelet	NGLDM	HHL
Wavelet	NGLDM	HHL
Wavelet	NGLDM	HHL
Wavelet	NGLDM	HHL
Wavelet	NGLDM	HHL
Wavelet	NGLDM	HHL
Wavelet	NGLDM	HHL
Wavelet	NGLDM	HHL
Wavelet	NGLDM	HHL
Wavelet	NGLDM	HHL
Wavelet	intensity	HLH
Wavelet	intensity	HLH
Wavelet	intensity	HLH
Wavelet	intensity	HLH
Wavelet	intensity	HLH
Wavelet	intensity	HLH
Wavelet	intensity	HLH
Wavelet	intensity	HLH
Wavelet	intensity	HLH
Wavelet	intensity	HLH
Wavelet	intensity	HLH
Wavelet	intensity	HLH
Wavelet	intensity	HLH
Wavelet	intensity	HLH
Wavelet	intensity	HLH
Wavelet	intensity	HLH
Wavelet	intensity	HLH
Wavelet	GLCM	HLH
Wavelet	GLCM	HLH
Wavelet	GLCM	HLH
Wavelet	GLCM	HLH
Wavelet	GLCM	HLH
Wavelet	GLCM	HLH
Wavelet	GLCM	HLH
Wavelet	GLCM	HLH
Wavelet	GLCM	HLH
Wavelet	GLCM	HLH
Wavelet	GLCM	HLH
Wavelet	GLCM	HLH
Wavelet	GLCM	HLH
Wavelet	GLCM	HLH
Wavelet	GLCM	HLH
Wavelet	GLCM	HLH
Wavelet	GLCM	HLH
Wavelet	GLCM	HLH

Wavelet	GLCM	HLH
Wavelet	GLCM	HLH
Wavelet	GLCM	HLH
Wavelet	GLCM	HLH
Wavelet	GLCM	HLH
Wavelet	GLCM	HLH
Wavelet	GLCM	HLH
Wavelet	GLCM	HLH
Wavelet	mGLCM	HLH
Wavelet	mGLCM	HLH
Wavelet	mGLCM	HLH
Wavelet	mGLCM	HLH
Wavelet	mGLCM	HLH
Wavelet	mGLCM	HLH
Wavelet	mGLCM	HLH
Wavelet	mGLCM	HLH
Wavelet	mGLCM	HLH
Wavelet	mGLCM	HLH
Wavelet	mGLCM	HLH
Wavelet	mGLCM	HLH
Wavelet	mGLCM	HLH
Wavelet	mGLCM	HLH
Wavelet	mGLCM	HLH
Wavelet	mGLCM	HLH
Wavelet	mGLCM	HLH
Wavelet	mGLCM	HLH
Wavelet	mGLCM	HLH
Wavelet	mGLCM	HLH
Wavelet	mGLCM	HLH
Wavelet	mGLCM	HLH
Wavelet	mGLCM	HLH
Wavelet	mGLCM	HLH
Wavelet	mGLCM	HLH
Wavelet	mGLCM	HLH
Wavelet	NGTDM	HLH
Wavelet	NGTDM	HLH
Wavelet	NGTDM	HLH
Wavelet	NGTDM	HLH
Wavelet	NGTDM	HLH
Wavelet	GLRLM	HLH
Wavelet	GLRLM	HLH
Wavelet	GLRLM	HLH
Wavelet	GLRLM	HLH
Wavelet	GLRLM	HLH
Wavelet	GLRLM	HLH
Wavelet	GLRLM	HLH
Wavelet	GLRLM	HLH
Wavelet	GLRLM	HLH
Wavelet	GLRLM	HLH
Wavelet	GLRLM	HLH

Wavelet	GLRLM	HLH
Wavelet	GLRLM	HLH
Wavelet	GLRLM	HLH
Wavelet	GLRLM	HLH
Wavelet	GLRLM	HLH
Wavelet	mGLRLM	HLH
Wavelet	mGLRLM	HLH
Wavelet	mGLRLM	HLH
Wavelet	mGLRLM	HLH
Wavelet	mGLRLM	HLH
Wavelet	mGLRLM	HLH
Wavelet	mGLRLM	HLH
Wavelet	mGLRLM	HLH
Wavelet	mGLRLM	HLH
Wavelet	mGLRLM	HLH
Wavelet	mGLRLM	HLH
Wavelet	mGLRLM	HLH
Wavelet	mGLRLM	HLH
Wavelet	mGLRLM	HLH
Wavelet	mGLRLM	HLH
Wavelet	mGLRLM	HLH
Wavelet	GLSZM	HLH
Wavelet	GLSZM	HLH
Wavelet	GLSZM	HLH
Wavelet	GLSZM	HLH
Wavelet	GLSZM	HLH
Wavelet	GLSZM	HLH
Wavelet	GLSZM	HLH
Wavelet	GLSZM	HLH
Wavelet	GLSZM	HLH
Wavelet	GLSZM	HLH
Wavelet	GLSZM	HLH
Wavelet	GLSZM	HLH
Wavelet	GLSZM	HLH
Wavelet	GLSZM	HLH
Wavelet	GLSZM	HLH
Wavelet	GLSZM	HLH
Wavelet	GLSZM	HLH
Wavelet	GLDZM	HLH
Wavelet	GLDZM	HLH
Wavelet	GLDZM	HLH
Wavelet	GLDZM	HLH
Wavelet	GLDZM	HLH
Wavelet	GLDZM	HLH
Wavelet	GLDZM	HLH
Wavelet	GLDZM	HLH
Wavelet	GLDZM	HLH
Wavelet	GLDZM	HLH
Wavelet	GLDZM	HLH
Wavelet	GLDZM	HLH
Wavelet	GLDZM	HLH

Wavelet	GLDZM	HLH
Wavelet	GLDZM	HLH
Wavelet	GLDZM	HLH
Wavelet	NGLDM	HLH
Wavelet	NGLDM	HLH
Wavelet	NGLDM	HLH
Wavelet	NGLDM	HLH
Wavelet	NGLDM	HLH
Wavelet	NGLDM	HLH
Wavelet	NGLDM	HLH
Wavelet	NGLDM	HLH
Wavelet	NGLDM	HLH
Wavelet	NGLDM	HLH
Wavelet	NGLDM	HLH
Wavelet	NGLDM	HLH
Wavelet	NGLDM	HLH
Wavelet	NGLDM	HLH
Wavelet	NGLDM	HLH
Wavelet	NGLDM	HLH
Wavelet	intensity	HLL
Wavelet	intensity	HLL
Wavelet	intensity	HLL
Wavelet	intensity	HLL
Wavelet	intensity	HLL
Wavelet	intensity	HLL
Wavelet	intensity	HLL
Wavelet	intensity	HLL
Wavelet	intensity	HLL
Wavelet	intensity	HLL
Wavelet	intensity	HLL
Wavelet	intensity	HLL
Wavelet	intensity	HLL
Wavelet	intensity	HLL
Wavelet	intensity	HLL
Wavelet	intensity	HLL
Wavelet	intensity	HLL
Wavelet	GLCM	HLL
Wavelet	GLCM	HLL
Wavelet	GLCM	HLL
Wavelet	GLCM	HLL
Wavelet	GLCM	HLL
Wavelet	GLCM	HLL
Wavelet	GLCM	HLL
Wavelet	GLCM	HLL
Wavelet	GLCM	HLL
Wavelet	GLCM	HLL
Wavelet	GLCM	HLL
Wavelet	GLCM	HLL
Wavelet	GLCM	HLL
Wavelet	GLCM	HLL

Wavelet	GLCM	HLL
Wavelet	GLCM	HLL
Wavelet	GLCM	HLL
Wavelet	GLCM	HLL
Wavelet	GLCM	HLL
Wavelet	GLCM	HLL
Wavelet	GLCM	HLL
Wavelet	GLCM	HLL
Wavelet	GLCM	HLL
Wavelet	GLCM	HLL
Wavelet	GLCM	HLL
Wavelet	GLCM	HLL
Wavelet	mGLCM	HLL
Wavelet	mGLCM	HLL
Wavelet	mGLCM	HLL
Wavelet	mGLCM	HLL
Wavelet	mGLCM	HLL
Wavelet	mGLCM	HLL
Wavelet	mGLCM	HLL
Wavelet	mGLCM	HLL
Wavelet	mGLCM	HLL
Wavelet	mGLCM	HLL
Wavelet	mGLCM	HLL
Wavelet	mGLCM	HLL
Wavelet	mGLCM	HLL
Wavelet	mGLCM	HLL
Wavelet	mGLCM	HLL
Wavelet	mGLCM	HLL
Wavelet	mGLCM	HLL
Wavelet	mGLCM	HLL
Wavelet	mGLCM	HLL
Wavelet	mGLCM	HLL
Wavelet	mGLCM	HLL
Wavelet	mGLCM	HLL
Wavelet	mGLCM	HLL
Wavelet	mGLCM	HLL
Wavelet	mGLCM	HLL
Wavelet	mGLCM	HLL
Wavelet	NGTDM	HLL
Wavelet	NGTDM	HLL
Wavelet	NGTDM	HLL
Wavelet	NGTDM	HLL
Wavelet	NGTDM	HLL
Wavelet	GLRLM	HLL
Wavelet	GLRLM	HLL
Wavelet	GLRLM	HLL
Wavelet	GLRLM	HLL
Wavelet	GLRLM	HLL
Wavelet	GLRLM	HLL
Wavelet	GLRLM	HLL

Wavelet	GLRLM	HLL
Wavelet	GLRLM	HLL
Wavelet	GLRLM	HLL
Wavelet	GLRLM	HLL
Wavelet	GLRLM	HLL
Wavelet	GLRLM	HLL
Wavelet	GLRLM	HLL
Wavelet	GLRLM	HLL
Wavelet	GLRLM	HLL
Wavelet	mGLRLM	HLL
Wavelet	mGLRLM	HLL
Wavelet	mGLRLM	HLL
Wavelet	mGLRLM	HLL
Wavelet	mGLRLM	HLL
Wavelet	mGLRLM	HLL
Wavelet	mGLRLM	HLL
Wavelet	mGLRLM	HLL
Wavelet	mGLRLM	HLL
Wavelet	mGLRLM	HLL
Wavelet	mGLRLM	HLL
Wavelet	mGLRLM	HLL
Wavelet	mGLRLM	HLL
Wavelet	mGLRLM	HLL
Wavelet	mGLRLM	HLL
Wavelet	mGLRLM	HLL
Wavelet	GLSZM	HLL
Wavelet	GLSZM	HLL
Wavelet	GLSZM	HLL
Wavelet	GLSZM	HLL
Wavelet	GLSZM	HLL
Wavelet	GLSZM	HLL
Wavelet	GLSZM	HLL
Wavelet	GLSZM	HLL
Wavelet	GLSZM	HLL
Wavelet	GLSZM	HLL
Wavelet	GLSZM	HLL
Wavelet	GLSZM	HLL
Wavelet	GLSZM	HLL
Wavelet	GLSZM	HLL
Wavelet	GLSZM	HLL
Wavelet	GLSZM	HLL
Wavelet	GLDZM	HLL
Wavelet	GLDZM	HLL
Wavelet	GLDZM	HLL
Wavelet	GLDZM	HLL
Wavelet	GLDZM	HLL
Wavelet	GLDZM	HLL
Wavelet	GLDZM	HLL
Wavelet	GLDZM	HLL
Wavelet	GLDZM	HLL

Wavelet	GLDZM	HLL
Wavelet	GLDZM	HLL
Wavelet	GLDZM	HLL
Wavelet	GLDZM	HLL
Wavelet	GLDZM	HLL
Wavelet	GLDZM	HLL
Wavelet	GLDZM	HLL
Wavelet	NGLDM	HLL
Wavelet	NGLDM	HLL
Wavelet	NGLDM	HLL
Wavelet	NGLDM	HLL
Wavelet	NGLDM	HLL
Wavelet	NGLDM	HLL
Wavelet	NGLDM	HLL
Wavelet	NGLDM	HLL
Wavelet	NGLDM	HLL
Wavelet	NGLDM	HLL
Wavelet	NGLDM	HLL
Wavelet	NGLDM	HLL
Wavelet	NGLDM	HLL
Wavelet	NGLDM	HLL
Wavelet	NGLDM	HLL
Wavelet	NGLDM	HLL
Wavelet	intensity	LHH
Wavelet	intensity	LHH
Wavelet	intensity	LHH
Wavelet	intensity	LHH
Wavelet	intensity	LHH
Wavelet	intensity	LHH
Wavelet	intensity	LHH
Wavelet	intensity	LHH
Wavelet	intensity	LHH
Wavelet	intensity	LHH
Wavelet	intensity	LHH
Wavelet	intensity	LHH
Wavelet	intensity	LHH
Wavelet	intensity	LHH
Wavelet	intensity	LHH
Wavelet	intensity	LHH
Wavelet	intensity	LHH
Wavelet	GLCM	LHH
Wavelet	GLCM	LHH
Wavelet	GLCM	LHH
Wavelet	GLCM	LHH
Wavelet	GLCM	LHH
Wavelet	GLCM	LHH
Wavelet	GLCM	LHH
Wavelet	GLCM	LHH
Wavelet	GLCM	LHH
Wavelet	GLCM	LHH

Wavelet	GLCM	LHH
Wavelet	GLCM	LHH
Wavelet	GLCM	LHH
Wavelet	GLCM	LHH
Wavelet	GLCM	LHH
Wavelet	GLCM	LHH
Wavelet	GLCM	LHH
Wavelet	GLCM	LHH
Wavelet	GLCM	LHH
Wavelet	GLCM	LHH
Wavelet	GLCM	LHH
Wavelet	GLCM	LHH
Wavelet	GLCM	LHH
Wavelet	GLCM	LHH
Wavelet	GLCM	LHH
Wavelet	GLCM	LHH
Wavelet	mGLCM	LHH
Wavelet	mGLCM	LHH
Wavelet	mGLCM	LHH
Wavelet	mGLCM	LHH
Wavelet	mGLCM	LHH
Wavelet	mGLCM	LHH
Wavelet	mGLCM	LHH
Wavelet	mGLCM	LHH
Wavelet	mGLCM	LHH
Wavelet	mGLCM	LHH
Wavelet	mGLCM	LHH
Wavelet	mGLCM	LHH
Wavelet	mGLCM	LHH
Wavelet	mGLCM	LHH
Wavelet	mGLCM	LHH
Wavelet	mGLCM	LHH
Wavelet	mGLCM	LHH
Wavelet	mGLCM	LHH
Wavelet	mGLCM	LHH
Wavelet	mGLCM	LHH
Wavelet	mGLCM	LHH
Wavelet	mGLCM	LHH
Wavelet	mGLCM	LHH
Wavelet	mGLCM	LHH
Wavelet	mGLCM	LHH
Wavelet	mGLCM	LHH
Wavelet	NGTDM	LHH
Wavelet	NGTDM	LHH
Wavelet	NGTDM	LHH
Wavelet	NGTDM	LHH
Wavelet	NGTDM	LHH
Wavelet	GLRLM	LHH
Wavelet	GLRLM	LHH
Wavelet	GLRLM	LHH

Wavelet	GLRLM	LHH
Wavelet	GLRLM	LHH
Wavelet	GLRLM	LHH
Wavelet	GLRLM	LHH
Wavelet	GLRLM	LHH
Wavelet	GLRLM	LHH
Wavelet	GLRLM	LHH
Wavelet	GLRLM	LHH
Wavelet	GLRLM	LHH
Wavelet	GLRLM	LHH
Wavelet	GLRLM	LHH
Wavelet	GLRLM	LHH
Wavelet	GLRLM	LHH
Wavelet	mGLRLM	LHH
Wavelet	mGLRLM	LHH
Wavelet	mGLRLM	LHH
Wavelet	mGLRLM	LHH
Wavelet	mGLRLM	LHH
Wavelet	mGLRLM	LHH
Wavelet	mGLRLM	LHH
Wavelet	mGLRLM	LHH
Wavelet	mGLRLM	LHH
Wavelet	mGLRLM	LHH
Wavelet	mGLRLM	LHH
Wavelet	mGLRLM	LHH
Wavelet	mGLRLM	LHH
Wavelet	mGLRLM	LHH
Wavelet	mGLRLM	LHH
Wavelet	mGLRLM	LHH
Wavelet	mGLRLM	LHH
Wavelet	GLSZM	LHH
Wavelet	GLSZM	LHH
Wavelet	GLSZM	LHH
Wavelet	GLSZM	LHH
Wavelet	GLSZM	LHH
Wavelet	GLSZM	LHH
Wavelet	GLSZM	LHH
Wavelet	GLSZM	LHH
Wavelet	GLSZM	LHH
Wavelet	GLSZM	LHH
Wavelet	GLSZM	LHH
Wavelet	GLSZM	LHH
Wavelet	GLSZM	LHH
Wavelet	GLSZM	LHH
Wavelet	GLSZM	LHH
Wavelet	GLSZM	LHH
Wavelet	GLSZM	LHH
Wavelet	GLDZM	LHH
Wavelet	GLDZM	LHH
Wavelet	GLDZM	LHH
Wavelet	GLDZM	LHH
Wavelet	GLDZM	LHH

Wavelet	GLDZM	LHH
Wavelet	GLDZM	LHH
Wavelet	GLDZM	LHH
Wavelet	GLDZM	LHH
Wavelet	GLDZM	LHH
Wavelet	GLDZM	LHH
Wavelet	GLDZM	LHH
Wavelet	GLDZM	LHH
Wavelet	GLDZM	LHH
Wavelet	GLDZM	LHH
Wavelet	GLDZM	LHH
Wavelet	NGLDM	LHH
Wavelet	NGLDM	LHH
Wavelet	NGLDM	LHH
Wavelet	NGLDM	LHH
Wavelet	NGLDM	LHH
Wavelet	NGLDM	LHH
Wavelet	NGLDM	LHH
Wavelet	NGLDM	LHH
Wavelet	NGLDM	LHH
Wavelet	NGLDM	LHH
Wavelet	NGLDM	LHH
Wavelet	NGLDM	LHH
Wavelet	NGLDM	LHH
Wavelet	NGLDM	LHH
Wavelet	NGLDM	LHH
Wavelet	intensity	LHL
Wavelet	intensity	LHL
Wavelet	intensity	LHL
Wavelet	intensity	LHL
Wavelet	intensity	LHL
Wavelet	intensity	LHL
Wavelet	intensity	LHL
Wavelet	intensity	LHL
Wavelet	intensity	LHL
Wavelet	intensity	LHL
Wavelet	intensity	LHL
Wavelet	intensity	LHL
Wavelet	intensity	LHL
Wavelet	intensity	LHL
Wavelet	intensity	LHL
Wavelet	intensity	LHL
Wavelet	intensity	LHL
Wavelet	GLCM	LHL
Wavelet	GLCM	LHL
Wavelet	GLCM	LHL
Wavelet	GLCM	LHL
Wavelet	GLCM	LHL
Wavelet	GLCM	LHL

Wavelet	GLCM	LHL
Wavelet	GLCM	LHL
Wavelet	GLCM	LHL
Wavelet	GLCM	LHL
Wavelet	GLCM	LHL
Wavelet	GLCM	LHL
Wavelet	GLCM	LHL
Wavelet	GLCM	LHL
Wavelet	GLCM	LHL
Wavelet	GLCM	LHL
Wavelet	GLCM	LHL
Wavelet	GLCM	LHL
Wavelet	GLCM	LHL
Wavelet	GLCM	LHL
Wavelet	GLCM	LHL
Wavelet	GLCM	LHL
Wavelet	GLCM	LHL
Wavelet	GLCM	LHL
Wavelet	GLCM	LHL
Wavelet	GLCM	LHL
Wavelet	mGLCM	LHL
Wavelet	mGLCM	LHL
Wavelet	mGLCM	LHL
Wavelet	mGLCM	LHL
Wavelet	mGLCM	LHL
Wavelet	mGLCM	LHL
Wavelet	mGLCM	LHL
Wavelet	mGLCM	LHL
Wavelet	mGLCM	LHL
Wavelet	mGLCM	LHL
Wavelet	mGLCM	LHL
Wavelet	mGLCM	LHL
Wavelet	mGLCM	LHL
Wavelet	mGLCM	LHL
Wavelet	mGLCM	LHL
Wavelet	mGLCM	LHL
Wavelet	mGLCM	LHL
Wavelet	mGLCM	LHL
Wavelet	mGLCM	LHL
Wavelet	mGLCM	LHL
Wavelet	mGLCM	LHL
Wavelet	mGLCM	LHL
Wavelet	mGLCM	LHL
Wavelet	mGLCM	LHL
Wavelet	mGLCM	LHL
Wavelet	mGLCM	LHL
Wavelet	NGTDM	LHL
Wavelet	NGTDM	LHL
Wavelet	NGTDM	LHL
Wavelet	NGTDM	LHL

Wavelet	NGTDM	LHL
Wavelet	GLRLM	LHL
Wavelet	GLRLM	LHL
Wavelet	GLRLM	LHL
Wavelet	GLRLM	LHL
Wavelet	GLRLM	LHL
Wavelet	GLRLM	LHL
Wavelet	GLRLM	LHL
Wavelet	GLRLM	LHL
Wavelet	GLRLM	LHL
Wavelet	GLRLM	LHL
Wavelet	GLRLM	LHL
Wavelet	GLRLM	LHL
Wavelet	GLRLM	LHL
Wavelet	GLRLM	LHL
Wavelet	GLRLM	LHL
Wavelet	GLRLM	LHL
Wavelet	mGLRLM	LHL
Wavelet	mGLRLM	LHL
Wavelet	mGLRLM	LHL
Wavelet	mGLRLM	LHL
Wavelet	mGLRLM	LHL
Wavelet	mGLRLM	LHL
Wavelet	mGLRLM	LHL
Wavelet	mGLRLM	LHL
Wavelet	mGLRLM	LHL
Wavelet	mGLRLM	LHL
Wavelet	mGLRLM	LHL
Wavelet	mGLRLM	LHL
Wavelet	mGLRLM	LHL
Wavelet	mGLRLM	LHL
Wavelet	mGLRLM	LHL
Wavelet	mGLRLM	LHL
Wavelet	mGLRLM	LHL
Wavelet	GLSZM	LHL
Wavelet	GLSZM	LHL
Wavelet	GLSZM	LHL
Wavelet	GLSZM	LHL
Wavelet	GLSZM	LHL
Wavelet	GLSZM	LHL
Wavelet	GLSZM	LHL
Wavelet	GLSZM	LHL
Wavelet	GLSZM	LHL
Wavelet	GLSZM	LHL
Wavelet	GLSZM	LHL
Wavelet	GLSZM	LHL
Wavelet	GLSZM	LHL
Wavelet	GLSZM	LHL
Wavelet	GLSZM	LHL
Wavelet	GLSZM	LHL
Wavelet	GLSZM	LHL
Wavelet	GLSZM	LHL
Wavelet	GLDZM	LHL

Wavelet	GLDZM	LHL
Wavelet	GLDZM	LHL
Wavelet	GLDZM	LHL
Wavelet	GLDZM	LHL
Wavelet	GLDZM	LHL
Wavelet	GLDZM	LHL
Wavelet	GLDZM	LHL
Wavelet	GLDZM	LHL
Wavelet	GLDZM	LHL
Wavelet	GLDZM	LHL
Wavelet	GLDZM	LHL
Wavelet	GLDZM	LHL
Wavelet	GLDZM	LHL
Wavelet	GLDZM	LHL
Wavelet	GLDZM	LHL
Wavelet	NGLDM	LHL
Wavelet	NGLDM	LHL
Wavelet	NGLDM	LHL
Wavelet	NGLDM	LHL
Wavelet	NGLDM	LHL
Wavelet	NGLDM	LHL
Wavelet	NGLDM	LHL
Wavelet	NGLDM	LHL
Wavelet	NGLDM	LHL
Wavelet	NGLDM	LHL
Wavelet	NGLDM	LHL
Wavelet	NGLDM	LHL
Wavelet	NGLDM	LHL
Wavelet	NGLDM	LHL
Wavelet	NGLDM	LHL
Wavelet	intensity	LLH
Wavelet	intensity	LLH
Wavelet	intensity	LLH
Wavelet	intensity	LLH
Wavelet	intensity	LLH
Wavelet	intensity	LLH
Wavelet	intensity	LLH
Wavelet	intensity	LLH
Wavelet	intensity	LLH
Wavelet	intensity	LLH
Wavelet	intensity	LLH
Wavelet	intensity	LLH
Wavelet	intensity	LLH
Wavelet	intensity	LLH
Wavelet	intensity	LLH
Wavelet	intensity	LLH
Wavelet	intensity	LLH
Wavelet	intensity	LLH
Wavelet	GLCM	LLH
Wavelet	GLCM	LLH

Wavelet	GLCM	LLH
Wavelet	GLCM	LLH
Wavelet	GLCM	LLH
Wavelet	GLCM	LLH
Wavelet	GLCM	LLH
Wavelet	GLCM	LLH
Wavelet	GLCM	LLH
Wavelet	GLCM	LLH
Wavelet	GLCM	LLH
Wavelet	GLCM	LLH
Wavelet	GLCM	LLH
Wavelet	GLCM	LLH
Wavelet	GLCM	LLH
Wavelet	GLCM	LLH
Wavelet	GLCM	LLH
Wavelet	GLCM	LLH
Wavelet	GLCM	LLH
Wavelet	GLCM	LLH
Wavelet	GLCM	LLH
Wavelet	GLCM	LLH
Wavelet	GLCM	LLH
Wavelet	GLCM	LLH
Wavelet	GLCM	LLH
Wavelet	GLCM	LLH
Wavelet	mGLCM	LLH
Wavelet	mGLCM	LLH
Wavelet	mGLCM	LLH
Wavelet	mGLCM	LLH
Wavelet	mGLCM	LLH
Wavelet	mGLCM	LLH
Wavelet	mGLCM	LLH
Wavelet	mGLCM	LLH
Wavelet	mGLCM	LLH
Wavelet	mGLCM	LLH
Wavelet	mGLCM	LLH
Wavelet	mGLCM	LLH
Wavelet	mGLCM	LLH
Wavelet	mGLCM	LLH
Wavelet	mGLCM	LLH
Wavelet	mGLCM	LLH
Wavelet	mGLCM	LLH
Wavelet	mGLCM	LLH
Wavelet	mGLCM	LLH
Wavelet	mGLCM	LLH
Wavelet	mGLCM	LLH
Wavelet	mGLCM	LLH
Wavelet	mGLCM	LLH
Wavelet	mGLCM	LLH
Wavelet	mGLCM	LLH
Wavelet	mGLCM	LLH

Wavelet	NGTDM	LLH
Wavelet	NGTDM	LLH
Wavelet	NGTDM	LLH
Wavelet	NGTDM	LLH
Wavelet	NGTDM	LLH
Wavelet	GLRLM	LLH
Wavelet	GLRLM	LLH
Wavelet	GLRLM	LLH
Wavelet	GLRLM	LLH
Wavelet	GLRLM	LLH
Wavelet	GLRLM	LLH
Wavelet	GLRLM	LLH
Wavelet	GLRLM	LLH
Wavelet	GLRLM	LLH
Wavelet	GLRLM	LLH
Wavelet	GLRLM	LLH
Wavelet	GLRLM	LLH
Wavelet	GLRLM	LLH
Wavelet	GLRLM	LLH
Wavelet	GLRLM	LLH
Wavelet	mGLRLM	LLH
Wavelet	mGLRLM	LLH
Wavelet	mGLRLM	LLH
Wavelet	mGLRLM	LLH
Wavelet	mGLRLM	LLH
Wavelet	mGLRLM	LLH
Wavelet	mGLRLM	LLH
Wavelet	mGLRLM	LLH
Wavelet	mGLRLM	LLH
Wavelet	mGLRLM	LLH
Wavelet	mGLRLM	LLH
Wavelet	mGLRLM	LLH
Wavelet	mGLRLM	LLH
Wavelet	mGLRLM	LLH
Wavelet	mGLRLM	LLH
Wavelet	mGLRLM	LLH
Wavelet	GLSZM	LLH
Wavelet	GLSZM	LLH
Wavelet	GLSZM	LLH
Wavelet	GLSZM	LLH
Wavelet	GLSZM	LLH
Wavelet	GLSZM	LLH
Wavelet	GLSZM	LLH
Wavelet	GLSZM	LLH
Wavelet	GLSZM	LLH
Wavelet	GLSZM	LLH
Wavelet	GLSZM	LLH
Wavelet	GLSZM	LLH
Wavelet	GLSZM	LLH

Wavelet	GLSZM	LLH
Wavelet	GLSZM	LLH
Wavelet	GLSZM	LLH
Wavelet	GLDZM	LLH
Wavelet	GLDZM	LLH
Wavelet	GLDZM	LLH
Wavelet	GLDZM	LLH
Wavelet	GLDZM	LLH
Wavelet	GLDZM	LLH
Wavelet	GLDZM	LLH
Wavelet	GLDZM	LLH
Wavelet	GLDZM	LLH
Wavelet	GLDZM	LLH
Wavelet	GLDZM	LLH
Wavelet	GLDZM	LLH
Wavelet	GLDZM	LLH
Wavelet	GLDZM	LLH
Wavelet	GLDZM	LLH
Wavelet	GLDZM	LLH
Wavelet	NGLDM	LLH
Wavelet	NGLDM	LLH
Wavelet	NGLDM	LLH
Wavelet	NGLDM	LLH
Wavelet	NGLDM	LLH
Wavelet	NGLDM	LLH
Wavelet	NGLDM	LLH
Wavelet	NGLDM	LLH
Wavelet	NGLDM	LLH
Wavelet	NGLDM	LLH
Wavelet	NGLDM	LLH
Wavelet	NGLDM	LLH
Wavelet	NGLDM	LLH
Wavelet	NGLDM	LLH
Wavelet	NGLDM	LLH
Wavelet	NGLDM	LLH
Wavelet	intensity	LLL
Wavelet	intensity	LLL
Wavelet	intensity	LLL
Wavelet	intensity	LLL
Wavelet	intensity	LLL
Wavelet	intensity	LLL
Wavelet	intensity	LLL
Wavelet	intensity	LLL
Wavelet	intensity	LLL
Wavelet	intensity	LLL
Wavelet	intensity	LLL
Wavelet	intensity	LLL
Wavelet	intensity	LLL
Wavelet	intensity	LLL
Wavelet	intensity	LLL
Wavelet	intensity	LLL

Wavelet	intensity	LLL
Wavelet	intensity	LLL
Wavelet	GLCM	LLL
Wavelet	GLCM	LLL
Wavelet	GLCM	LLL
Wavelet	GLCM	LLL
Wavelet	GLCM	LLL
Wavelet	GLCM	LLL
Wavelet	GLCM	LLL
Wavelet	GLCM	LLL
Wavelet	GLCM	LLL
Wavelet	GLCM	LLL
Wavelet	GLCM	LLL
Wavelet	GLCM	LLL
Wavelet	GLCM	LLL
Wavelet	GLCM	LLL
Wavelet	GLCM	LLL
Wavelet	GLCM	LLL
Wavelet	GLCM	LLL
Wavelet	GLCM	LLL
Wavelet	GLCM	LLL
Wavelet	GLCM	LLL
Wavelet	GLCM	LLL
Wavelet	GLCM	LLL
Wavelet	GLCM	LLL
Wavelet	GLCM	LLL
Wavelet	GLCM	LLL
Wavelet	GLCM	LLL
Wavelet	mGLCM	LLL
Wavelet	mGLCM	LLL
Wavelet	mGLCM	LLL
Wavelet	mGLCM	LLL
Wavelet	mGLCM	LLL
Wavelet	mGLCM	LLL
Wavelet	mGLCM	LLL
Wavelet	mGLCM	LLL
Wavelet	mGLCM	LLL
Wavelet	mGLCM	LLL
Wavelet	mGLCM	LLL
Wavelet	mGLCM	LLL
Wavelet	mGLCM	LLL
Wavelet	mGLCM	LLL
Wavelet	mGLCM	LLL
Wavelet	mGLCM	LLL
Wavelet	mGLCM	LLL
Wavelet	mGLCM	LLL
Wavelet	mGLCM	LLL
Wavelet	mGLCM	LLL
Wavelet	mGLCM	LLL
Wavelet	mGLCM	LLL

Wavelet	mGLCM	LLL
Wavelet	mGLCM	LLL
Wavelet	mGLCM	LLL
Wavelet	mGLCM	LLL
Wavelet	NGTDM	LLL
Wavelet	NGTDM	LLL
Wavelet	NGTDM	LLL
Wavelet	NGTDM	LLL
Wavelet	NGTDM	LLL
Wavelet	GLRLM	LLL
Wavelet	GLRLM	LLL
Wavelet	GLRLM	LLL
Wavelet	GLRLM	LLL
Wavelet	GLRLM	LLL
Wavelet	GLRLM	LLL
Wavelet	GLRLM	LLL
Wavelet	GLRLM	LLL
Wavelet	GLRLM	LLL
Wavelet	GLRLM	LLL
Wavelet	GLRLM	LLL
Wavelet	GLRLM	LLL
Wavelet	GLRLM	LLL
Wavelet	GLRLM	LLL
Wavelet	GLRLM	LLL
Wavelet	GLRLM	LLL
Wavelet	mGLRLM	LLL
Wavelet	mGLRLM	LLL
Wavelet	mGLRLM	LLL
Wavelet	mGLRLM	LLL
Wavelet	mGLRLM	LLL
Wavelet	mGLRLM	LLL
Wavelet	mGLRLM	LLL
Wavelet	mGLRLM	LLL
Wavelet	mGLRLM	LLL
Wavelet	mGLRLM	LLL
Wavelet	mGLRLM	LLL
Wavelet	mGLRLM	LLL
Wavelet	mGLRLM	LLL
Wavelet	mGLRLM	LLL
Wavelet	mGLRLM	LLL
Wavelet	mGLRLM	LLL
Wavelet	GLSZM	LLL
Wavelet	GLSZM	LLL
Wavelet	GLSZM	LLL
Wavelet	GLSZM	LLL
Wavelet	GLSZM	LLL
Wavelet	GLSZM	LLL
Wavelet	GLSZM	LLL
Wavelet	GLSZM	LLL
Wavelet	GLSZM	LLL

Wavelet	GLSZM	LLL
Wavelet	GLSZM	LLL
Wavelet	GLSZM	LLL
Wavelet	GLSZM	LLL
Wavelet	GLSZM	LLL
Wavelet	GLSZM	LLL
Wavelet	GLSZM	LLL
Wavelet	GLDZM	LLL
Wavelet	GLDZM	LLL
Wavelet	GLDZM	LLL
Wavelet	GLDZM	LLL
Wavelet	GLDZM	LLL
Wavelet	GLDZM	LLL
Wavelet	GLDZM	LLL
Wavelet	GLDZM	LLL
Wavelet	GLDZM	LLL
Wavelet	GLDZM	LLL
Wavelet	GLDZM	LLL
Wavelet	GLDZM	LLL
Wavelet	GLDZM	LLL
Wavelet	GLDZM	LLL
Wavelet	GLDZM	LLL
Wavelet	GLDZM	LLL
Wavelet	NGLDM	LLL
Wavelet	NGLDM	LLL
Wavelet	NGLDM	LLL
Wavelet	NGLDM	LLL
Wavelet	NGLDM	LLL
Wavelet	NGLDM	LLL
Wavelet	NGLDM	LLL
Wavelet	NGLDM	LLL
Wavelet	NGLDM	LLL
Wavelet	NGLDM	LLL
Wavelet	NGLDM	LLL
Wavelet	NGLDM	LLL
Wavelet	NGLDM	LLL
Wavelet	NGLDM	LLL
Wavelet	NGLDM	LLL
Wavelet	NGLDM	LLL